ELECTROCHEMICAL STUDIES OF GE WAFER AND THE FORMATION OF GERMANENE IN AQUEOUS MEDIA

by

MARIA ALEKSEYEVNA LEDINA

(Under the Direction of John Lewellen Stickney)

ABSTRACT

This dissertation discusses studies of germanium electrodeposition, Te deposition onto Ge wafer and electrochemical formation of germanene in aqueous media. Germanene, similar to graphene, is a two-dimensional honeycomb structure. According to theoretical calculations, energetically stable structure of germanene is a low-buckled one, where half of the Ge atoms should be higher than the other half by 0.07 nm. Germanene is predicted to have similar unique properties and applications to those of graphene.

The electrodeposition of germanene has been studied by means of voltammetry, coulometry, in situ Scanning Tunneling microscopy (EC-STM), and micro-Raman spectroscopy. EC-STM investigations have demonstrated that initial Ge deposition was kinetically slow and formed deposits were somewhat unstable. It also has been identified that alloy between Ge and Au is observed to form as early as -300 mV vs. Ag/AgCl in pH 4.5 solution if the potential was held long enough. Moreover, presence of the Ge species in Au surface or as adsorbed species has been observed to cause a modification of Au(111) herringbone reconstruction.

EC-STM studies of electrodeposition of more than a monolayer of Ge demonstrated a honeycomb-like structure where the atomic distances were found to be about 0.44 ± 0.02 nm, which is only 10% of from what is expected. However, germanene domains identified in the STM images were incoherent. A micro-Raman shift corresponding to germanene signal was observed on one of Ge nanofilms, grown on Cu substrate. The EC-STM data and difficulty to find Raman signal indicates that the deposition of germanene structure has to be improved to more consistently produce the Raman shift.

Electrochemical deposition of Te onto Ge(100) wafer has been studied by means of cyclic voltammetry and ultrahigh vacuum surface characterization techniques, such as Auger Electron Spectroscopy (AES) and Low Energy Electron Diffraction (LEED). The investigations have shown that Te bulk was formed between -0.6 V and -0.85 V, whereas the deposition at -0.94 V have resulted in Te atomic layer, and no Te was observed at -1.6 V and lower.

INDEX WORDS: Germanene, Germanium, in situ Scanning Tunneling Microscopy, EC-STM, Electrodeposition, Electrochemistry, Cyclic Voltammetry, Raman Spectroscopy, UHV, AES, LEED.

ELECTROCHEMICAL STUDIES OF GE WAFER AND THE FORMATION OF GERMANENE IN AQUEOUS MEDIA

by

MARIA ALEKSEYEVNA LEDINA

BS, Saint-Petersburg State University, Russia, 2006

MS, Saint-Petersburg State University, Russia, 2008

A Dissertation Submitted to the Graduate Faculty of The University of Georgia in Partial Fulfillment of the Requirements for the Degree

DOCTOR OF PHILOSOPHY

ATHENS, GEORGIA

2015

ELECTROCHEMICAL STUDIES OF GE WAFER AND THE FORMATION OF GERMANENE IN AQUEOUS MEDIA

by

MARIA ALEKSEYEVNA LEDINA

Major Professor: John Lewellen Stickney

Committee: I. Jonathan Amster
Jeffrey L. Urbauer

Electronic Version Approved:

Suzanne Barbour
Dean of the Graduate School
The University of Georgia
December 2015

DEDICATION

I would like to dedicate this dissertation to my amazing parents, Liudmila and Aleksey, my incredible sister, Margarita, and my wonderful husband, Petr. None of this would have been possible without their constant encouragement and support throughout the years.

ACKNOWLEDGEMENTS

I would like to thank my major advisor, Professor John L. Stickney, for his guidance and support throughout the years. Without his timely advices my research studies would be a lot harder and not as productive and interesting. Moreover, I would like to thank Professor Jonathan Amster and Professor Jeffrey Urbauer, for serving on my committee, as well as for their support and advice. Last, but not least, I would like to thank all of the former and current members of Stickney's group for always being there for me. It was great working in such friendly environment.

TABLE OF CONTENTS

CHAPTER 1

INTRODUCTION AND LITERATURE REVIEW

Semiconductors play very important part in nowadays life, especially germanium. [1-4] Even though germanium was initially the first material used to fabricate a transistor, it has been very quickly substituted in industry by Si, since the last has stable native oxide. [5] However, since the thickness of the gate oxide in transistors has to decrease in order to keep improving its performance, SiO_2 is now reaching its critical thickness before gate leakage current will occur. [6] On the other hand, utilization of high-k material as a gate oxide, for example germanium, will allow continuing to decrease its size as well as to lower the power consumption in transistor. [7]

Most commonly used techniques for fabrication of Ge, especially to obtain good quality epitaxial films, are chemical vapor depositions[8-9] and molecular beam epitaxy. [10-11] The obtained deposits are high in quality, however, strict requirements, time and high cost needed to achieve it that makes these techniques good for research purposes, but not for implementation into the industry. One of the techniques that also commonly used but does not need those harsh conditions, such as vacuum, where the deposition can be performed in atmosphere, and no high temperatures used, is electrodeposition. Moreover, the last is very cost effective. Electrodeposition of germanium has been studied for a long time. [12-13] It has been determined that the electrodeposition of Ge in aqueous media is suspended to several monolayers (monolayer here is defined as one adsorbate per one substrate atom) due to low hydrogen overpotential, that starts before any more Ge can be

deposited. [13] However, utilization of nonaqueous solution does not have that problem and thick deposits can be achieved. [14-19] Endres et al. have studied Ge electrochemical deposition in various nonaqueous liquids such as ionic ones and molten salts. [15, 20-23] In their reports electrodeposition from GeI_4, $GeCl_4$ and $GeBr_4$ as a source of Ge were reported, moreover, not only the electrochemical studies from those precursors were showed but also in situ Scanning Tunneling Microscopy investigation were demonstrated. It was identified that the electrodeposition from GeI_4 precursor was limited to about 20 nm, due attack of the iodides species in solution on the interface of the deposit. [22] However, micrometer thick deposits were also obtained. [15] Huang et al. have been studying a formation of single-crystalline germanium films on Si substrates where the electrodeposited amorphous films were annealed. [16] Chandrasekharan et al. have reported a formation of germanium films utilizing electrochemical anodic deposition from ethylenediamine solutions of K_4Ge_9 containing deltahedral Zintl anions. [17] The characterization techniques have demonstrated that the obtained films were flat and consisted from aggregated nanoparticles. Another group, Jawad et al., have showed a formation of Ge films several micrometers thick utilizing a solution, Ge species in which were electrochemically obtained from Ge target from dissolving it. [24] Various nanostructures were obtained in those studies. In fact there are quite a few reports on formation of Ge nanostructures. Carim et al. have utilized a simple method called electrochemical Liquid-Liquid-Solid (ec-LLS) where germanium nanostructures were grown from aqueous solution containing Ge^{+4} species. The mechanism of the growth was explained as Ge is dissolved in liquid electrode, creating an alloy between intercalated Ge and the liquid substrate, and after reaching a saturation of Ge, nanostructures start to

grow from the alloy, producing crystalline Ge structures. [25] Ge nanowires were also grown from template assisted electrodeposition. [26-27] Another approach that was used to grow Ge nanowires was described by Mahenderkar et al. report. [28] The used substrate, Indium Tin Oxide (ITO) was electrochemically reduced to create In nanoparticles on the surface which were a nucleation spots for Ge crystallization. Supercritical liquids were also used to electrodeposit Ge. [29] Ge films were obtained from precursors containing compound of Ge(II) or Ge(IV). It was found that the deposit obtained from Ge(II) species in electrolyte were poorly reproducible and heavily contaminated. On the other hand, deposits synthesized from compounds of Ge(IV) were much more better, but amorphous. UV-assisted electrochemical deposition of Ge was also studied by Lahiri et al. on ITO. [30] It was identified that the electrodeposition of Ge will earlier (reduction) if UV light is applied during the formation of the deposit.

Aqueous electrodeposition of Ge was studied by Stickney et al. [31-33] The formation of Ge monolayer has been studied by means of cyclic voltammetry, coulometry and electrochemical Scanning Tunneling Microscopy (EC-STM). [31] It has been found that Ge coverage will depend on the pH of the precursor solution. Thus the maximum coverage was found to be in pH 9.2, whereas very little was obtained in pH 1.2. It is probably associated with earlier hydrogen evolution since proton concentration is higher. On the other hand, as was also reported, the deposition in very basic conditions is also ceased, it is not clear why, so it is something that needs to be studied in the future. Ge structures on Au(111) were demonstrated to start from formation of $(\sqrt{3} \times \sqrt{3})R30^{\circ}$ or (3×3) unit cells relative to the Au in pH 4.5 solution. Moreover, EC-STM studies showed the formation of an alloy between Ge and Au after -850 mV vs. Ag/AgCl. It was

concluded due to observation of the pitted surface after Ge deposit was stripped and also due to roughening of Moirè structure obtained by that potential. It was also reported that Ge electrodeposition has a very slow kinetics and in order to reach a maximum coverage at a particular potential, the last has to be held. In another article, Liang et al. developed an electrochemical cycle to grow Ge nanofilms utilizing a scheme "Bait and Switch" with surface-limited reaction by electrochemical Atomic Layer Deposition (E-ALD). [32] E-ALD is an electrochemical method where material is deposited by one atomic layer at a time using surface-limited reactions. [34-37] The E-ALD deposition is performed in condensed phase at room temperature in atmosphere. The surface-limited reaction usually referred as underpotential deposition, where the one element is deposited on a second one at a potential prior to (or under) that needed to deposit the element on itself, thus before a bulk formation. Linag et al. have described a cycle to grow Ge nanofilms with help of atomic layer of Te. The cycle would be started with deposition of the self-limited amount of Ge onto the substrate of choice. In the studies copper electrode was used over Au due to higher hydrogen overpotential. After the self-limited amount of Ge was grown, Te would be introduced into the flow cell without loosing of the potential control and deposited as bulk amount, and then the potential would be stepped to where atomic layer of Te would be left on the surface. Then Ge would be introduced into the cell and deposited onto the Te layer. The cycle would be finished with switching the potential to a very negative value for aqueous solutions (-1.6 V), to reductively and completely strip Te from the surface, leaving behind only newly deposited Ge. Then the cycle can be repeated as many times as needed to grow the desired thickness. It was identified that Ge films can be grown in a linear fashion depending on the number of cycles.

Characterization of the Ge deposits with Raman spectroscopy and XRD has showed that the grown films were amorphous in nature. And the third paper presented by Liang et al. was about a formation of $Ge_xSb_yTe_z$ films using E-ALD, the potential application of those phase change materials is optical storage. As a result of the studies of formation of alternated binary cycles conformal nanodeposits were obtained with good crystallinity. [33]

The second chapters of this dissertation will be discussing a continuation of initial deposition of Ge in pH 4.5 solution by means of Cyclic Voltammetry, coulometry, and Raman Spectroscopy. In particular, the main technique utilized in this dissertation is in situ STM studies will be performed on STM instrument (Digital Instruments, Veeco), schematic of which is presented in Figure 1.1. The electrochemical STM instrumentation allows performing experiment in the condensed phase under the potential control in real time. Moreover, it allows obtaining atomically resolved images at the solid-liquid interface. In order to see the interface an atomically sharp tip is needed to create the flow of tunneling current between the tip and the surface. The tip is usually a tungsten one, prepared by etching the W wire in hydroxide solution. [38-39] Another important part of the EC-STM studies is a preparation of the Au single crystal bead sample. The modification of Clavier method was utilized in the present studies, where the bead will be repeatedly heated in hydrogen flame and slowly cooled down to create large Au(111) terraces. [40]

Chapter 3 discusses the investigation into electrochemical formation of germanene structure on Au(111) surface. Germanene is a honeycomb single layer of Ge atoms. Cahangirov et al. have demonstrated a theoretical report where the formation of germanene and silicene was described for the first time. [41] The interest in formation of those structures started to increase after the isolation the separate layers of graphene from

Highly Oriented Pyrolytic Graphite (HOPG) using a very simple method such as scotch exfoliation, which allowed studying its application and properties. [42-45]

Germanene structure will be very similar to the structure of graphene, however, it was theoretically predicted that the energetically stable one would be low buckled by 0.07 nm, which would promote mixed sp^2-sp^3 hybridization. [46] The structure of germanene is demonstrated in Figure 1.2. Ge-Ge neighbor atomic distances were predicted to be around 0.24 nm. Germanene predicted to have only about 24 meV band gap, which means it would be practically a gapless material. [47-49] Furthermore, *ab initio* calculations shows that germanene structure should have a Raman shift around 290 cm^{-1}. [50-55]

As known, germanene structure does not exist in nature as graphene does in HOPG. However, a few reports have already been published where the experimental results for synthesis of the germanene structures have been published. Pt (111) surface was used as a substrate by Li et al. to produce a buckled $\sqrt{19} \times \sqrt{19}$ germanene structure indentified by STM and theoretical calculations, where germanium was physical vapor deposited by electron beam at room temperature, and sequential annealing of the deposit. [56] It was also concluded from DFT calculations that only one out of six atoms was higher than the rest of five atoms in ring structure. Davila et al. have also presented a formation of germanene deposit onto Au(111) surface utilizing MBE. [57] As earlier report, the obtained STM images of germanene structure were compared with *ab initio* calculations and concluded that the formed structure was $\sqrt{7} \times \sqrt{7}$ relative trot the Au(111), however, it the observed honeycomb structure was nearly flat. Derivaz et al. have demonstrated a formation of germanene structure also using gas phase method. [58] STM images of the

deposit as well as the theoretical calculations have showed that the formed deposit was a honeycomb (3 × 3) superstructure relative to the Al(111). Moreover, the formation of germanane was also reported by Bianco et al. utilizing a topochemical deintercalation of the $CaGe_2$. [59] Interestingly, it was reported that the formed germanane could have been easily exfoliated.

The recent report by our group about investigation into electrochemical formation of germanene structure was an impetus for this dissertation. [60] The incoherence of the observed germanene domains as well as irreproducibility of Raman signal implies that a better understanding is necessary to obtain a better germanene deposits. The studies are needed to be performed in order to identify the conditions for formation of defect free germanene domains, and in order to more reproducibly exhibit Raman shift that correspond to germanene. Thus the very initial deposition amount will be studied in order to identify whether it is important for the final structure, what role alloy formation plays in the consequent deposition process, whether the deposition can be improved by finding a different conditions, and if the germanene structure will be better when it is fabricated slow vs. fast deposition.

Chapter 4 will discuss Te electrodeposition onto Ge(100) wafer. UHV system combined with electrochemical instrumentations was utilized in the studies which allowed transferring the substrate after electrochemical experiment into UHV main chamber to characterize the surface without its exposure to air. UHV techniques used were Auger Electron Spectroscopy (AES) and Low Energy Electron Diffraction (LEED). The studies are of interest for identification of the electrochemical potentials where an atomic layer of Te can be formed as well as where no Te will be present on Ge surface.

This data then can be applied in the Ge films growth cycle where Te is used as a sacrificial layer. Thus by determining better conditions for Te deposition, Ge nanofilms can be grown with improved quality for potential growth of germanene structure.

References

1. Soref, R., Mid-infrared photonics in silicon and germanium. *Nature photonics* **2010,** *4* (8), 495-497.

2. Chroneos, A., Defect engineering strategies for germanium. *J. Mater. Sci.: Mater. Electron.* **2013,** *24* (6), 1741-1747.

3. Chen, L., Ultra-low capacitance and high speed germanium photodetectors on silicon. *Optics express* **2009,** *17* (10), 7901-7906.

4. Liow, T.-Y.; Tan, K.-M.; Lee, R. T. P.; Zhu, M.; Tan, B. L. H.; Balasubramanian, N.; Yeo, Y.-C., Germanium source and drain stressors for ultrathin-body and nanowire field-effect transistors. *IEEE Electron Device Lett.* **2008,** *29* (7), 808-810.

5. Bardeen, J.; Brattain, W. H., THE TRANSISTOR, A SEMI-CONDUCTOR TRIODE. *Physical review* **1948,** *74* (2), 230-231.

6. Chaudhry, A., *Fundamentals of Nanoscaled Field Effect Transistors*. Springer: 2013.

7. Kamata, Y., High-k/Ge MOSFETs for future nanoelectronics. *Mater. Today (Oxford, U. K.)* **2008,** *11* (1-2), 29-38.

8. Hartmann, J. M.; Papon, A. M.; Destefanis, V.; Billon, T., Reduced pressure chemical vapor deposition of Ge thick layers on Si(001), Si(011) and Si(111). *J. Cryst. Growth* **2008,** *310* (24), 5287-5296.

9. Wintterlin, J.; Avouris, P., Scanning tunneling microscopy (STM) studies of the chemical vapor deposition of Ge on Si(111) from Ge hydrides and a comparison with molecular beam epitaxy. *J. Chem. Phys.* **1994,** *100* (1), 687-704.

10. Persans, P. D.; Deelman, P. W.; Stokes, K. L.; Schowalter, L. J.; Byrne, A., Optical studies of Ge islanding on Si(111). *Appl. Phys. Lett.* **1997,** *70* (4), 472-474.

11. Smith, D. J.; Chandrasekhar, D.; Chaparro, S. A.; Crozier, P. A.; Drucker, J.; Floyd, M.; McCartney, M. R.; Zhang, Y., Microstructural evolution of Ge/Si(100) nanoscale islands. *J. Cryst. Growth* **2003,** *259* (3), 232-244.

12. Szekely, G., Electrodeposition of germanium. *J. Electrochem. Soc.* **1951,** *98*, 318-24.

13. Pourbaix, M., *Atlas of Electrochemical Equilibria in Aqueous Solutions*. Pergamon Press: 1966.

14. Wu, M.; Brooks, N. R.; Schaltin, S.; Binnemans, K.; Fransaer, J., Electrodeposition of germanium from the ionic liquid 1-butyl-1-methylpyrrolidinium dicyanamide. *Phys. Chem. Chem. Phys.* **2013,** *15* (14), 4955-4964.

15. Endres, F.; Zein El Abedin, S., Nanoscale electrodeposition of germanium on Au(111) from an ionic liquid: an in situ STM study of phase formation. Part I. Ge from GeBr4. *Phys. Chem. Chem. Phys.* **2002,** *4* (9), 1640-1648.

16. Huang, Q.; Bedell, S. W.; Saenger, K. L.; Copel, M.; Deligianni, H.; Romankiw, L. T., Single-crystalline germanium thin films by electrodeposition and solid-phase epitaxy. *Electrochem Solid St* **2007,** *10* (11), D124-D126.

17. Chandrasekharan, N.; Sevov, S. C., Anodic Electrodeposition of Germanium Films from Ethylenediamine Solutions of Deltahedral Ge94- Zintl Ions. *J. Electrochem. Soc.* **2010,** *157* (4), C140-C145.

18. Lahiri, A.; Pulletikurthi, G.; Zein El Abedin, S.; Endres, F., Electrodeposition of Ge, Sn and GexSn1-x from two different room temperature ionic liquids. *J. Solid State Electrochem.* **2015,** *19* (3), 785-793.

19. Wu, M.; Vanhoutte, G.; Brooks, N. R.; Binnemans, K.; Fransaer, J., Electrodeposition of germanium at elevated temperatures and pressures from ionic liquids. *Phys. Chem. Chem. Phys.* **2015,** *17* (18), 12080-12089.

20. Endres, F.; Zein El Abedin, S., Electrodeposition of stable and narrowly dispersed germanium nanoclusters from an ionic liquid. *Chem. Commun. (Cambridge, U. K.)* **2002,** (8), 892-893.

21. Endres, F.; Zein El Abedin, S., Nanoscale electrodeposition of germanium on Au(111) from an ionic liquid: an in situ STM study of phase formation. Part II. Ge from GeCl4. *Phys. Chem. Chem. Phys.* **2002,** *4* (9), 1649-1657.

22. Endres, F.; Schrodt, C., In situ STM studies on germanium tetraiodide electroreduction on Au(111) in the room temperature molten salt 1-butyl-3-methylimidazolium hexafluorophosphate. *Phys. Chem. Chem. Phys.* **2000,** *2* (24), 5517-5520.

23. Endres, F., Electrodeposition of a thin germanium film on gold from a room temperature ionic liquid. *Phys. Chem. Chem. Phys.* **2001,** *3* (15), 3165-3174.

24. Jawad, M. J.; Hashim, M. R.; Ali, N. K.; Corcoles, E. P.; Sharifabad, M. E., An Alternative Method to Grow Ge Thin Films on Si by Electrochemical Deposition for Photonic Applications. *J. Electrochem. Soc.* **2012,** *159* (2), D124-D128.

25. Carim, A. I.; Collins, S. M.; Foley, J. M.; Maldonado, S., Benchtop Electrochemical Liquid-Liquid-Solid Growth of Nanostructured Crystalline Germanium. *J. Am. Chem. Soc.* **2011,** *133* (34), 13292-13295.

26. Al-Salman, R.; Mallet, J.; Molinari, M.; Fricoteaux, P.; Martineau, F.; Troyon, M.; El Abedin, S. Z.; Endres, F., Template assisted electrodeposition of germanium and silicon nanowires in an ionic liquid. *Phys. Chem. Chem. Phys.* **2008,** *10* (41), 6233-6237.

27. Martineau, F.; Namur, K.; Mallet, J.; Delavoie, F.; Endres, F.; Troyon, M.; Molinari, M., Electrodeposition at room temperature of amorphous silicon and germanium nanowires in ionic liquid. *IOP Conf. Ser.: Mater. Sci. Eng.* **2009,** *6*, 012012/1-012012/4.

28. Mahenderkar, N. K.; Liu, Y.-C.; Koza, J. A.; Switzer, J. A., Electrodeposited germanium nanowires. *ACS Nano* **2014,** *8* (9), 9524-9530.

29. Ke, J.; Bartlett, P. N.; Cook, D.; Easun, T. L.; George, M. W.; Levason, W.; Reid, G.; Smith, D.; Su, W. T.; Zhang, W. J., Electrodeposition of germanium from supercritical fluids. *Physical Chemistry Chemical Physics* **2012,** *14* (4), 1517-1528.

30. Lahiri, A.; Zein El Abedin, S.; Endres, F., UV-Assisted Electrodeposition of Germanium from an Air- and Water-Stable Ionic Liquid. *J. Phys. Chem. C* **2012,** *116* (33), 17739-17745.

31. Liang, X.; Kim, Y.-G.; Gebergziabiher, D. K.; Stickney, J. L., Aqueous electrodeposition of Ge monolayers. *Langmuir* **2010,** *26* (4), 2877-84.

32. Liang, X.; Zhang, Q.; Lay, M. D.; Stickney, J. L., Growth of Ge Nanofilms Using Electrochemical Atomic Layer Deposition, with a "Bait and Switch" Surface-Limited Reaction. *J. Am. Chem. Soc.* **2011,** *133* (21), 8199-8204.

33. Liang, X.; Jayaraju, N.; Thambidurai, C.; Zhang, Q.; Stickney, J. L., Controlled Electrochemical Formation of GexSbyTez using Atomic Layer Deposition (ALD). *Chem. Mater.* **2011,** *23* (7), 1742-1752.

34. Banga, D. O.; Kim, Y.-G.; Cox, S.; Happek, U.; Stickney, J. L., Optimization of PbSe nanofilms formation by electrochemical atomic layer deposition (ALD). *ECS Trans.* **2009,** *19* (3, State-of-the-Art Program on Compound Semiconductors 50 (SOTAPOCS 50) and Processes at the Semiconductor Solution Interface 3), 245-272.

35. Gebregziabiher, D. K.; Kim, Y.-G.; Thambidurai, C.; Ivanova, V.; Haumesser, P.-H.; Stickney, J. L., Electrochemical atomic layer deposition of copper nanofilms on ruthenium. *J. Cryst. Growth* **2010,** *312* (8), 1271-1276.

36. Kim, J. Y.; Kim, Y.-G.; Stickney, J. L., Copper Nanofilm Formation by Electrochemical Atomic Layer Deposition. Ultrahigh-Vacuum Electrochemical and In Situ STM Studies. *J. Electrochem. Soc.* **2007,** *154* (4), D260-D266.

37. Lay, M. D.; Stickney, J. L., EC-STM Studies of Te and CdTe Atomic Layer Formation from a Basic Te Solution. *J. Electrochem. Soc.* **2004,** *151* (6), C431-C435.

38. Kim, Y.-G.; Kim, J. Y.; Thambidurai, C.; Stickney, J. L., Pb deposition on I-coated Au(111). UHV-EC and EC-STM studies. *Langmuir* **2007,** *23* (5), 2539-45.

39. Suggs, D. W.; Bard, A. J., Scanning Tunneling Microscopic Study with Atomic Resolution of the Dissolution of Cu(111) in Aqueous Chloride Solutions. *J. Am. Chem. Soc.* **1994,** *116* (23), 10725-33.

40. Clavilier, J.; Faure, R.; Guinet, G.; Durand, R., Preparation of monocrystalline platinum microelectrodes and electrochemical study of the plane surfaces cut in the direction of the {111} and {110} planes. *J. Electroanal. Chem. Interfacial Electrochem.* **1980,** *107* (1), 205-9.

41. Cahangirov, S.; Topsakal, M.; Akturk, E.; Sahin, H.; Ciraci, S., Two- and One-Dimensional Honeycomb Structures of Silicon and Germanium. *Phys. Rev. Lett.* **2009,** *102* (23), 236804/1-236804/4.

42. Zhu, Y.; Murali, S.; Cai, W.; Li, X.; Suk, J. W.; Potts, J. R.; Ruoff, R. S., Graphene and Graphene Oxide: synthesis, Properties, and Applications. *Adv. Mater. (Weinheim, Ger.)* **2010,** *22* (35), 3906-3924.

43. Novoselov, K. S.; Geim, A. K.; Morozov, S. V.; Jiang, D.; Zhang, Y.; Dubonos, S. V.; Grigorieva, I. V.; Firsov, A. A., Electric Field Effect in Atomically Thin Carbon Films. *Science (Washington, DC, U. S.)* **2004,** *306* (5696), 666-669.

44. Li, X.; Zhu, Y.; Cai, W.; Borysiak, M.; Han, B.; Chen, D.; Piner, R. D.; Colombo, L.; Ruoff, R. S., Transfer of Large-Area Graphene Films for High-Performance Transparent Conductive Electrodes. *Nano Lett.* **2009,** *9* (12), 4359-4363.

45. Li, D.; Mueller, M. B.; Gilje, S.; Kaner, R. B.; Wallace, G. G., Processable aqueous dispersions of graphene nanosheets. *Nat. Nanotechnol.* **2008,** *3* (2), 101-105.

46. Bechstedt, F.; Matthes, L.; Gori, P.; Pulci, O., Infrared absorbance of silicene and germanene. *Applied Physics Letters* **2012,** *100* (26).

47. Li, L.; Zhao, M., First-principles identifications of superstructures of germanene on Ag(111) surface and h-BN substrate. *Physical Chemistry Chemical Physics* **2013,** *15* (39), 16853-16863.

48. Kaloni, T. P.; Schwingenschlogl, U., Stability of germanene under tensile strain. *arXiv.org, e-Print Arch., Condens. Matter* **2013**, 1-11, arXiv:1311.2807v1 [cond-mat.mtrl-sci].

49. Ye, M.; Quhe, R.; Zheng, J.; Ni, Z.; Wang, Y.; Yuan, Y.; Tse, G.; Shi, J.; Gao, Z.; Lu, J., Tunable band gap in germanene by surface adsorption. *Phys. E (Amsterdam, Neth.)* **2014,** *59*, 60-65.

50. Houssa, M.; Pourtois, G.; Afanas'ev, V. V.; Stesmans, A., Electronic properties of two-dimensional hexagonal germanium. *Applied Physics Letters* **2010,** *96* (8).

51. Wei, W.; Dai, Y.; Huang, B.; Jacob, T., Many-body effects in silicene, silicane, germanene and germanane. *Physical Chemistry Chemical Physics* **2013,** *15* (22), 8789-8794.

52. Kaltsas, D.; Tsetseris, L., Stability and electronic properties of ultrathin films of silicon and germanium. *Physical Chemistry Chemical Physics* **2013,** *15* (24), 9710-9715.

53. Scalise, E.; Houssa, M.; Pourtois, G.; Broek, B.; Afanas'ev, V.; Stesmans, A., Vibrational properties of silicene and germanene. *Nano Res.* **2013,** *6* (1), 19-28.

54. Matthes, L.; Pulci, O.; Bechstedt, F., Massive Dirac quasiparticles in the optical absorbance of graphene, silicene, germanene, and tinene. *Journal of Physics-Condensed Matter* **2013,** *25* (39).

55. Roome, N. J.; Carey, J. D., Beyond Graphene: Stable Elemental Monolayers of Silicene and Germanene. *ACS Appl. Mater. Interfaces* **2014,** *6* (10), 7743-7750.

56. Li, L.; Lu, S.-z.; Pan, J.; Qin, Z.; Wang, Y.-q.; Wang, Y.; Cao, G.-y.; Du, S.; Gao, H.-J., Buckled Germanene Formation on Pt(111). *Advanced Materials* **2014,** *26* (28), 4820-+.

57. Davila, M. E.; Xian, L.; Cahangirov, S.; Rubio, A.; Le Lay, G., Germanene: a novel two-dimensional germanium allotrope akin to graphene and silicene. *New J. Phys.* **2014,** *16* (Sept.), 095002/1-095002/10, 10 pp.

58. Derivaz, M.; Dentel, D.; Stephan, R.; Hanf, M.-C.; Mehdaoui, A.; Sonnet, P.; Pirri, C., Continuous germanene layer on Al(111). *Nano Lett.* **2015,** *15* (4), 2510-2516.

59. Bianco, E.; Butler, S.; Jiang, S.; Restrepo, O. D.; Windl, W.; Goldberger, J. E., Stability and Exfoliation of Germanane: A Germanium Graphane Analogue. *Acs Nano* **2013,** *7* (5), 4414-4421.

60. Ledina, M.; Liang, X.; Kim, Y.-G.; Jung, J.; Perdue, B.; Tsang, C.; Soriaga, M. P.; Stickney, J. L., (Invited) Investigations into the Formation of Germanene Using Electrochemical Atomic Layer Deposition (E-ALD). *Ecs Transactions* **2015,** *66* (6), 129-140.

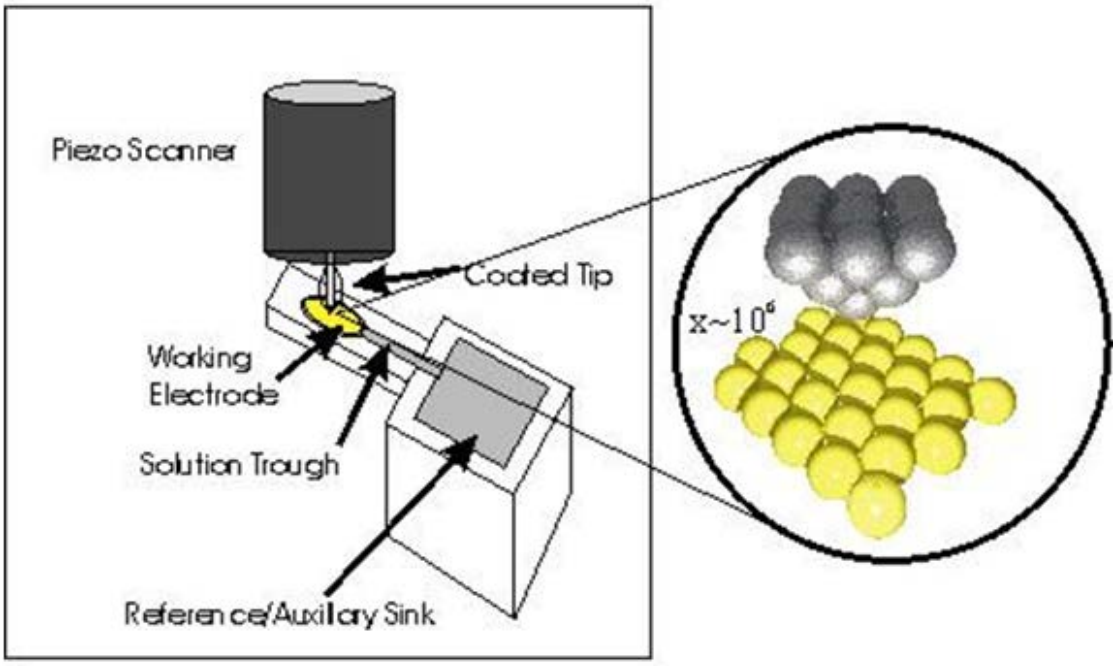

Figure1.1. In situ Scanning Tunneling Microscope schematic

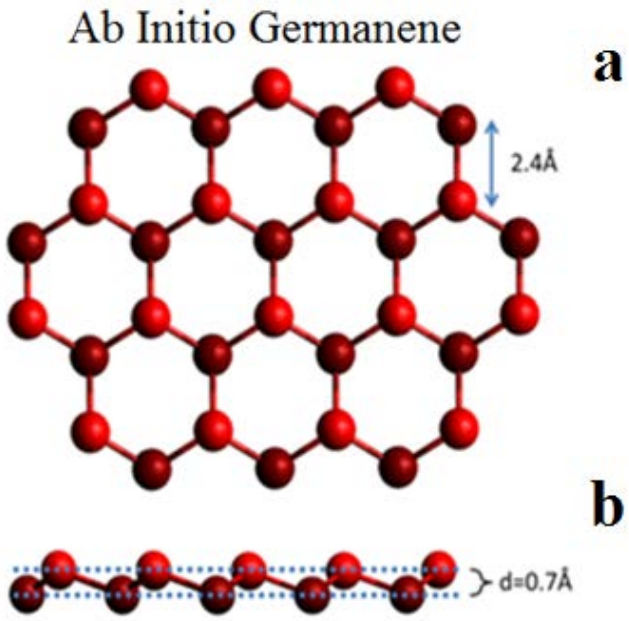

Figure 1.2. A proposed low buckled structure of germanene.

CHAPTER 2

ELECTROCHEMICAL SCANNING TUNNELING MICROSCOPY STUDIES OF THE INITIAL GE DEPOSITION ON AU(111) SURFACES IN AQUEOUS MEDIA[1]

[1] M.A. Ledina, J. Jung, J.L. Stickney, To be submitted to *Journal of the Electrochemical Society*

Abstract

The electrochemical deposition studies of Ge low coverages (less than a monolayer) onto Au(111) were performed in aqueous solution pH 4.5. A monolayer (ML) is defined as one adsorbate per one surface atom. The investigations were conducted by means of cyclic voltammetry, coulometry and electrochemical scanning tunneling microscopy (EC-STM). It was identified that alloy between Au and Ge can be formed as early as -300 mV vs. Ag/AgCl in this pH, if the potential was held. The alloy development was observed as appearance of “lines”-like features, the atomic distances in which were found to correspond to 0.5 nm. The distances between “lines” were around 0.9 nm. These structures tended to form groups of lines positioned parallel to each other. At -700 mV vs. Ag/AgCl, where maximum Ge coverage correspond to ⅓ of a ML, a formation of holes (depletions), due to place exchange, were identified in spots where the double ridges were changing its direction, elbows, or at defects present in the surface. Moreover, an unusual Au(111) herringbone reconstruction was noticed. Instead of normal ridges of $\sqrt{3} \times 22$ structure, the surface demonstrated multiple broken parts of double ridges. Furthermore, some parts of Au(111) herringbone surface were found to have even more unusually modified surface where single soliton walls were forming triangles, the directions of which (walls) were found to be in $[1\bar{1}0]$, rather than in normal $[11\bar{2}]$ direction. An appearance of nanoribbons-like features was also showed at -700 mV vs. Ag/AgCl. The distance between the nanoribbons was found to be about 1.1 nm. Furthermore, nanoribbons did not uplift the Au(111) herringbone reconstruction and were very mobile during imaging process. Such modifications of the Au(111) herringbone reconstruction surface seem to be associated with the Ge species present in form of these

nanoribbons as well as the formation of Ge-Au alloy structure. The atomic distances for an alloy Ge-Au structure that was imaged at -800 mV was measured to be 0.52 nm, corresponding to $\sqrt{3} \times \sqrt{3}$ structure relative to Au(111).

Introduction

Germanium is an important semiconductor in electronics and photonics.[1-4] In fact, the first transistor, a semi-conductor triode, described in the literature was Ge one, reported by Bardeen et al. in 1948. [5] However, even though Ge had higher hole and electron mobilities[6] than Si, an existence of stable native oxide, SiO_2, was one of the reasons for Si to be used over Ge in semiconductor industry. Now the situation is changing in Ge favor, due to potential gate leakage current as thickness of Si gate oxide decrease and due to a possibility of utilization of high-k material as the gate oxide, which will decrease the power consumption in transistor. [6]

Some techniques, that have been used to synthesize Ge, such as chemical vapor deposition[7-8], molecular beam epitaxy[9-10] require high temperature and vacuum conditions, and thus are more expensive. Electrodeposition, on the other hand, can be performed in air at room temperature, and considered to be cost effective. The electrodeposition of Ge has been studied since the middle of the twentieth century. [11] It has been identified, that electrochemical deposition of Ge in aqueous media is limited[12] due to high overpotential for Ge deposition and low hydrogen evolution potential. [13] Thus the electrodeposition of Ge was mostly studied in nonaqueous media. [12, 14-22] Since the potential window in nonaqueous media can be as high as 4 V, micrometer thick Ge films can be deposited.[16] Moreover, single-crystal germanium films on Si substrate can be

fabricated, however, amorphous as synthesized deposits had to be annealed after electrodeposition. [23] Not only Ge films were studied in the literature, but also nanostructures were, due to possible confinement effect. A few groups have reported formation of electrochemical deposition from ionic liquid of Ge nanowires utilizing a template. [21, 24] Furthermore, to fabricate Ge crystalline nanostructures, aqueous solution with dissolved Ge^{+4} species was used, where the electrodeposition of Ge was obtained due to saturation of the mercury electrode with Ge, creating an alloy, and thus promoting a growth of polycrystalline Ge structures. [25] Mahenderkar et al. also reported formation of the Ge nanowires on reduced ITO, where the Ge nanowires were forming on In nanoparticles. [26] Supercritical fluids were also used to electrodeposit Ge films. Best results were obtained from electrochemical deposition using germanium tetrachloride in liquid CH_2F_2 and supercritical CH_2F_2. [27]

Electrochemical deposition of Ge from aqueous solution has been studied in our group several years ago. [28-30] In particular, Liang et al. have studied the initial deposition of Ge, formation of several Ge layers on Au surface, to understand the nature of its deposition. [28] It was demonstrated that Ge electrodeposition is limited, but the coverage will also depend on the pH of the aqueous solution used. The maximum coverage, that can be deposited in pH 9.2 solution containing Ge^{+4} species, corresponds to about 4 ML. [28] Moreover, it was reported the formation of Ge on Au(111) surface starts from ($\sqrt{3} \times \sqrt{3}$)R30˚ or (3 × 3) unit cells with coverages of 1/3 ML or 4/9 ML, respectfully.

Interestingly, a few papers have been published on experimental formation of germanene, a two-dimensional (2D) allotrope of Ge. Germanene has a hexagonal honeycomb structure, similar to graphene, however, half of Ge atoms in germanene will

be lower than the other one by 0.07 nm. [31] It is expected that germanene will have similar properties and applications to those of graphene, however, the integration of Ge into Si industry is expected to be more facile. [32-33] Li et al. have showed a formation of germanene structure, where Ge deposit was annealed after it was sputtered onto Pt(111). [34] According to STM studies the structure was assigned to ($\sqrt{19} \times \sqrt{19}$). Davila et al. have demonstrated a formation of germanene by molecular beam epitaxy on Au(111). [35] The reported structure was ($\sqrt{7} \times \sqrt{7}$)R19.1˚ relative to the Au(111). There was also a report by Derivaz et al. where germanene has been evaporated onto Al(111) and (3×3) structure has been identified. No reports to date are known about formation of germanene structure in aqueous solutions.

Electrochemical studies from our group show indications that germanene has been formed electrochemically, however, as a minority species. Raman signal obtained for one of Ge nanofilms grown on Cu corresponded to the theoretical value in germanene. Moreover, an STM image of honeycomb-like structure has been obtained. [36] It is hypothesized, taking into account Raman and STM data, it is necessary to find conditions which allow obtaining a better structure of germanene to observe Raman shift reproducibly. In the present studies, a continuation of Ge electrodeposition studies discribed by Liang[28] will be reported in order to understand the stages of its initial deposition better.

Experimental

Electrochemical scanning tunneling microscopy studies were performed on Nanoscope III (Digital Instruments, Veeco) which included in-house built STM cell. The

instrumentation and setup were described elsewhere. [37] The electrochemical setup consisted of an STM cell (Kel-F), Au bead, attached by the stem to a gold plate, and Teflon O-ring sandwiched between the cell and the Au plate to create the seal. Au bead and Au plate were 99.999% pure Au. All potentials reported here were versus Ag/AgCl (3M NaCl, Basi) reference electrode. Pt wire was used as an auxiliary electrode. All glassware and other parts used in the assembly were cleaned on daily basis and rinsed carefully with DI water. The Au bead sample was kept in nitric acid when not in use. The imaging was done on Au(111) facet, which was routinely obtained by utilizing one of the variations of Clavier method. [38] In particular, before every experiment the Au bead sample was annealed in hydrogen flame, slowly cooled down in hydrogen atmosphere, and then quenched in hydrogen saturated ultrapure DI water to cool down completely to produce large terraces. After the Au bead sample was completely cooled down, it was taken out of the DI water and quickly assembled together with electrochemical cell to avoid air contaminations. Terraces observed after the Au sample preparation were typically about 300-500 nm. STM tips were 0.25 mm W wires etched in 1 M KOH (15 V ac), rinsed with DI water and covered completely with transparent nail polish, but the apex of the tip, to exclude Faradaic processes. The tip potential E_t was typically around -150 mV vs. Ag/AgCl. The electrochemical cell and scanning head on top of the instrument were also covered with Plexiglas hood and purged constantly with nitrogen, thus creating a positive atmosphere inside the hood to exclude the air. All EC-STM experiments were performed in constant current mode (height mode). STM instrument was calibrated with HOPG sample.

All solutions contained ultrapure DI water (> 18 MΩ) and grade reagent chemicals. Blank and germanium solutions contained 50 mM $NaClO_4$ (Aldrich, 99.99% trace metals basis) and 50 mM $NaClO_4$ and 1 mM GeO_2 (Alfa Aesar, 99.999% trace metals basis), respectively. All solutions were pH 4.5-4.7. The experiments discussed below were all started from assembling the cell with Au sample, filling up with a solution, connecting the leads for all electrodes and defining an open circuit potential (OCP), and then connecting the scanning STM head with W etched tip covered with nail polish.

Electrochemical studies were done on automated flow cell deposition system (Electrochemical ALD L.C., Athens, GA). The E-ALD hardware consisted of valves, electrochemical flow cell, pump, and a potentiostat, all controlled via specialized software. To exclude oxygen, solutions were purged with nitrogen, and valves and tubing were confined in a nitrogen atmosphere. Flow cell also contained a three-electrode configuration. Polycrystalline Au on Ta on glass substrate was used as a working electrode, Ag/AgCl (3M NaCl, Basi) was used as reference electrode and Au wire was used as an auxiliary electrode. Cleaning of Au substrate was usually performed in 0.1 M sulfuric acid before any experiment until a typical reproducible cyclic voltammogram was observed.

Results and discussions

Electrodeposition of Ge is kinetically slow and time is required to complete reduction process. Figure 2.1 demonstrates a series of cyclic voltammograms of polycrystalline Au substrate in Ge solution (pH 4.5). Figure 2.1a shows CVs where potential of a working electrode is scanned from 500 mV to a chosen negative limit and

without holding the potential, scanned back to 500 mV. Figure 2.1b, on the other hand, demonstrates similar series of CVs where the potential ranges are the same, however, when the scanned potential reaches a chosen negative limit, it is held there for 700 sec and only then scanned back to the positive limit. Colors for the same potential ranges are the same on Figure 2.1a and 2.1b. As can be seen on both figures, reduction peaks are the same, however, when the potential is held at negative limits (Figure 2.1b), reductive currents were dropping with time. Moreover, oxidative features were different in CVs after hold from CVs without, as well as self-limited at all studied potential limits. The oxidation charges for green scan on Figure 2.1b are evidently larger than on Figure 2.1a, due to more Ge reduced. It is also revealed that left peak in the green scan on Figure 2.1b has three subpeaks, which might be associated with different facets of Au surface on which Ge is reduced and/or different positions of Ge atoms oxidizing from the surface, such as dislocated spots, edge spots or spots on terraces. It should be noted that the left peak does not correspond to Ge oxidation to soluble species, but rather to intermediate species that still remain present on the surface. That was confirmed by an experiment, where clean Au electrode was scanned from 500 mV to -700 mV and held there for 700 sec to reach its maximum coverage. The potential then was scanned through the left peak while the electrode was still in the Ge solution, then the solution was exchanged, without losing potential control, with a blank one. After making sure no Ge species were present in the solution, the potential was scanned negative. A reductive peak was observed to appear which suggests that Ge species present on the surface were reduced again. The potential then was switched to a positive direction and scanned to 500 mV. The left peak was observed again, implying that the oxidation process that takes place did not produce

Ge soluble species. Moreover, the peaks were observed before and were deducted to be Ge hydride/hydroxide couple. [28]

Red CVs on both Figure 2.1a and Figure 2.1b demonstrate larger differences for no hold vs. 700 sec hold. In addition to a larger left and right oxidation peaks, middle peak shows up after the potential is held at -900 mV. The right peaks are probably associated with oxidation of Ge directly bonded with Au. The middle peak seemed to appear after coverage of more than half of a ML is deposited. In particular, the coverage for oxidation peaks in red CV (Figure 2.1b) corresponds to about 0.78 ML, taking into account 4 e^- process. Ge species produced during oxidation process in the middle peak scan are soluble. Figure 2.1a reveals that only after the potential is scanned to -1000 mV, the left peak, similar to the left peak in green CV in Figure 2.1b, shows up. However, still no middle peak is yet observed. The blue scans show even more drastic differences between no holding and holding the potential. The Figure 2.1b shows that after hold of the potential at -1000 mV the middle peak charge increases dramatically compared to the red scan. Moreover, it is observed that the left peak is decreasing in size, and both left and right peak are riding on the middle peak sides. It is hypothesized, that as more Ge was deposited the more stable deposit is formed on the Au surface since it is harder to oxidize, as the oxidation potential shifts more positive.

Ge reduction can be identified even at much earlier potentials where first reduction peak is not even observed. Figure 2.2 demonstrates the CV of polycrystalline Au in Ge solution where the potential was scanned to -400 mV and then held there for 30 min and scanned back to the original positive limit. The coverage that is obtained after holding corresponds to 0.08 ML (for 4 e^- process). EC-STM studies were done at or

around this potential. Figure 2.3 shows usual Au herringbone reconstruction of Au before any Ge reduction is taken place. Figure 2.4 demonstrates STM images of Au(111) reconstructed surface after the potential was held at -300 mV in Ge solution for about an hour. The observed Au terraces are about 50 nm wide. Au herringbone reconstruction is still present on the surface. “Lines”-like features are found on the edges of the Au steps as well as on some areas close to other Au steps. The “lines” look ordered and packed in parallel stacks. From the images observed the average width of the “lines” was found to be around 6 nm. The height was measured to be between 0.06 and 0.08 nm. However, angles, measured between the “lines” and the Au herringbone ridges, did not have a particular direction relative to the Au. If these “lines” appeared due to an alloy formation between the Au and Ge atoms, the fact the “lines” are observed might mean that the alloy is ordered, but then the angles should give information about its orientation. It is possible that due to the drift present during the scanning process does not allow to define the direction. Another reason might be the instability of the lines as the scanning is taking place. Although, the “lines” seem to stay in place throughout the particular experiment, some of them look distorted. It appears that the formation of the “lines” happens near the edges where it is probably easier for Ge atoms to enter the surface. Next, after the observed scanned area was zoomed out, a larger terrace was found and zoomed into (Figure 2.5a). By that time the potential was held at -300 mV for about 1 hour. No “lines” lines were present. Then the potential was stepped to -400 mV. On the next image, taken only 30 sec later (Figure 2.5b), it can already be observed that a higher (0.08 nm) layer was appearing on the edges of the Au terrace. And in the next minute (Figure 2.5c and 2.5d), the spots where the formation of the layer is taking place were where the

herringbone reconstruction changes its directions, right at the elbows. According to the[39] these are preferable spots for deposited atoms to go in due to higher surface energy and since there are no visible defects present on the surface. As the potential was held further, images on Figure 2.6 were observed. At the time Figure 2.6b was obtained, the potential was stepped to -500 mV. No rapid changes were observed. The layer was continuing to grow from the spots where originally they were noticed and around them. As the layer was growing, formation of islands was also noticed, the height of which was about 0.22 nm, close to the height of the Au or Ge islands. The observed islands might be Au that started to appear due to uplifting of the Au reconstruction and due to Ge intercalation. Since the height of the islands on Figure 2.6c were measured between the island and the growing layer, same layer was also formed on top of the island. 0.22 nm islands were only appearing outside of the growing layer, on Au surface. Figure 2.6d demonstrates the increased amount of 0.22 nm islands throughout the image, as well as almost completely covered with layer terrace. It is assumed that the growing 0.08 nm layer also contains "lines"-like feature, however, due to probably lower resolution or a large area scanned were not clearly visible.

Another experiment demonstrates that the presence of the defects on the substrate increases the kinetics of layer with "lines" features growth. Figure 2.7a was obtained after potential sweeping has been performed of the electrode in Ge solution. The potential was scanned from 500 mV to -1.2 V, coverage corresponds to 1.4 ML (for 4 e- process), and then back to 500 mV. The image was taken at the 220 mV (Figure 2.7a). The surface was found completely pitted with lots of small Au islands which were also pitted. The observations on image suggest that an alloy has been formed between Ge and Au. The

potential has been changed to -400 mV (Figure 2.7b), “lines” were observed formed on the pitted surface as well on the islands only after about 6 min after the potential was stepped to -400 mV. It is evident the more substrate contains defects the easier it is for Ge atoms to enter the surface, to create an intermixed layer, or an alloy, on a faster time scale.

The maximum coverage that can be reached after holding the potential at -500 mV was found to be 0.11 ML (Figure 2.8), where only one peak (right peak) observed for Ge oxidation. Figure 2.9 shows images after the Au bead electrode was in Ge solution at -400 mV and -500 mV. “Lines” features were again found on one of the imaged areas. Additionally, it can be observed that some parts of the intermixed layer do not contain “lines”. The height of the layer with “lines” present was found to be about 1 nm and without about 0.07 nm. As the potential was stepped to -500 mV, a third of an atom high layer continued to grow. The 0.22 nm islands were also observed to appear. These islands are probably Au islands that started to form due to uplifting of Au reconstruction as well as due to intercalation of Ge atoms into the surface, thus causing ejection of Au atoms, similar to what was observed at -400 mV. Figures 2.9c and 2.9d show a closer look at “lines”. The atomic distances were measured to be around 0.52 nm. Distances between lines were close to 0.9 nm. Directions though were still hard to identify due to possible drift during imaging. After about 30 min of potential holding the imaged surface was completely covered. The height difference between the islands and the newly formed layer was found to be about 0.22 nm, which means that the islands were also covered with the third of an atom high layer. Figure 2.9f demonstrates the surface imaged in the “Up” direction after the potential was stepped to 200 mV (bottom part of the image), at

which no Ge should be left on the surface. Even though the resolution of the image was lost to some degree, it can be clearly observed that after the potential stepping the surface was left pitted as well as the islands. Since the large islands were still found to be present after the oxidative step confirms that these were Au islands. It also implies that the "lines" are most likely to consist of Au atoms. The presence of the holes confirms that the observed layer was an alloy between the Ge and Au atoms. The fact that the layer with "lines" features are present suggest that the alloy might be ordered.

When the potential was not held at initial values (from -300 mV to -500 mV), but was stepped rather quickly through them, the surface was found to have usual herringbone reconstruction (Figure 2.10a). At -600 mV, an area with unusually modified Au(111) reconstruction was observed (Figure 2.10b). Germanium maximum coverage on Au substrate after potential is held at -600 mV corresponds to 0.24 ML (Figure 2.11). The cyclic voltammogram demonstrates peak at -50 mV, which was observed after Ge deposition at more positive potentials, and also an appearance of left oxidative peak, at -500 mV, which corresponds to oxidation of Ge species on the surface, however not to soluble species. As can be seen in Figure 2.12a soliton walls of the Au herringbone reconstruction, highlighted in the yellow circle, do not correspond to [11^{-}2] or √3 direction. In fact, it is evident that some of the soliton walls are parallel to the [1^{-}10] or n-by direction (notice two arrows with assigned directions taken from a spot with an unmodified Au herringbone reconstruction) and have formed triangular-like network. Figure 2.12a demonstrates an example of modifications to double ridges, and which still correspond to the √3 direction highlighted in red circle. After 6 min the image (Figure 2.12b) shows the double ridges came apart forming a triangular-like shape. According to

the studies by Sun and coworkers[40], similar triangles were observed on Au reconstructed surface after molecular adsorption of perylene and iron phthalocyanine (FePc). It was concluded in the report that the Au surface electronic state was different due to adsorption of the molecules which was affecting the surface stress and thus producing a different reconstructed pattern. It is hypothesized that in the present report similar effects are observed (Figure 2.12), however, the question is what could be absorbed onto the surface that could have caused the surface to change from the pristine reconstruction. Another similar modification of Au herringbone reconstruction was reported by Wu et al. which was induced by metal adlayer. [41] Irreversible adsorption and underpotential deposition of Sb was demonstrated to affect Au(111) reconstructed surface, where double ridges which should correspond to √3 direction, were relaxed and found to be in n-by direction, in the form of triangles. The observed phenomenon was justified as a result of different surface charge due to compromise between formation of bonding and dislocation-mediated alloying process. Moreover, Wu et al. showed that after introduction of less than 0.05 ML, after the studied potential was held for some time, the observed modified Au herringbone reconstruction was very similar to the one imaged in the present studies showed in Figure 2.13. The last figure was imaged after the working potential was held for about an hour at -500 mV. The Au reconstruction looked different from the normal one and demonstrated a multiple rotated ridges, multiple elbows, looking like multiple “checks”. Taking into account both papers,[40-41] it is clear that in our studies the observed modifications of Au reconstructed surface are due to a different surface stress caused either by adsorption of Ge species onto the surface or intercalation. An appearance of holes-like features at the elbows and spots where ridges were changing its

directions was also noticed. With time the size of the holes was increasing (Figures 2.12a and 2.12c). The depth of the holes was found to be around 0.04-0.05 nm. These dips are probably due to place exchange, where Ge atoms are intercalating into the Au surface. Similar features were also observed in the literature before.[42-43] The dips were also observed in FCC areas (outside of the triangles), where with time protrusion will appear (black circles in Figure 2.12a).

Figure 2.14a demonstrates a continuation of an experiment discussed earlier from Figure 2.12. A new feature appeared (Figure 2.14a), consisted from a flat pack of parallel to each other rows of nanoribbons. The last, in turn, seem to be composed from a row of molecule-like components, which should be Ge related. The distance between the molecules as well as the distance between the rows of nanoribbons were measured to be around 0.9 – 1 nm. The measured distances in the nanoribbon and between nanoribbons are too large to be between atoms, especially which are not in contact with Au surface. The height of the rows of nanoribbons was found to be 0.05-0.08 nm. However, it should be kept in mind that a height measured in STM is a reflection of conductivity of an imaged material, which means in the present case if the conductivity of the feature is less than that of Au, the height of the pack will seem lower than it actually is. The herringbone reconstruction, even though was observed to be modified, was not lifted. Figure 2.14b was imaged only after 30 sec later, no flat pack feature observed on Figure 2.14a was found and herringbone reconstruction seemed intact. That would mean that the rows of the nanoribbons are probably adsorbed onto the Au surface and not covalently bonded, and can easily be moved (possibly due to tunneling conditions).

Figure 2.15 shows images after rows of nanoribbons appeared again a couple of minutes later after the nanoribbons were observed in Figure 2.14a. In Figure 2.15 the rows of nanoribbons were found to be in a different direction and seemed to be building up as the imaging was taken place (black circles). As the scan was taken in the "Up" direction (Figure 2.15a), some curved-end rows were visible. The next image (Figure 2.15b), taken a half of minute later in the opposite direction, demonstrates already formed continuation to the rows. It might be as the scanning was taken place, before those molecules were forming rows, they were less stable than those that were already in a bundle, so they were more mobile. Five longer rows, as they were imaged in the middle of the Figure 2.15b (red circle), seemed to break off from the main structure and imaged at the bottom, moreover with one more row in the structure. It is interesting to note that the rows were imaged with dips in the structure, which corresponded to the dips in Au reconstructed surface. This phenomenon might be associated with lower conductivity of the nanoribbons. Additionally, some protrusions appeared in between corrugation lines and seemed to be forming in the FCC areas due to probably a formation of the alloy between the Au and Ge atoms.

The maximum coverage of Ge on Au surface at -700 mV should correspond to 0.24 ML (taking into account 4 e^- process). Figure 2.16 demonstrates CV after the potential was scanned to -700 mV and held there for 700 sec, time after which no more Ge can be deposited into the Au. The oxidative scan shows two peaks which are related to the same Ge species after oxidizing to some intermediate during the left peak, which ends at around -350 mV and peak from -350 mV to around 200 mV where soluble Ge^{+4} are produced. Even though a coverage of Ge should be a forth of a ML at this potential,

an area was found where neither changes to Au herringbone reconstruction nor a visible alloy layer were observed. As the potential was held at -700 mV, the Au reconstruction was not observed to change with time, however, dips were observed to appear and increase at the elbows and where the reconstruction double ridges were changing its direction (Figure 2.17). A formation of the 0.2 - 0.22 nm islands was also identified. Figures 2.17a-c demonstrate the progress of the nucleation and growth of these islands. On Figure 2.17a, three areas were highlighted with colored circles, where some depletion spots were identified. These, as was discussed earlier, are due to place exchange where Ge atoms are intercalating into the Au surface. As the potential was held, islands were appearing in the highlighted areas where the depletion spots were observed and growing with time (Figures 2.17b and 2.17c). The observed islands are probably Au islands formed due to ejection of Au atoms after Ge intercalation.

At -800 mV (Figure 2.18), Ge coverage on Au without holding the potential corresponds to 0.16 ML and the maximum coverage that can be reached at that potential to 0.45 ML (4 e^- process). Both CVs have two peaks, denoted in the present report as the left and the right. As can be seen in the CVs, the maximum amount for the right and left peaks can only be reached after the potential is held, and is more than twice as much as compared to charges without holding. The larger amount of the charge implies to slow kinetics for Ge deposition, as was discussed earlier. Moreover, the left peak after holding the potential has a different shape from the one without. That means as more Ge was deposited, some reduced Ge species were easier to oxidize since its oxidation charge starts earlier and some were harder to oxidize, since its potential shifted to more positive potential.

EC-STM images obtained at -800 mV are presented in Figure 2.19. Formation of a layer was observed, starting from -500 mV, the height of which was measured to be about 0.1 nm (Figure 2.19a). The potential was then shifted to more negative values stepwise reaching eventually -800 mV over 10 min and then kept there. As the potential was held, the layer was covering the imaged area. The shape of the layer was uneven on the edges and moreover, the layer was not whole but rather had holes and worm-like features in it. Moreover, as the potential was held, holes (due to place exchanges) were appearing where the Au reconstructed surface was still present, at dislocations and where the double ridges were changing its directions (Figure 2.19b). Small islands (0.22 nm) were observed to form where the holes were appearing. The 0.1 nm layer was zoomed in to obtain an atomic structure (Figure 2.19c). Figure 2.19d demonstrates atomically resolved image is the alloy layer between Ge and Au atoms. As can be observed the layer was not continuous and contained a lot of holes in it, however, it might be that some spots in the imaged area are not as conductive as the others. The atomic distances were measured to be about 0.52 nm in all directions, which is close to $\sqrt{3} \times \sqrt{3}$ structure relative to the Au(111).

Conclusion

The present report describes the studies of initial deposition of Ge onto Au(111) surface from -300 mV to -800 mV from pH 4.7 Ge solution. It was observed that Ge is forming an alloy with Au surface starting from as early as -300 mV. At potentials from -300 mV till -500 mV “lines”-like feature were observed. How fast the “lines”-like feature were forming was found to depend on the quality of the surface - the more defects were

present the easier it was probably for Ge atoms to enter the surface, creating “lines” with atomic distances between atoms in the “line” about 0.52 nm. At – 600 mV and -700 mV, areas with unusually modified herringbone reconstruction were observed. Some corrugation lines of the herringbone reconstruction were found to be in [11^{-}2] direction instead of [1^{-}10]. Some areas demonstrated Au(111) broke herringbone reconstruction. Taking into account the observed images and literature, the Au(111) reconstruction seem to be effected by presence of the Ge species either as a result of the Ge species in the Au surface, due to a formed alloy layer, or in the form of some adsorbed Ge molecules in shape of nanoribbons, which were observed at -700 mV. The distances between the molecules in the nanoribbons were found to be about 0.9 nm, and the distance between the ribbons was around 1 nm. Dips due to place exchange were observed as well throughout of the studies at -600 mV to -800 mV present at defects and dislocations, where Ge atoms are probably were entering the surface. An alloy observed throughout the studies had height of about 0.1 nm. The atomic distances in alloy structure were found to be around 0.52 nm, which corresponds to $\sqrt{3} \times \sqrt{3}$ relative to the Au(111) surface.

Acknowledgements

Support from the National Science Foundation, DMR #1410109, is gratefully acknowledged.

References

1. Soref, R., Mid-infrared photonics in silicon and germanium. *Nature photonics* **2010,** *4* (8), 495-497.

2. Chroneos, A., Defect engineering strategies for germanium. *J. Mater. Sci.: Mater. Electron.* **2013,** *24* (6), 1741-1747.

3. Chen, L., Ultra-low capacitance and high speed germanium photodetectors on silicon. *Optics express* **2009,** *17* (10), 7901-7906.

4. Liow, T.-Y.; Tan, K.-M.; Lee, R. T. P.; Zhu, M.; Tan, B. L. H.; Balasubramanian, N.; Yeo, Y.-C., Germanium source and drain stressors for ultrathin-body and nanowire field-effect transistors. *IEEE Electron Device Lett.* **2008,** *29* (7), 808-810.

5. Bardeen, J.; Brattain, W. H., THE TRANSISTOR, A SEMI-CONDUCTOR TRIODE. *Physical review* **1948,** *74* (2), 230-231.

6. Kamata, Y., High-k/Ge MOSFETs for future nanoelectronics. *Mater. Today (Oxford, U. K.)* **2008,** *11* (1-2), 29-38.

7. Hartmann, J. M.; Papon, A. M.; Destefanis, V.; Billon, T., Reduced pressure chemical vapor deposition of Ge thick layers on Si(001), Si(011) and Si(111). *J. Cryst. Growth* **2008,** *310* (24), 5287-5296.

8. Wintterlin, J.; Avouris, P., Scanning tunneling microscopy (STM) studies of the chemical vapor deposition of Ge on Si(111) from Ge hydrides and a comparison with molecular beam epitaxy. *J. Chem. Phys.* **1994,** *100* (1), 687-704.

9. Persans, P. D.; Deelman, P. W.; Stokes, K. L.; Schowalter, L. J.; Byrne, A., Optical studies of Ge islanding on Si(111). *Appl. Phys. Lett.* **1997,** *70* (4), 472-474.

10. Smith, D. J.; Chandrasekhar, D.; Chaparro, S. A.; Crozier, P. A.; Drucker, J.; Floyd, M.; McCartney, M. R.; Zhang, Y., Microstructural evolution of Ge/Si(100) nanoscale islands. *J. Cryst. Growth* **2003,** *259* (3), 232-244.

11. Szekely, G., Electrodeposition of germanium. *J. Electrochem. Soc.* **1951,** *98*, 318-24.

12. Jayakrishnan, S.; Pushpavanam, M.; Shenoi, B. A., Electrodeposition from organic solutions of metals that are difficult to deposit from aqueous solutions. *Surf. Technol.* **1981,** *13* (3), 225-40.

13. Pourbaix, M., *Atlas of Electrochemical Equilibria in Aqueous Solutions*. Pergamon Press: 1966.

14. Endres, F.; Schrodt, C., In situ STM studies on germanium tetraiodide electroreduction on Au(111) in the room temperature molten salt 1-butyl-3-methylimidazolium hexafluorophosphate. *Phys. Chem. Chem. Phys.* **2000,** *2* (24), 5517-5520.

15. Endres, F., Electrodeposition of a thin germanium film on gold from a room temperature ionic liquid. *Phys. Chem. Chem. Phys.* **2001,** *3* (15), 3165-3174.

16. Endres, F.; Zein El Abedin, S., Nanoscale electrodeposition of germanium on Au(111) from an ionic liquid: an in situ STM study of phase formation. Part I. Ge from GeBr4. *Phys. Chem. Chem. Phys.* **2002,** *4* (9), 1640-1648.

17. Endres, F.; Zein El Abedin, S., Nanoscale electrodeposition of germanium on Au(111) from an ionic liquid: an in situ STM study of phase formation. Part II. Ge from GeCl4. *Phys. Chem. Chem. Phys.* **2002,** *4* (9), 1649-1657.

18. Endres, F.; Zein El Abedin, S., Electrodeposition of stable and narrowly dispersed germanium nanoclusters from an ionic liquid. *Chem. Commun. (Cambridge, U. K.)* **2002,** (8), 892-893.

19. Freyland, W.; Zell, C. A.; Zein El-Abedin, S.; Endres, F., Nanoscale electrodeposition of metals and semiconductors from ionic liquids. *Electrochim. Acta* **2003,** *48* (20-22), 3053-3061.

20. Mukhopadhyay, I.; Freyland, W., Thickness induced metal-nonmetal transition in ultrathin electrodeposited Ge films. *Chem. Phys. Lett.* **2003,** *377* (1,2), 223-228.

21. Al-Salman, R.; Mallet, J.; Molinari, M.; Fricoteaux, P.; Martineau, F.; Troyon, M.; El Abedin, S. Z.; Endres, F., Template assisted electrodeposition of germanium and silicon nanowires in an ionic liquid. *Phys. Chem. Chem. Phys.* **2008,** *10* (41), 6233-6237.

22. Chandrasekharan, N.; Sevov, S. C., Anodic Electrodeposition of Germanium Films from Ethylenediamine Solutions of Deltahedral Ge94- Zintl Ions. *J. Electrochem. Soc.* **2010,** *157* (4), C140-C145.

23. Huang, Q.; Bedell, S. W.; Saenger, K. L.; Copel, M.; Deligianni, H.; Romankiw, L. T., Single-crystalline germanium thin films by electrodeposition and solid-phase epitaxy. *Electrochem Solid St* **2007,** *10* (11), D124-D126.

24. Martineau, F.; Namur, K.; Mallet, J.; Delavoie, F.; Endres, F.; Troyon, M.; Molinari, M., Electrodeposition at room temperature of amorphous silicon and germanium nanowires in ionic liquid. *IOP Conf. Ser.: Mater. Sci. Eng.* **2009,** *6*, 012012/1-012012/4.

25. Carim, A. I.; Collins, S. M.; Foley, J. M.; Maldonado, S., Benchtop Electrochemical Liquid-Liquid-Solid Growth of Nanostructured Crystalline Germanium. *J. Am. Chem. Soc.* **2011,** *133* (34), 13292-13295.

26. Mahenderkar, N. K.; Liu, Y.-C.; Koza, J. A.; Switzer, J. A., Electrodeposited germanium nanowires. *ACS Nano* **2014,** *8* (9), 9524-9530.

27. Ke, J.; Bartlett, P. N.; Cook, D.; Easun, T. L.; George, M. W.; Levason, W.; Reid, G.; Smith, D.; Su, W. T.; Zhang, W. J., Electrodeposition of germanium from supercritical fluids. *Physical Chemistry Chemical Physics* **2012,** *14* (4), 1517-1528.

28. Liang, X.; Kim, Y.-G.; Gebergziabiher, D. K.; Stickney, J. L., Aqueous electrodeposition of Ge monolayers. *Langmuir* **2010,** *26* (4), 2877-84.

29. Liang, X.; Zhang, Q.; Lay, M. D.; Stickney, J. L., Growth of Ge Nanofilms Using Electrochemical Atomic Layer Deposition, with a "Bait and Switch" Surface-Limited Reaction. *J. Am. Chem. Soc.* **2011,** *133* (21), 8199-8204.

30. Liang, X.; Jayaraju, N.; Thambidurai, C.; Zhang, Q.; Stickney, J. L., Controlled Electrochemical Formation of GexSbyTez using Atomic Layer Deposition (ALD). *Chem. Mater.* **2011,** *23* (7), 1742-1752.

31. Bechstedt, F.; Matthes, L.; Gori, P.; Pulci, O., Infrared absorbance of silicene and germanene. *Applied Physics Letters* **2012,** *100* (26).

32. Avouris, P.; Dimitrakopoulos, C., Graphene: synthesis and applications. *Mater. Today (Oxford, U. K.)* **2012,** *15* (3), 86-97.

33. Houssa, M.; Pourtois, G.; Afanas'ev, V. V.; Stesmans, A., Electronic properties of two-dimensional hexagonal germanium. *Applied Physics Letters* **2010,** *96* (8).

34. Li, L.; Lu, S.-z.; Pan, J.; Qin, Z.; Wang, Y.-q.; Wang, Y.; Cao, G.-y.; Du, S.; Gao, H.-J., Buckled Germanene Formation on Pt(111). *Advanced Materials* **2014,** *26* (28), 4820-+.

35. Davila, M. E.; Xian, L.; Cahangirov, S.; Rubio, A.; Le Lay, G., Germanene: a novel two-dimensional germanium allotrope akin to graphene and silicene. *New J. Phys.* **2014,** *16* (Sept.), 095002/1-095002/10, 10 pp.

36. Ledina, M.; Liang, X.; Kim, Y.-G.; Jung, J.; Perdue, B.; Tsang, C.; Soriaga, M. P.; Stickney, J. L., (Invited) Investigations into the Formation of Germanene Using Electrochemical Atomic Layer Deposition (E-ALD). *Ecs Transactions* **2015,** *66* (6), 129-140.

37. Suggs, D. W.; Bard, A. J., Scanning Tunneling Microscopic Study with Atomic Resolution of the Dissolution of Cu(111) in Aqueous Chloride Solutions. *J. Am. Chem. Soc.* **1994,** *116* (23), 10725-33.

38. Clavilier, J.; Faure, R.; Guinet, G.; Durand, R., Preparation of monocrystalline platinum microelectrodes and electrochemical study of the plane surfaces cut in the direction of the {111} and {110} planes. *J. Electroanal. Chem. Interfacial Electrochem.* **1980,** *107* (1), 205-9.

39. Baber, A. E.; Tierney, H. L.; Sykes, E. C. H., Atomic-Scale Geometry and Electronic Structure of Catalytically Important Pd/Au Alloys. *ACS Nano* **2010,** *4* (3), 1637-1645.

40. Sun, J. T.; Gao, L.; He, X. B.; Cheng, Z. H.; Deng, Z. T.; Lin, X.; Hu, H.; Du, S. X.; Liu, F.; Gao, H. J., Surface reconstruction transition of metals induced by molecular

adsorption. *Phys. Rev. B: Condens. Matter Mater. Phys.* **2011,** *83* (11), 115419/1-115419/4.

41. Wu, Q.; Shang, W. H.; Yan, J. W.; Xie, Z. X.; Mao, B. W., Metal Adlayer-Induced Relaxation of Au(111) Reconstruction under Electrochemical Control. *J. Phys. Chem. B* **2003,** *107* (17), 4065-4069.

42. Nahas, Y.; Repain, V.; Chacon, C.; Girard, Y.; Rousset, S., Interplay between ordered growth and intermixing of Pt on patterned Au surfaces. *Surf. Sci.* **2010,** *604* (9-10), 829-833.

43. Moller, F. A.; Magnussen, O. M.; Behm, R. J., Two-dimensional needle growth of electrodeposited Ni on reconstructed Au(111). *Phys Rev Lett* **1996,** *77* (15), 3165-3168.

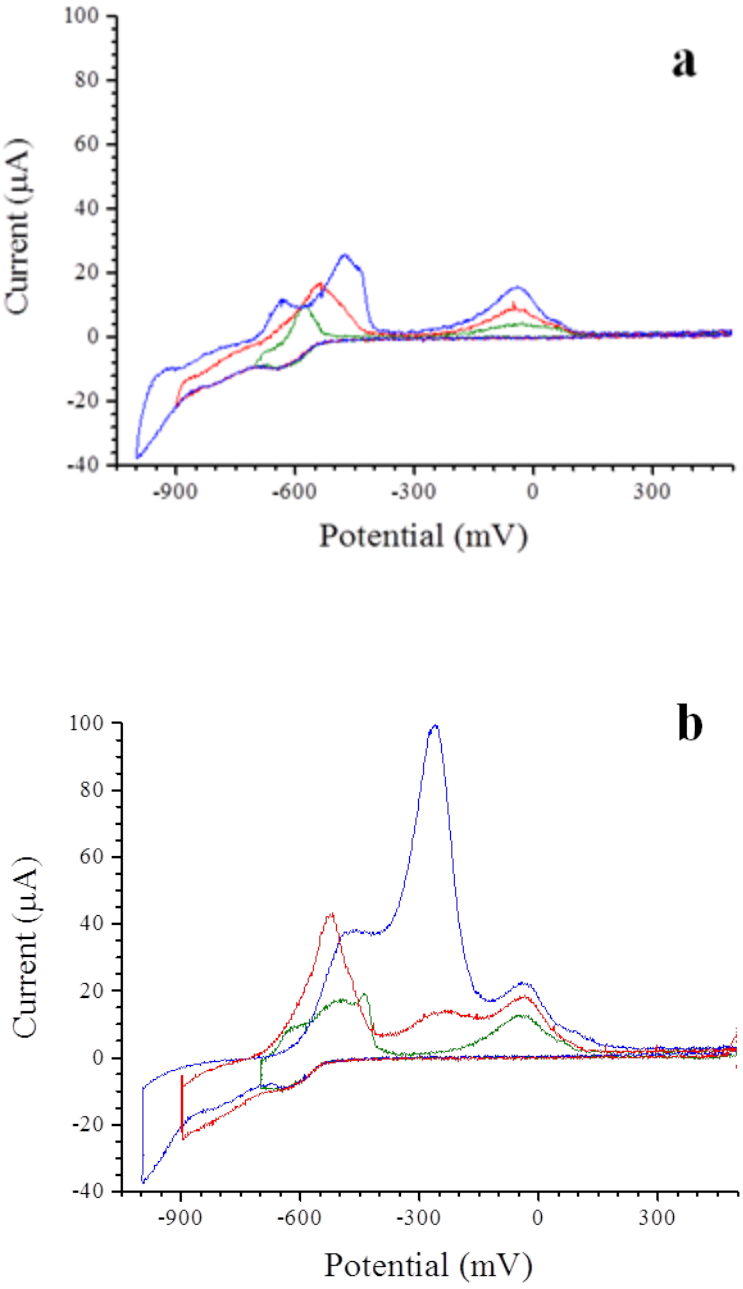

Figure 2.1. Cyclic voltammograms of polycrystalline Au in 0.5 mM GeO_2 (0.1 M $NaClO_4$, pH 4.5) solution, scan rate 10 mV/sec. a). No hold at negative values; b). Hold for 700 sec at negative values.

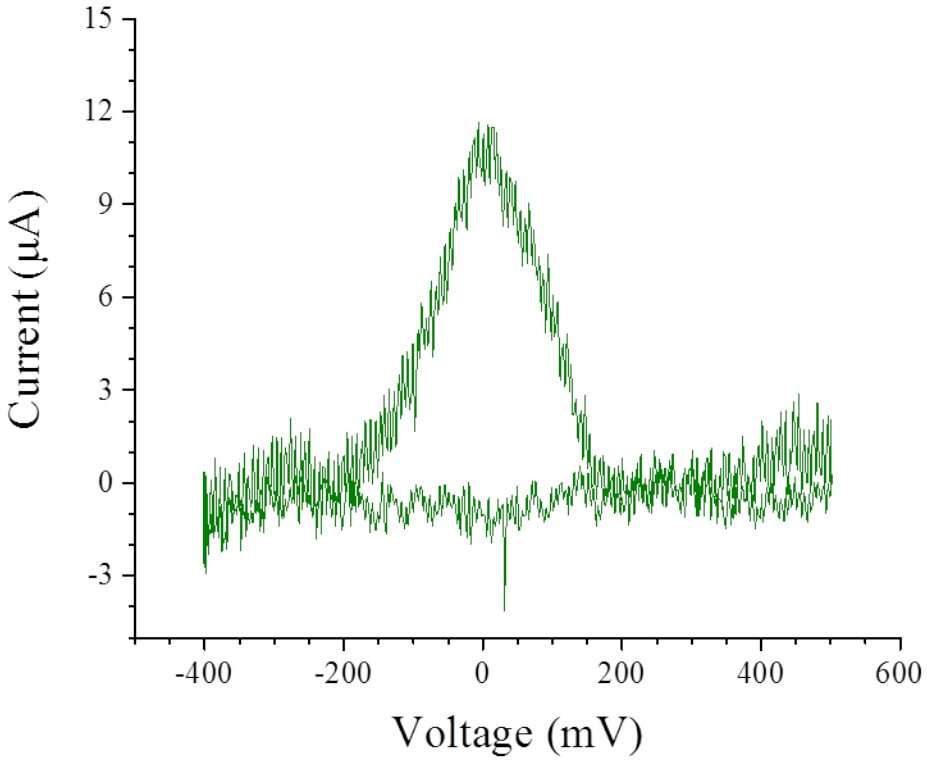

Figure 2.2. Cyclic voltammogram of polycrystalline Au in 0.5 mM GeO_2 (0.1 M $NaClO_4$, pH 4.5) solution after the potential was held at -400 mV (vs. Ag/AgCl) for 30 min, scan rate 10 mV/sec. Ge coverage corresponds to 0.08 ML relative to Au.

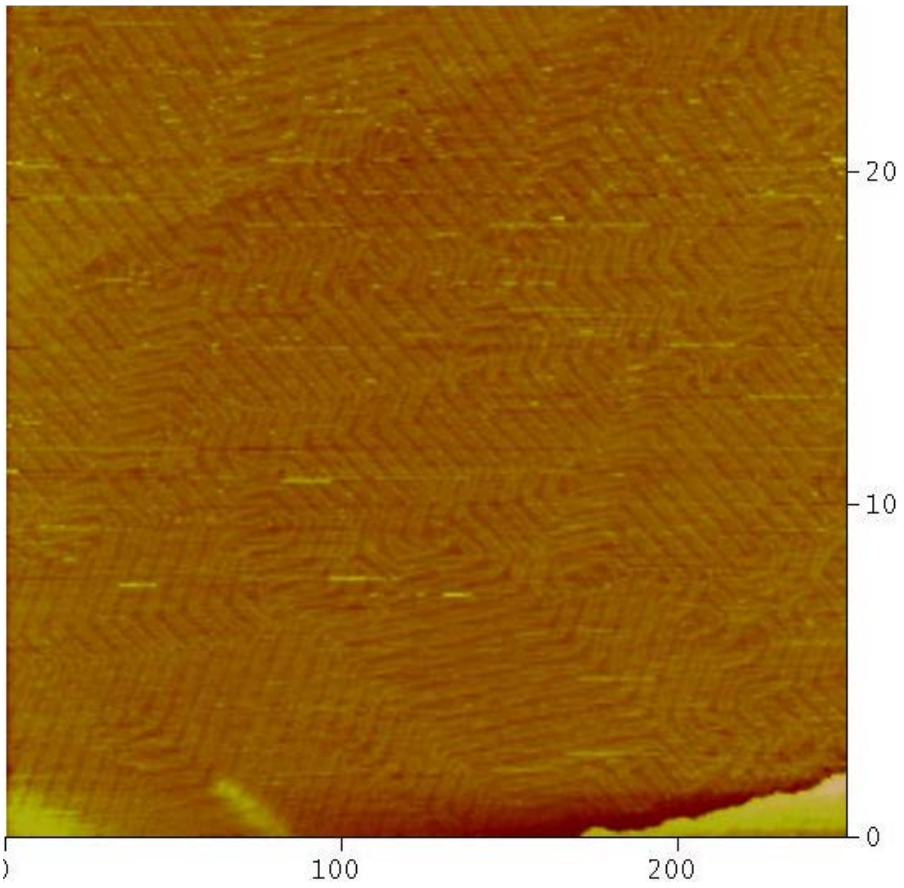

Figure 2.3. EC-STM image of Au(111) √3 × 22 herringbone reconstruction at -500 mV before any Ge deposition took place.

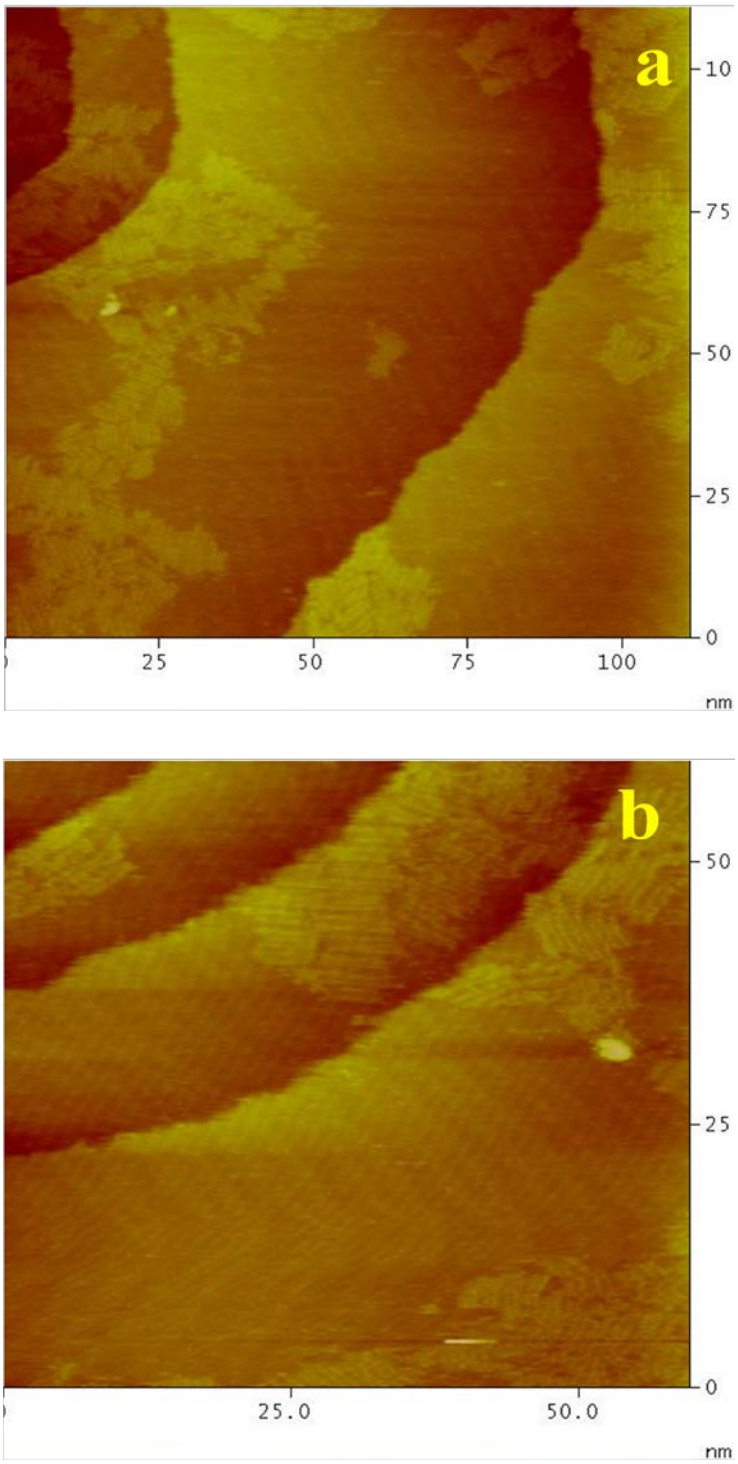

Figure 2.4. EC-STM image of Au(111) surface at -300 mV vs. Ag/AgCl after holding the potential for an hour in 1 mM GeO_2 (0.05 M $KClO_4$, pH 4.5) solution.

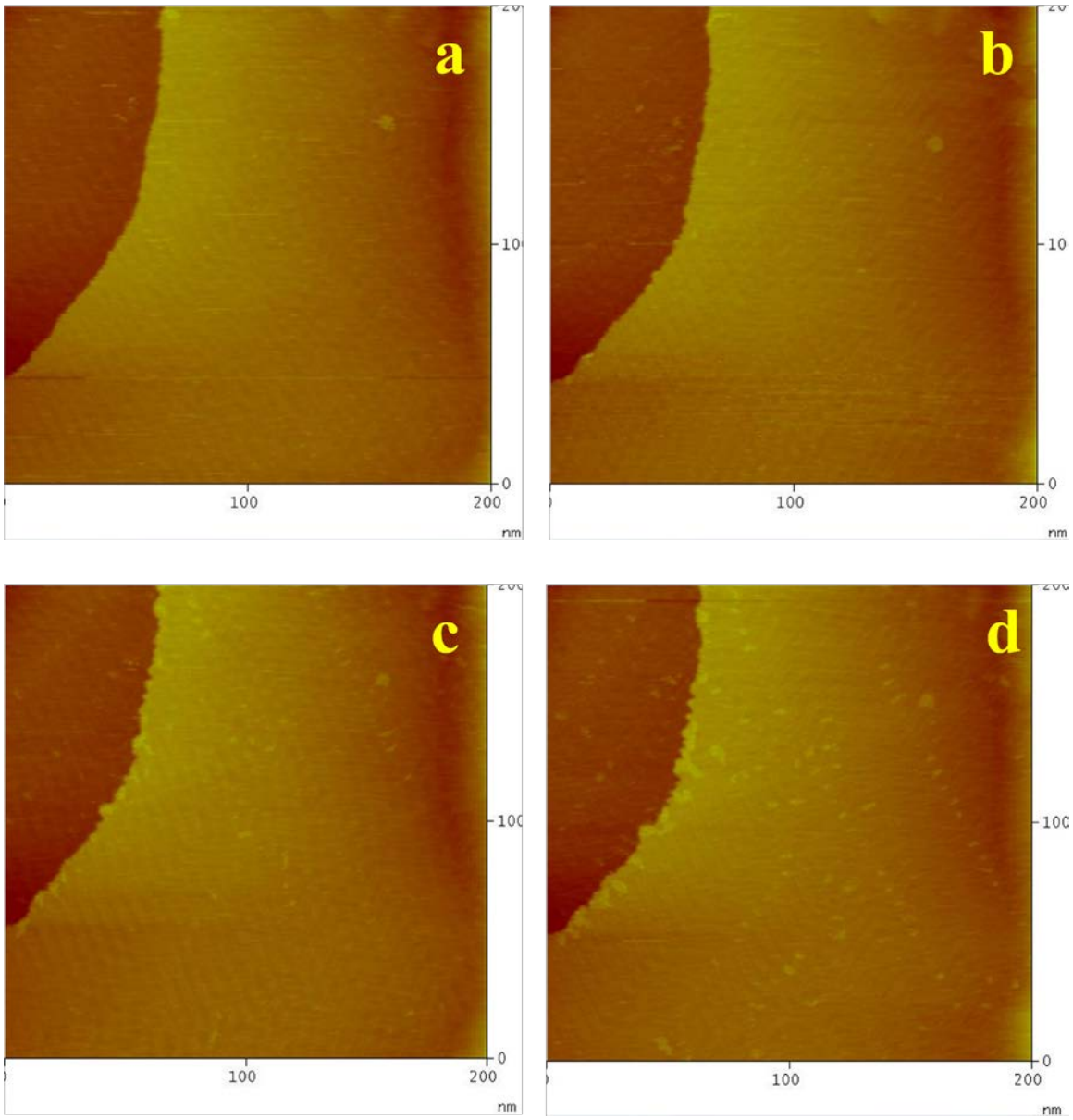

Figure 2.5. EC-STM image of Au(111) surface a). at -300 mV vs. Ag/AgCl; b), c), d) at -400 mV vs. Ag/AgCl in 1 mM GeO_2 (0.05 M $KClO_4$, pH 4.5) solution.

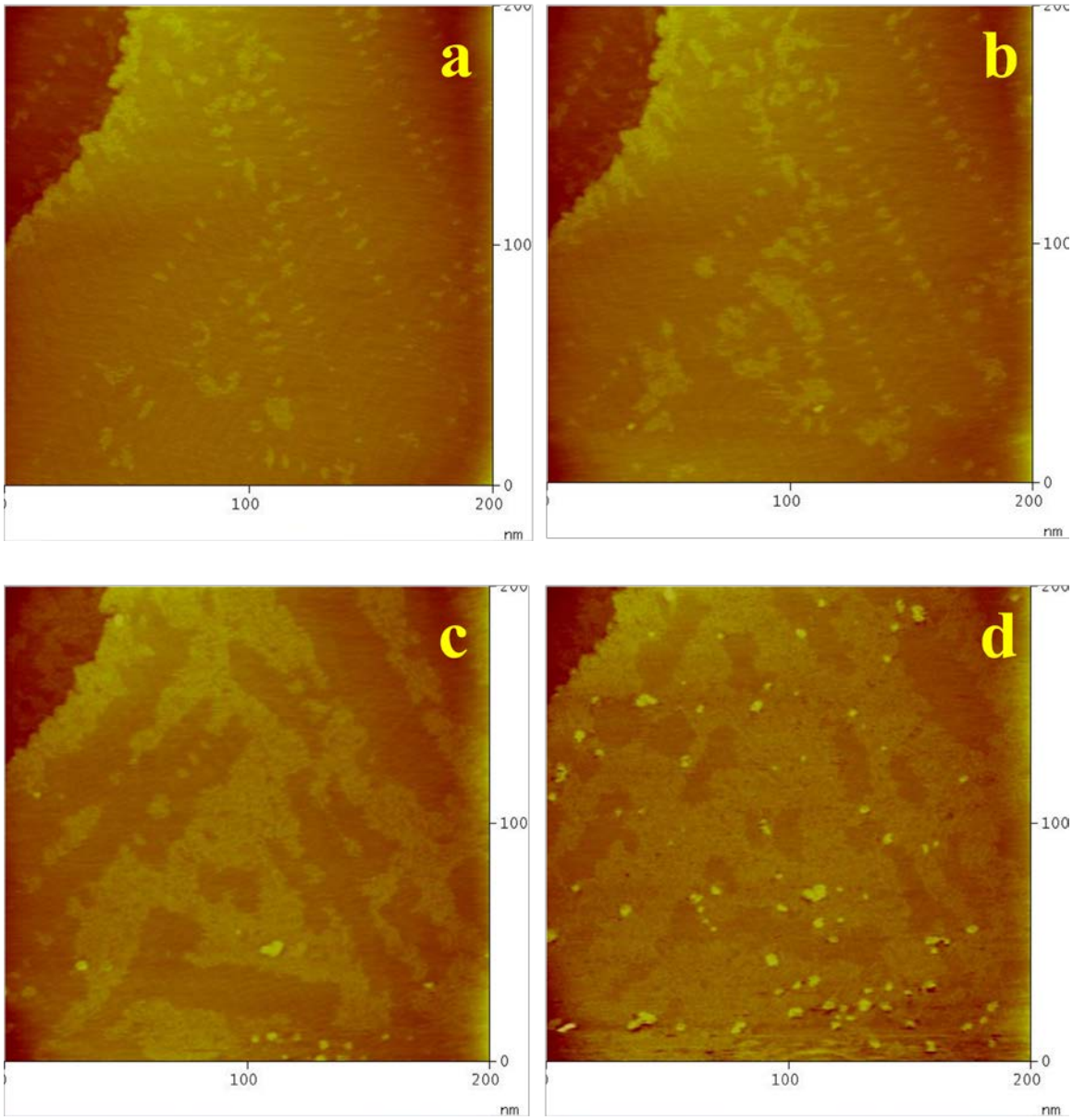

Figure 2.6. EC-STM image of Au(111) surface a). at -400 mV vs. Ag/AgCl; b), c), d). at -500 mV vs. Ag/AgCl in 1 mM GeO_2 (0.05 M $KClO_4$, pH 4.5) solution.

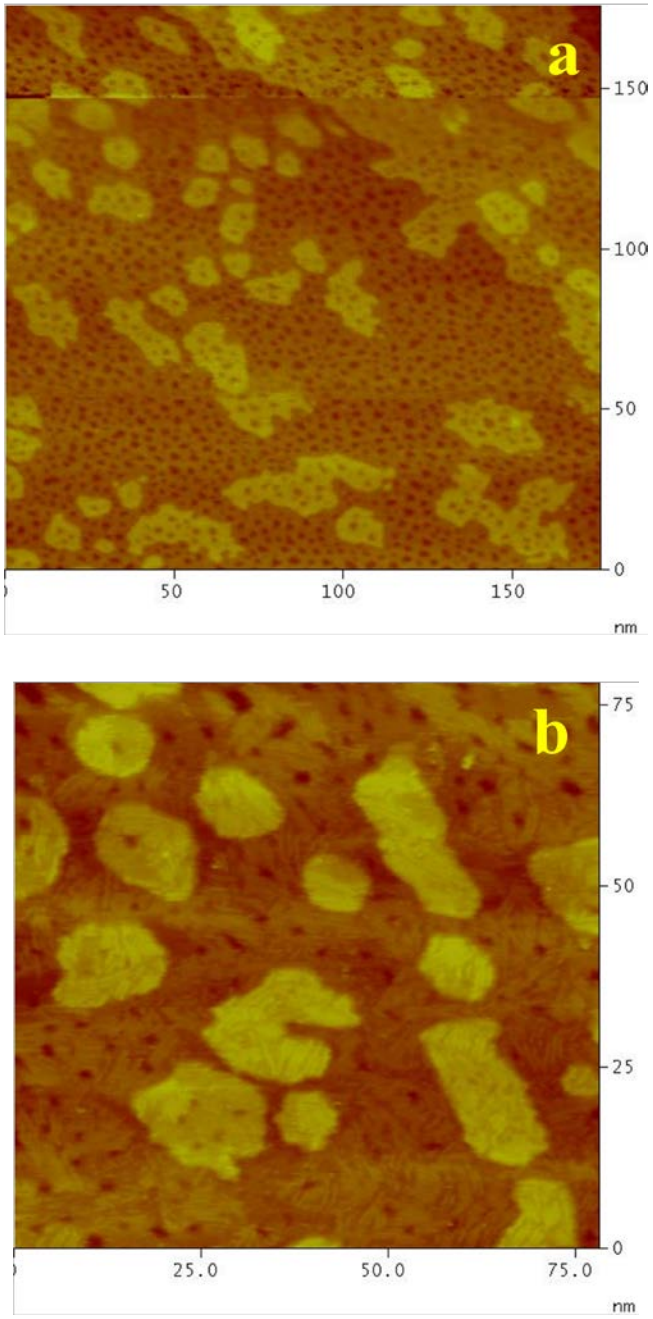

Figure 2.7. EC-STM image of Au(111) surface in 1 mM GeO_2 (0.05 M $KClO_4$, pH 4.5) solution. a). at 220 mV vs. Ag/AgCl after the potential of the Au electrode was scanned to -1.2 mV and then to 500 mV. b). Au(111) 1 min later after the potential was stepped to -400 mV vs. Ag/AgCl.

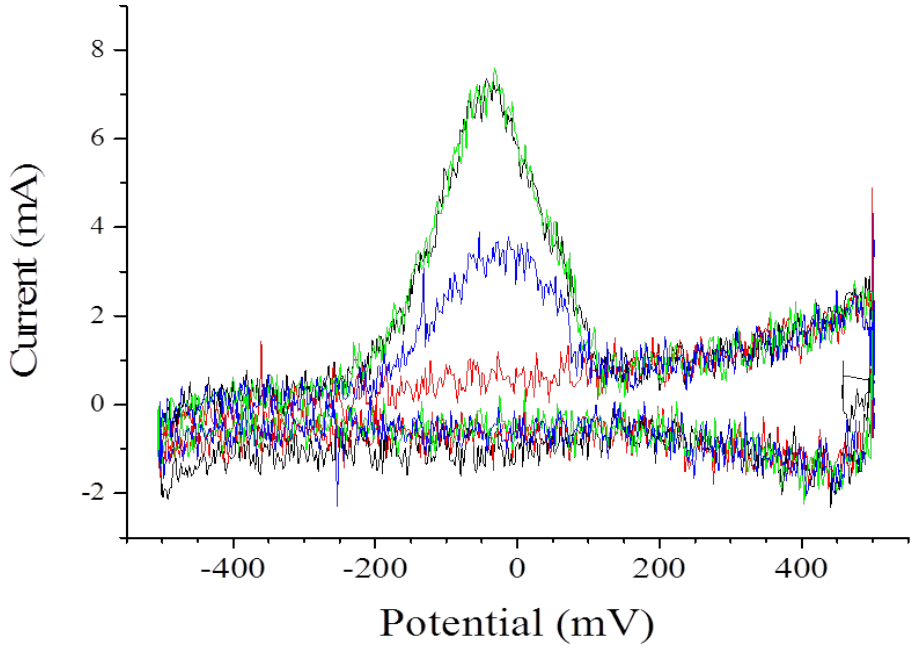

Figure 2.8. Cyclic voltammogram of polycrystalline Au in 0.5 mM GeO_2 (0.1 M $NaClO_4$, pH 4.5) solution after the potential was held at -500 mV vs. Ag/AgCl for 0 sec (red scan), 200 sec (blue scan), 500 sec (black scan) and 700 sec (green scan); scan rate 10 mV/sec. Ge maximum coverage corresponds to 0.18 ML relative to Au.

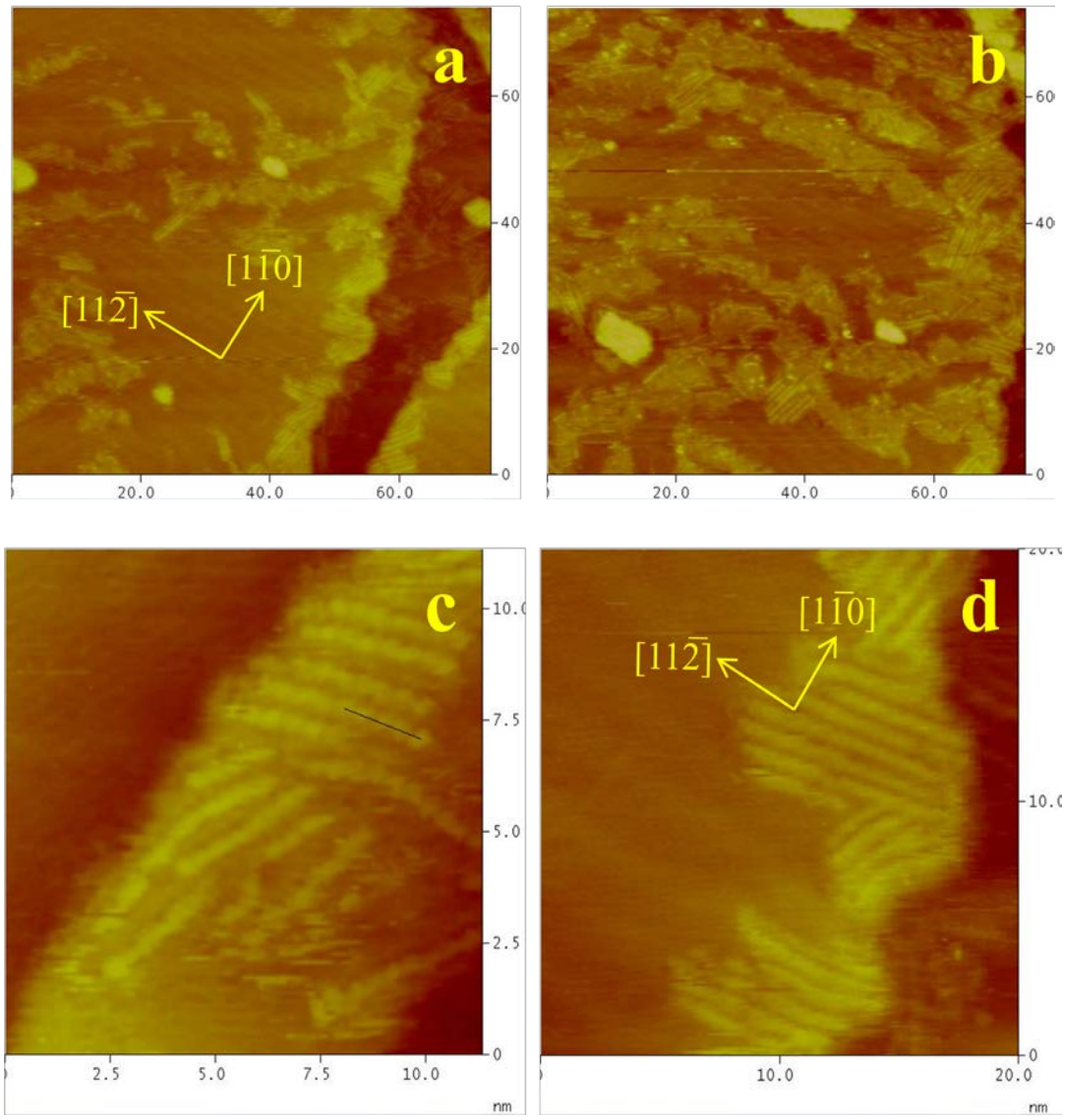

Figure 2.9. EC-STM image of Au(111) surface in 1 mM GeO_2 (0.05 M $KClO_4$, pH 4.5) solution. a, c, d). at -400 mV vs. Ag/AgCl. b) at -500 mV vs. Ag/AgCl. The distance between atoms in image c is 0.49 nm.

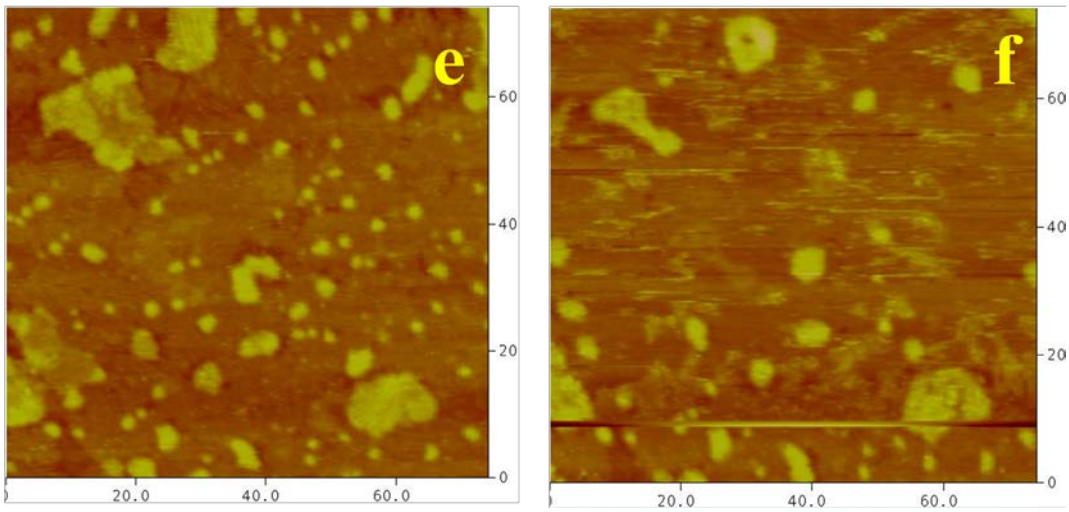

Figure 2.9. EC-STM image of Au(111) surface in 1 mM GeO_2 (0.05 M $KClO_4$, pH 4.5) solution. e). at -500 mV vs. Ag/AgCl. f) at 200 mV vs. Ag/AgCl.

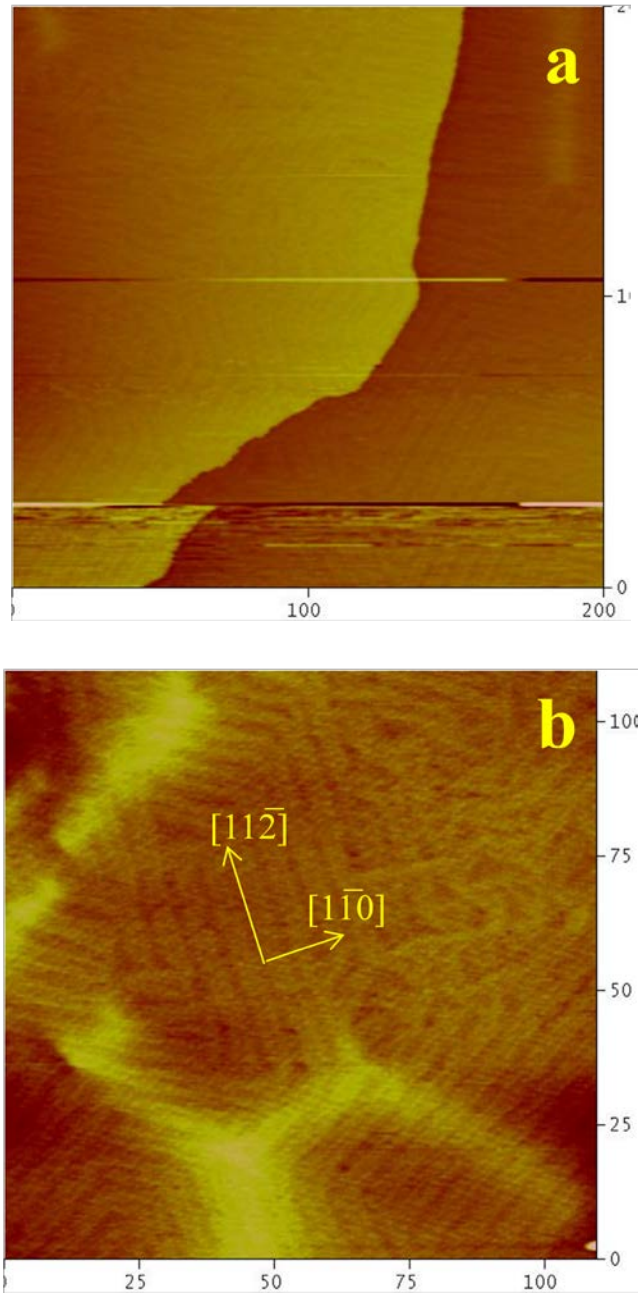

Figure 2.10. EC-STM image of Au(111) surface in 1 mM GeO_2 (0.05 M $KClO_4$, pH 4.5) solution. e). at -400 mV vs. Ag/AgCl. f) at -600 mV vs. Ag/AgCl.

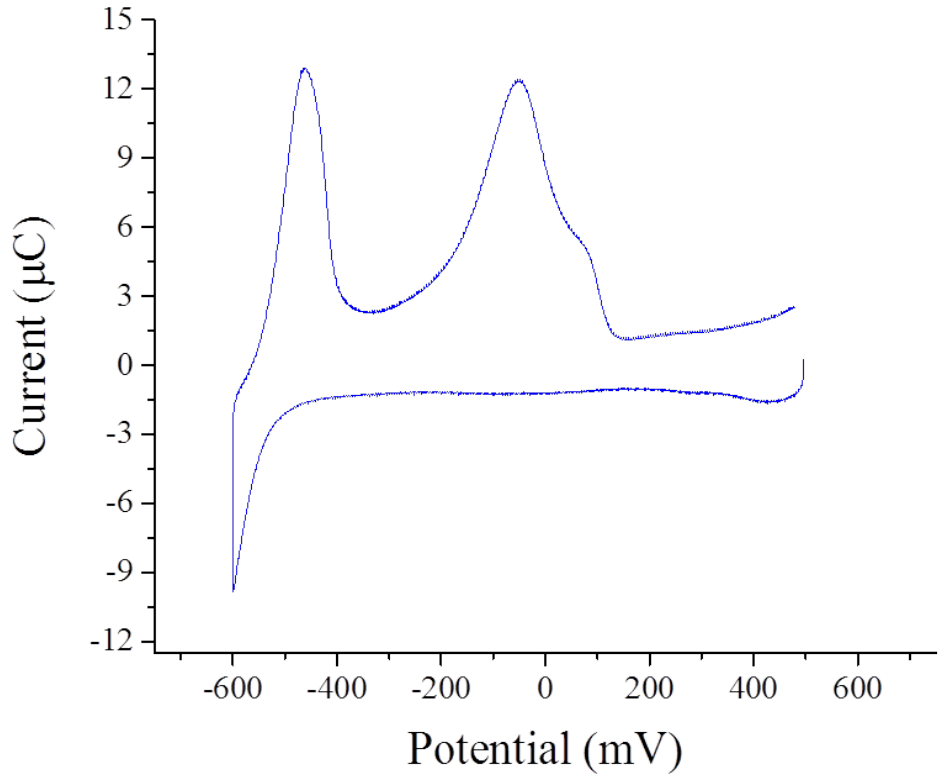

Figure 2.11. Cyclic voltammogram of polycrystalline Au in 0.5 mM GeO_2 (0.1 M $NaClO_4$, pH 4.5) solution after the potential was held at -600 mV vs. Ag/AgCl for 700 sec; scan rate 10 mV/sec. Ge maximum coverage corresponds to 0.24 ML relative to Au.

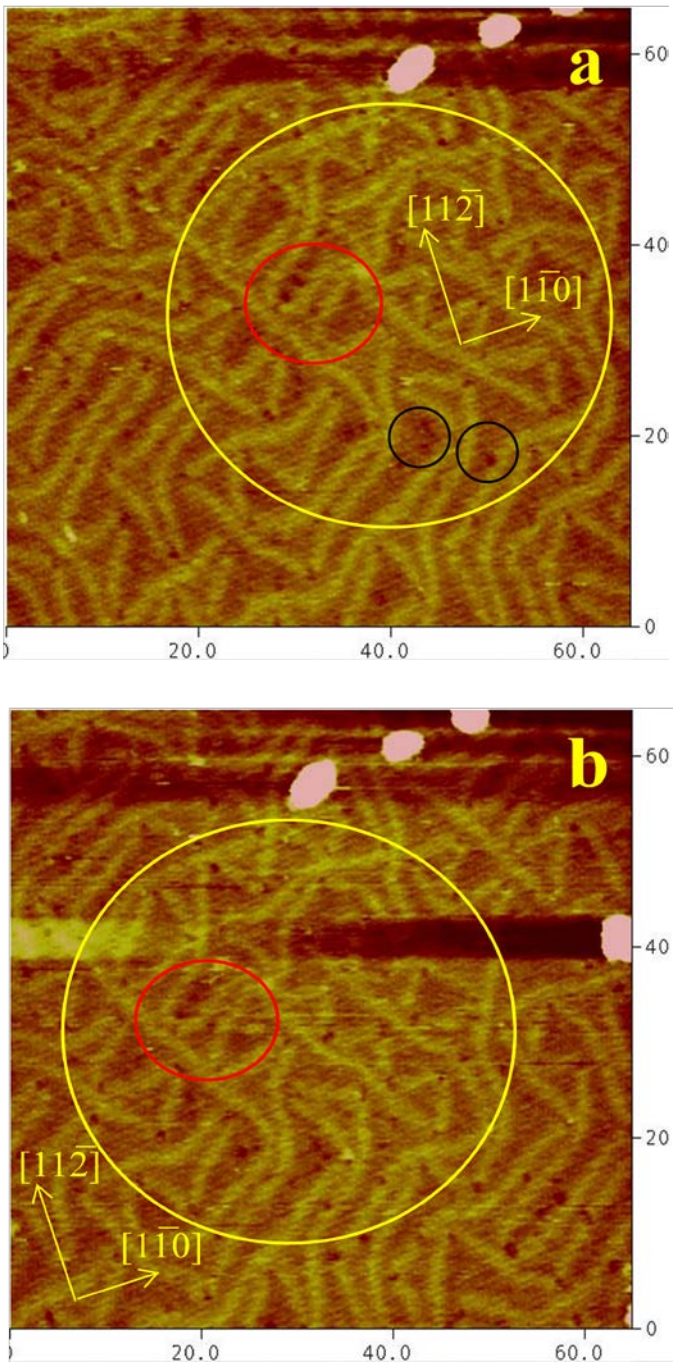

Figure 2.12. EC-STM image of Au(111) surface in 1 mM GeO_2 (0.05 M $KClO_4$, pH 4.5) solution. a). at -600 mV vs. Ag/AgCl; b) at -600 mV vs. Ag/AgCl 6 min. later;

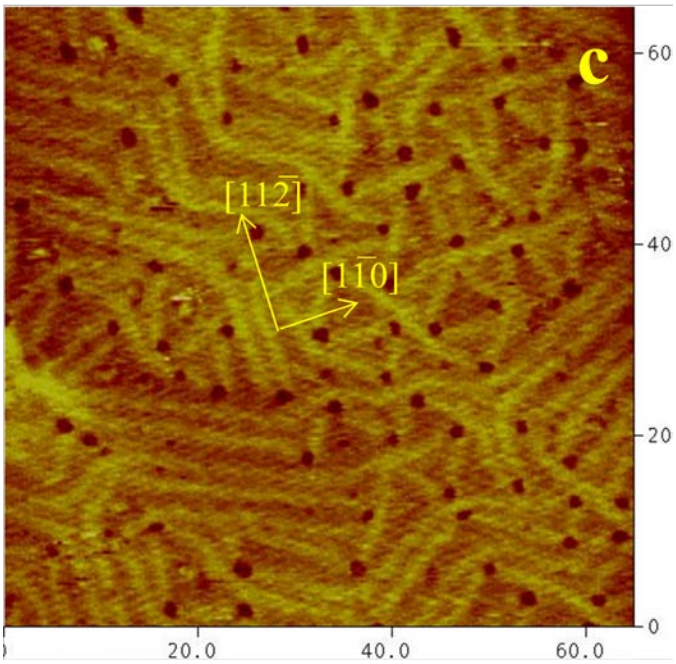

Figure 2.12. EC-STM image of Au(111) surface in 1 mM GeO_2 (0.05 M $KClO_4$, pH 4.5) solution. c). At -700 mV vs. Ag/AgCl.

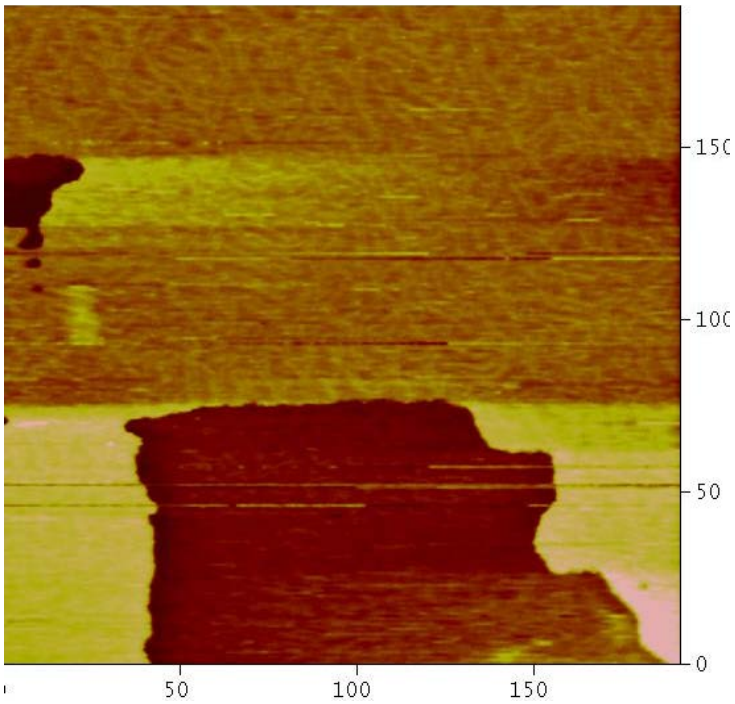

Figure 2.13. EC-STM image of Au(111) surface in 1 mM GeO_2 (0.05 M $KClO_4$, pH 4.5) solution at -500 mV vs. Ag/AgCl.

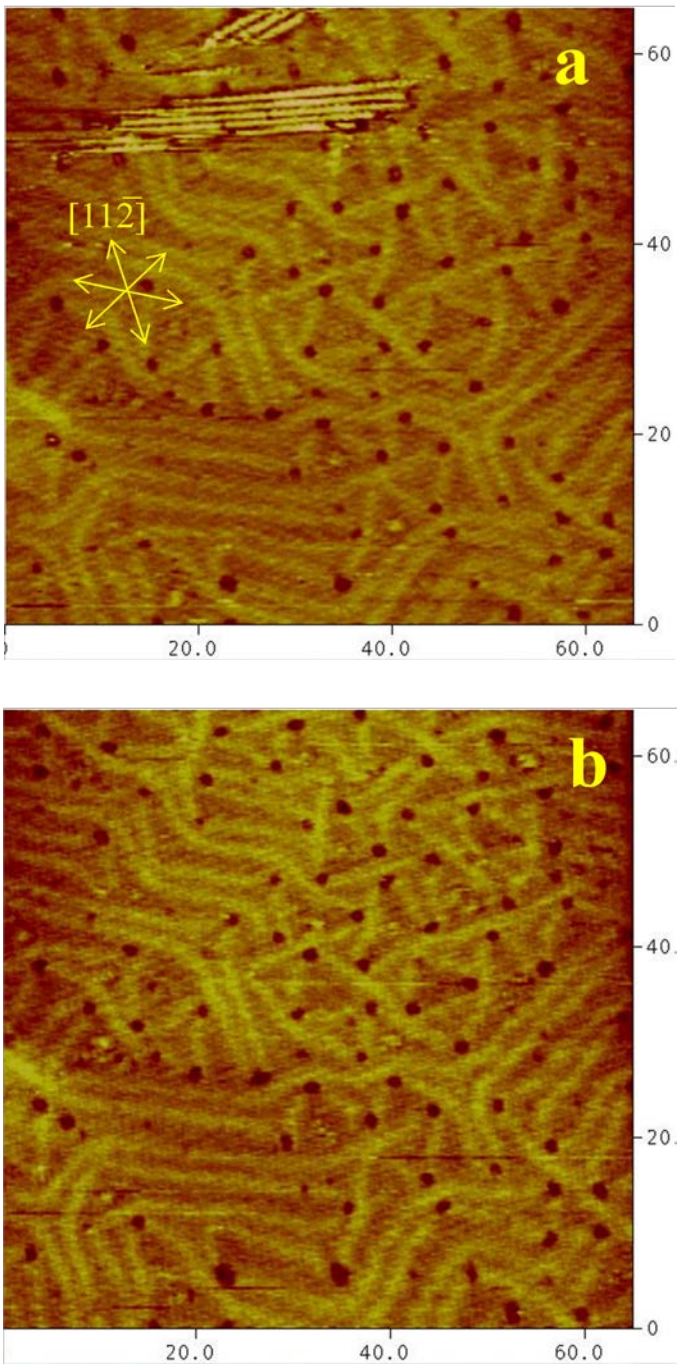

Figure 2.14. EC-STM image of Au(111) surface in 1 mM GeO_2 (0.05 M $KClO_4$, pH 4.5) solution. a). at -700 mV vs. Ag/AgCl; b) at -700 mV vs. Ag/AgCl 30 sec later.

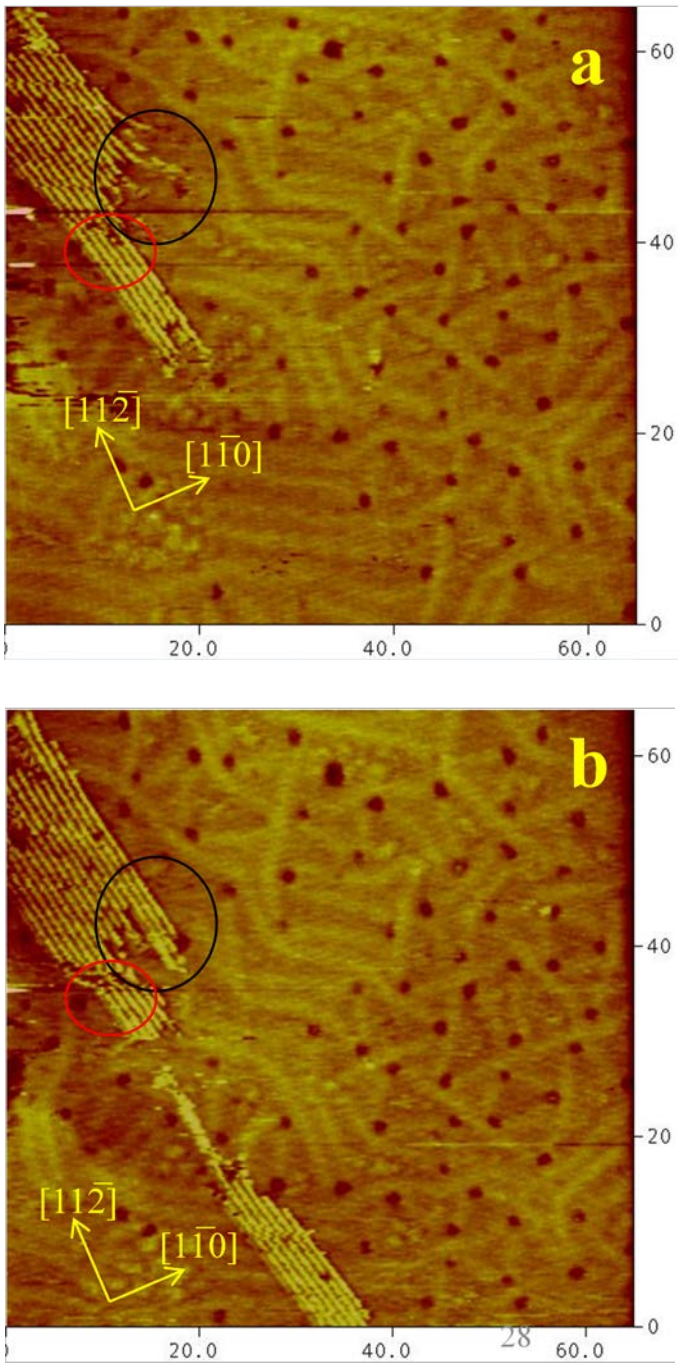

Figure 2.15. EC-STM image of Au(111) surface in 1 mM GeO_2 (0.05 M $KClO_4$, pH 4.5) solution. a). at -700 mV vs. Ag/AgCl; b) at -700 mV vs. Ag/AgCl 30 sec later.

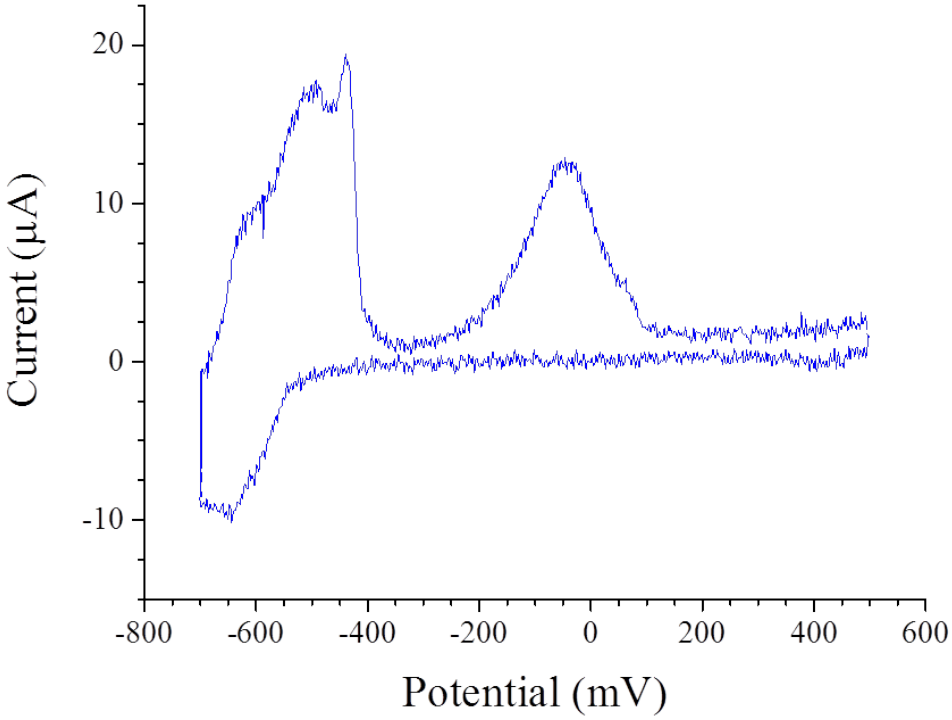

Figure 2.16. Cyclic voltammogram of polycrystalline Au in 0.5 mM GeO_2 (0.1 M $NaClO_4$, pH 4.5) solution after the potential was held at -700 mV vs. Ag/AgCl for 700 sec; scan rate 10 mV/sec. Ge maximum coverage corresponds to 0.33 ML relative to Au.

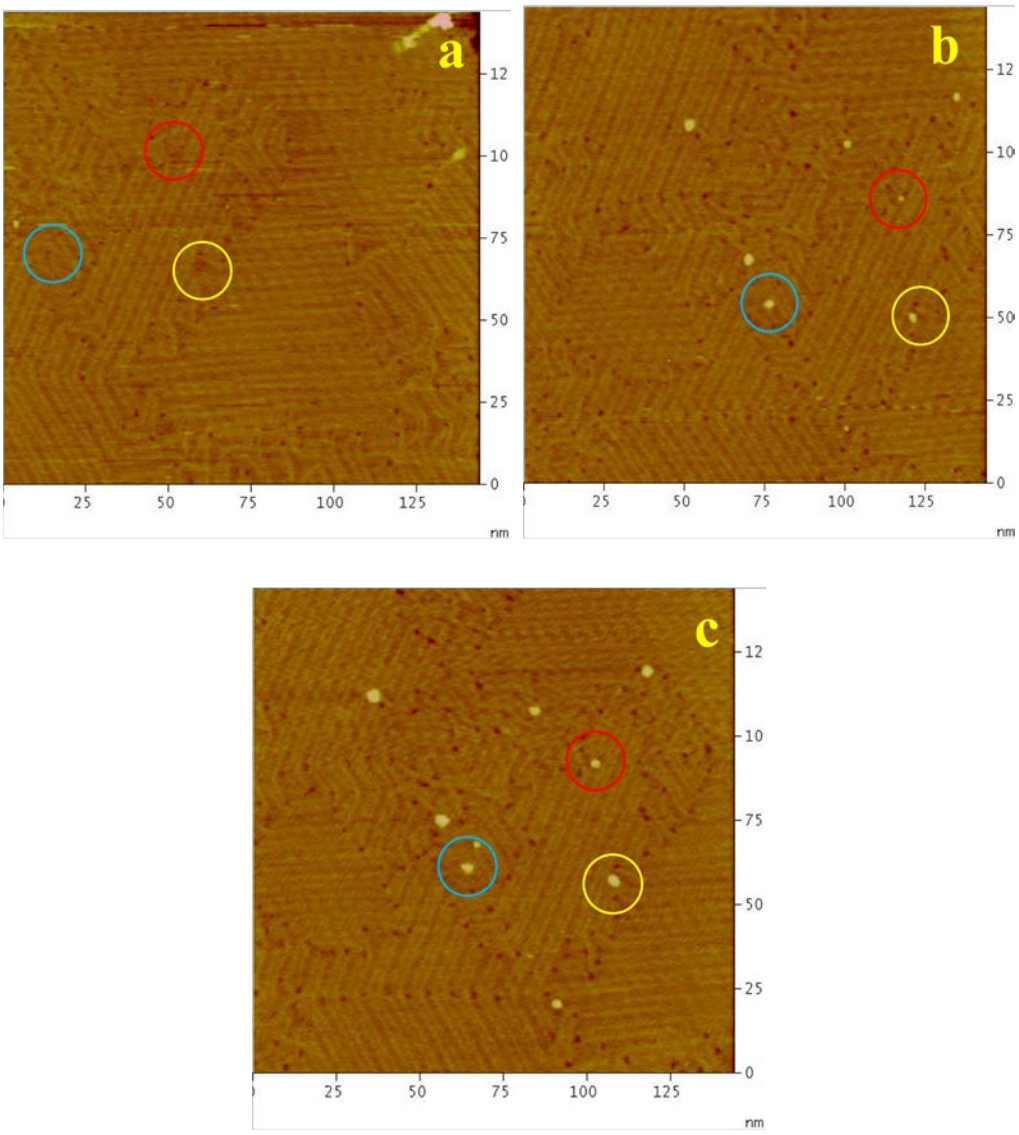

Figure 2.17. EC-STM image of Au(111) surface in 1 mM GeO_2 (0.05 M $KClO_4$, pH 4.5) solution at -700 mV vs. Ag/AgCl. Image b was taken 6 min later after image a, image c was taken 3 min later after image b.

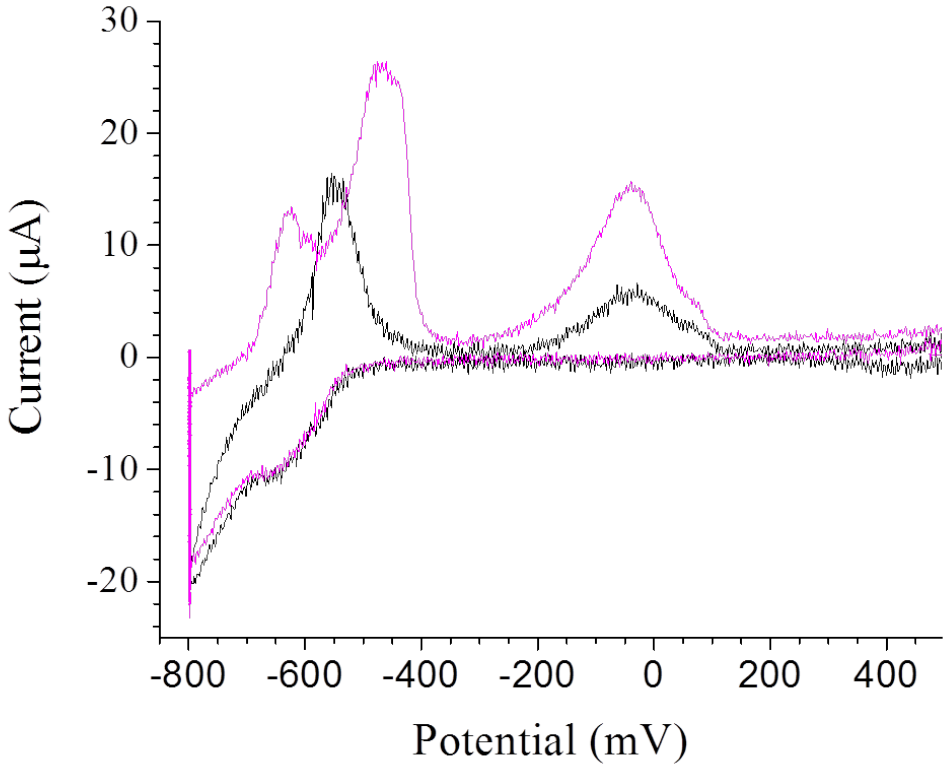

Figure 2.18. Cyclic voltammogram of polycrystalline Au in 0.5 mM GeO_2 (0.1 M $NaClO_4$, pH 4.5) solution after the potential was held at -800 mV vs. Ag/AgCl for 0 sec (black scan), 700 sec (pink scan); scan rate 10 mV/sec. Ge maximum coverage corresponds to 0.44 ML relative to Au.

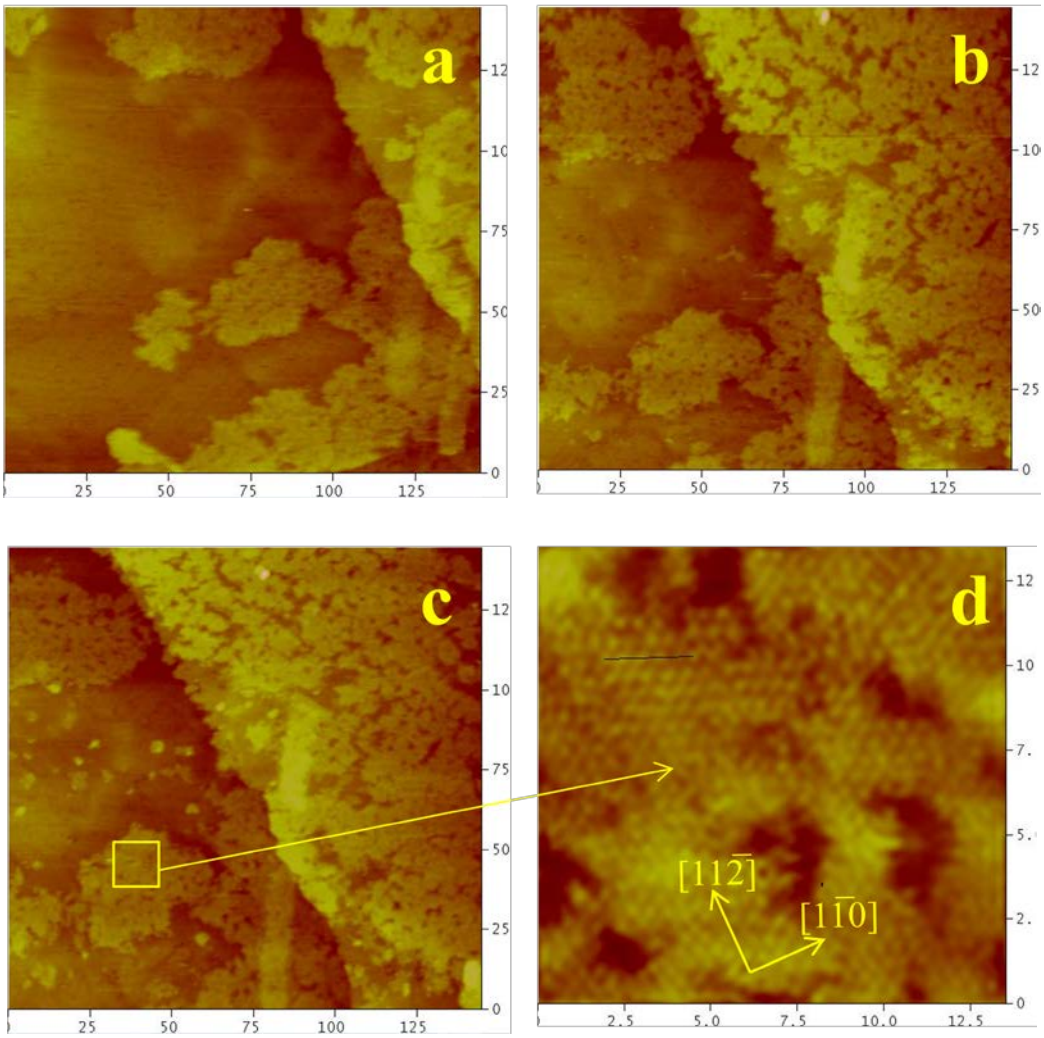

Figure 2.19. EC-STM image of Au(111) surface in 1 mM GeO_2 (0.05 M $KClO_4$, pH 4.5) solution. a). at -700 mV vs. Ag/AgCl; b,c,d) at -800 mV vs. Ag/AgCl. The distance between atoms in image d is 0.51 nm.

CHAPTER 3

ELECTROCHEMICAL STUDIES INTO FORMATION OF GERMANENE IN AQUEOUS SOLUTION[1]

[1] M.A. Ledina, X. Liang, Y.-G. Kim, J. Jung, B. Perdue, C. Tsang, M.P. Soriaga, J.L. Stickney, To be submitted to *Journal of the Electrochemical Society*

Abstract

The discovery of isolated sheets of graphene and its unique properties and applications has stimulated a great interest in other inorganic 2D materials. Germanene, which belongs in the same group as graphene, is predicted to share similar properties that make it a promising material for nanoelectronics applications. According to theoretical reports, germanene is a single layer allotrope of Ge, with a low buckled honeycomb structure. Investigations into formation of germanene in aqueous media will be discussed in this report. Electrochemical formation of germanene structure has been investigated by means of in situ electrochemical Scanning Tunneling Microscopy (EC-STM), voltammetry, coulometry, and micro-Raman. Electrochemical studies on Au(111) terraces have shown that the deposition of Ge at the initial stages is kinetically slow and somewhat unstable, however deposits with coverage more than half of a monolayer seem to be more stable. Moreover, EC-STM imaging on Au(111) of deposits with coverage higher than two monolayer of Ge demonstrated honeycomb-like structure with atomic distances of about 0.44 nm ± 0.02 nm, which is about 10% higher from what is expected if every other atom would be imaged in germanene. However, the domains observed in these images were incoherent. Micro-Raman was performed on Ge nanofilms grown on Cu. An area on one of the samples was found where a shift around 290 cm^{-1} was observed, which according to theoretical reports should correspond to Raman shift in germanene. Given the Raman and STM results, it appears that the coherence of the germanene domains will need to be increased in order to more consistently produce the Raman signal. The data presented suggest that germanene has been formed electrochemically, although only as a minority species.

Introduction

Two dimensional inorganic materials have or expected to have unique properties that make them very attractive for integration into the nanoelectronic industry. [1-3] Ever since the discovery of graphene, a single layer of carbon atoms in a hexagonal pattern, studies of its properties, such as large theoretical specific area, high intrinsic mobility, good electrical conductivity and others [4] have demonstrated its tremendous potential to be used in numerous applications. An example of these applications, just to name a few, would be nanoelectronics, sensors, batteries, supercapacitors, and in particular, field effect transistors and transparent conductive electrodes. [5-7] The isolation of single sheets of graphene and its studies have greatly stimulated to look for other two dimensional materials, such as germanene, a Ge analog of graphene. [8-11] Germanene structure has been first described in 2009 by Cahangirov et al. [12] in a theoretical report and since then more than two hundred papers has been published already.

Germanene structure is a van der Waals hexagonal two-dimensional (2D) array of Ge atoms, similar to honeycomb structure of graphene. However, in contrast to graphene, the energetically stable configuration of germanene is predicted to be low buckled by about 0.07 nm, and, hence, to have sp^2-sp^3 mixed hybridization. [13] It is expected that band gap will be more open in germanene than in graphene due to a buckled structure[14], although it will be still very small, about 24 meV. [15-17] According to theoretical reports germanene low buckled structure will be semimetallic. [18-19] Ge-Ge atoms neighbor distance was theoretically predicted to be about 0.24 nm. Figure 3.1 demonstrates the proposed structure of germanene, where one half of the atoms are 0.07

nm higher than the other. The *ab initio* reports also predict the Raman shift for germanene should be observed at about 290 cm^{-1}. [20-25]

Germanene is a unique material that does not exist in nature as graphene does in graphite. Due to a more facile integration of germanene into Si nanotechnology than graphene, [18, 26] it is quite intriguing to find experimental procedures for formation of germanene structures. Moreover, it is fundamental to investigate the mechanisms of its formation and growth, and find means for optimization of the synthesis conditions to produce free standing germanene sheets.

There have been several experimental reports on the formation of germanene in gas phase. On Pt(111), a $\sqrt{19} \times \sqrt{19}$ buckled germanene structure has been described, where Ge was synthesized by electron beam physical vapor deposition at room temperature, with consequent annealing of the sample. According to the STM image and theoretical DFT-based *ab initio* calculations it was concluded that only one atom is higher in the six-member Ge atoms hexagon structure. [27] Another group has reported a $\sqrt{3} \times \sqrt{3}$ germanene layer on $\sqrt{7} \times \sqrt{7}$ Au(111) supercell, that has been also deposited by molecular beam epitaxy (MBE). The observed in STM image a honeycomb-like structure was found to be nearly flat, and the atomic distances were deduced to be about 0.255 nm. [28] A (3×3) superstructure was observed on Al(111) by a different group using same method with similar identified atomic distances. The height of the germanene layer on Al(111) surface was found to be about 0.27 nm. [14] Formation of germanene structure was as well reported after evaporation of Pt onto Ge(110) and consequent flash annealing. [29] Moreover, a fabrication of multi-layered germanene (lonsdaleite germanium) on Si substrate has been reported. These germanene layers were synthesized first by epitaxial

growth of $Si_{0.65}Ge_{0.35}$, then immersing the sample into N_2 plasma and sequential annealing. [30] Finally, there was also a report on the formation of the germanane structure, a hydrogenated germanene, by topotactic deintercalation of $CaGe_2$. Moreover, Bianco et al. were able to exfoliate germanane. [31]

Ge electrodeposition has been studied in the literature in the past. Due to its low hydrogen overpotential and non-reactivity of Ge ions, the electrodeposition studies of germanium were mostly done in nonaqueous media. [32-36] For example, Szekely has reported a formation of Ge films by electrodeposition from a solution of germanium tetrachloride in propylene glycol with plating speed of 0.001 in./3 hr. [33] Endres et al. have published quite a few papers about Ge electrodeposition studies from molten salts and ionic liquids accompanied with STM and in situ STM studies of its deposition. [37-41] Some studies, that were done with germanium tetraiodide, have shown that even after Ge electrodeposition in such solutions maximum thickness of the deposits was found to be less than 20 nm. [37] Cyclic voltammetry studies in nonaquoues media discussed in the literature agree on reduction process to correspond to a reduction of Ge^{+4} species to Ge^{+2} species, and then Ge^{+2} to Ge^{0}. [35, 40-45] Ge electroplating was also reported to be feasible on semiconducting substrates, such as Si. [46] There are also reports about formation of the thick Ge nanostructures. [47-49] For example, Carim et al. showed that depending on potential Ge various nanostructures can be grown from aqueous solution by dissolution and saturation in the liquid Hg electrode. [49] Ge nanowires were also formed by Al-Salman et al. by utilizing a solution of Ge in ionic liquids. [43] Ke et al. have studied electrodeposition of Ge from various supercritical fluids containing Ge(II) or Ge(IV)

compounds, and were able to obtain amorphous Ge films from Ge(IV), however, films grown from Ge(II) compound were heavily contaminated. [45]

Stickney's group has been investigating the electrodeposition of Ge onto Au and Cu substrates in the past. [50-52] The direct electrodeposition of Ge in aqueous media is limited to a several or less monolayers (ML, a monolayer is referred here as one adsorbate per one surface atoms), depending on a potential and precursors solution pH used. However, even though it is not possible to grow more than 3 ML in aqueous media because of low hydrogen overpotential, Stickney's group has developed a cycle of electrochemical growth of Ge nanofilms utilizing deposition of a Te layer as a bait, which allows to deposit a new layer of Ge onto it, with a sequential stripping of Te layer at very negative potential, leaving behind newly deposited Ge layer. The created cycle can be repeated as many times as needed to grow the desired thickness of the film. It should be noted that at the time of the studies, Raman spectroscopy has been performed on the Ge deposits and it was concluded by that electrodeposited Ge was amorphous, as Raman shift was observed around 270 cm^{-1}. [52]

No reports are known to date of the synthesis of germanene structure in aqueous media. As mentioned above, germanene structure has been reported to be formed in gas phase, which requires ultrahigh vacuum conditions and elevated temperatures. The present paper will discuss the investigations into the electrochemical formation of the germanene layer on Au electrode in an aqueous phase at room temperature by EC-STM, cyclic voltammetry and micro-Raman. The investigations into germanene's formation mechanism will provide the necessary tools and understanding of germanene synthesis

with good quality, possibility of studying its properties and future applications of germanene in various fields.

Experimental

Electrochemical deposition of germanium onto a Au surface was studied with electrochemical scanning tunneling microscopy (EC-STM). EC-STM studies were performed with a Nanoscope III (Digital Instruments, Veeco). All images were done in a constant current mode. A three-electrode configuration was used for all electrochemical studies. Reference electrode was Ag/AgCl (3 M NaCl, Basi). Platinum wire was used as an auxiliary electrode. Au bead sample was used as a working electrode, where Au(111) facet which was the imaging surface, which was prepared by one the variations of the Clavier method. [53] Before every experiment Au bead was flame annealed, cooled down in hydrogen atmosphere and quenched in ultrapure water (> 18.2 MΩ, bubbled with hydrogen), to ensure the formation of large (111) terraces and cleanliness. The bead usually then was quickly put into a EC-STM cell to exclude contaminations. STM tips used in experiments were 0.25 mm tungsten wires. All tips were freshly electrochemically etched in 1 M potassium hydroxide solution (15 V ac) and covered with nail polish to reduce contact of W wire with solution, leaving only apex of the tip uncovered in order to avoid Faradaic reactions on W wire. Tip potential E_t was usually around -150 mV vs. Ag/AgCl. STM was calibrated with HOPG sample. Typically observed terraces were about 300-500 nm. All glassware and other parts of assembly were cleaned on daily basis.

Electrochemical studies were also done on automated flow cell deposition system (Electrochemical ALD L.C., Athens, GA). The E-ALD hardware consisted of valves, electrochemical flow cell, pump, and a potentiostat, all controlled via specialized software. To exclude oxygen, solutions were purged with nitrogen, and valves and tubing were confined in a nitrogen atmosphere. Flow cell also contained a three-electrode configuration. Polycrystalline Au on Ta on glass substrate was used as a working electrode, Ag/AgCl (3M NaCl, Basi) was used as reference electrode and Au wire was used as an auxiliary electrode. Cleaning of Au substrate was usually performed in 0.1 M sulfuric acid before any experiment until a typical reproducible cyclic voltammogram was observed.

Solutions for both EC-STM and flow cell studies were prepared with reagent grade chemicals and ultrapure water (Milipore-Q system with resistance of 18 MΩ fed with in-house DI water). Blank and germanium solutions contained 0.1 or 0.05 M $KClO_4$ (Aldrich, 99.99% trace metals basis), and germanium solution contained 1 mM GeO_2 (Alfa Aesar, 99.999% metals basis) additionally to electrolyte. All solutions were pH 4.5 – 4.7. All experiments were started with assembling the flow cell or EC-STM cell, filling up with solution and connecting the leads without applying any potential control. The open circuit was usually about 300 mV for both EC-STM and flow cell. All potentials reported here are vs. Ag/AgCl (3M KCl). A Renishaw InVia Raman microscope (Renishaw, Inc., Hoffman Estates. IL) was used to analyze Ge films with 514 nm laser.

Results and discussions

Cyclic voltammetry studies of Ge deposition on polycrystalline Au surface are presented in Figure 3.2 from a solution that contains germanium oxide and potassium perchlorate electrolyte, with no buffer added. In these series of the cyclic voltammograms (CVs) the potential is scanned from 500 mV to different negative potential limits and then scanned back to 500 mV. The evaluation of these voltammograms suggests that the electrodeposition of Ge starts at about -550 mV. However, it is not the case if the potential is held.

Figure 3.3 shows a window opening CVs of time dependent studies where the potential was scanned from 500 mV to a chosen negative potential, held for 700 sec and then scanned back to 500 mV. The graph demonstrates that Ge electrodeposition is kinetically slow and time is needed in order to reach its maximum deposition at a certain potential. Furthermore, time dependent studies show that Ge can be deposited even before -550 mV if the potential is held long enough. An example is presented in Figure 3.4. Note the CV with no holding (red line) vs. the CV after the potential was held for 700 sec (green line), where oxidation charge seems to be already limited after 500 sec and corresponds to less than 0.1 ML.

Figure 3.5 shows ($\sqrt{3} \times 22$) herringbone reconstruction on Au(111) at -300 mV with no Ge present on the surface. The Au (111) reconstruction was observed on daily basis before any Ge deposition took place. Figure 3.6 shows STM images taken at more negative potentials such as -600 mV and -700 mV. In Figure 3.6a the Au(111) reconstruction is very disordered and has multiple elbows and rotations. Moreover, the Figure 3.6b the Au(111) shows reconstruction that follows not only the $\sqrt{3}$ direction ([11^{-}

2] directions, main crystallographic orientations), but also goes in n-by directions ([110] direction), which is unusual for pristine Au(111) surface reconstruction.

Formations of the dark spots should also be noted the where the reconstructed Au herringbone ridges change its direction or the where they end. According to the measurements performed on the imaged surface, the depth of the dark spots was found to be 0.04-0.05 nm. As imaging of the same spot continued without changing the potential (-600 mV), the spots were increasing in size. These holes might be where Ge atoms start to nucleate on the Au surface; however, since the radius of Ge is smaller, the height of the features will be lower. Another possibility is that these features are formation of an alloy between Ge and Au, where Ge substitutes Au atoms, hence the height of the feature will be lower again. Similar behavior has been observed in the literature. [54-56] For example, Nahas et al. have reported similar effects after deposition of Pt onto Au(111). [55] They also observed a random insertion of Pt atoms into the substrate surface. Similar behavior was observed in the present studies. Careful inspection of the image 6b reveals that dips were observed in hcp and fcc regions on the Au reconstructed surface. The reason that Ge atoms would likely to go to the elbows on the Au surface is due to a presence of the edge dislocation that always present on the surfaces and will likely behave like a preferred spot for atoms to bind to. [57-58] Moreover, Nahas et al. also suggested that random intrusion of Pt atoms into the surface might have caused modifications of the Au herringbone reconstruction. Unusual behavior of the Au observed in the present studies, as was discussed earlier, might also be influenced by random intrusion of the Ge atoms as well. Furthermore, according to the Sun et al. [59] such unusual behavior of $22 \times \sqrt{3}$ reconstructed Au(111) surface was observed after adsorption

of perylene (FePc) molecules at a monolayer coverage. That might be the case in the present studies if germanium molecules adsorbed would be some conjugated Ge systems, for example germanene related structures that were adsorbed onto the surface which have caused the change in Au reconstruction directions. However, there are no other suggestions that at that potential germanene would already be formed. Moreover, such a disordered surface was not always observed. And in the cases when it was observed, unusual herringbone reconstruction was only observed on some parts of imaged Au terraces.

However, lowering the potential slowly stepwise produced images with features which were observed already at -400 mV. Figure 3.7 shows STM images of the surfaces that were taken after the potential of Au was held at -400 mV. Figure 3.7a was taken after the potential was stepped negatively by 100 mV from 300 mV to -400 mV. Figure 3.7b was observed after the same stepping sequence and imaged at -400 mV, but first, the potential of the Au bead electrode was scanned to -1.2 V and then to 500 mV (CV not shown), to electrodeposit Ge and strip it from the Au surface. STM image that was taken after the CV at 220 mV have demonstrated a surface that was completely covered with pits (image not shown), which implies the Ge and Au were forming an alloy, which when stripped leaves the surface pitted. Moreover, pits are still visible on Figure 3.7b. “Lines-like” features were observed on both EC-STM images. It should be noted that both images were found as soon as imaging started and not formed as the scanning was taken place. However, as of presently, it is not understood if there is any tip effect present that can affect the formation of the ‘lines’-like features. The last (Figure 3.7a) were mostly observed on the edges of the Au terrace, on the second image (Figure 3.7b), they were

completely covering whole imaged Au terrace. The surface observed on Figure 3.7a after about 20 min of imaging was completely covered with the layer containing “lines-like” features layer. Moreover, the imaged area demonstrates two types of layers with different heights. The height of the layer without lines present on it was about 0.06 nm, and with “lines-like” features the height was about 1 nm. Both heights are not enough to be a separate layer. It is hypothesized that “lines-like” features are probably Au atoms lifted up due to intercalation of Ge atoms into the Au layer underneath. If the layer underneath has a different lattice constant, Au atoms in the top layer will not nest in the layer below, thus they should stick out and be higher than the surrounding Au atoms. Hence if the Au atoms on the top layer form lines, that would imply that the intercalated Ge atoms underneath are also in the lines-like positions. “Lines-like” features were observed throughout the studies done at around -400 mV. They seem to appear as stacked lines parallel to each other. Since they were usually found when the imaging just started, drift might have played a crucial role in identifying angles between the Au herringbone reconstruction ridges and the lines. The measurements have shown various angles relative to the Au herringbone reconstruction ridges, however, it seems that $\sqrt{3}$ was identified more than other directions, but more studies are needed to confirm that. The distance between the lines was found to be around 0.9 nm. As formation of the layer with lines continued appearance of 0.22 nm islands were also observed. These islands are probably Au islands formed due to uplifting of the Au reconstruction[60] as well as due to a substitution of Au with Ge atoms, however, that might be a minor part. It is also noted that the Au islands were forming only on the Au surface, and the new layer was forming around them, as well as on them (image not shown) as soon as the Au island has formed.

It appears that “lines-like” features start to form at edges, defects or dislocations first, since these are spots have higher surface energy compared to the rest of the surface which needs to be lowered. Thus, since the surface was already pitted (image not shown) before new deposition of Ge, lines were observed already after 4 min after the potential had reached -400 mV (Figure 3.7b). After the surface was completely covered, the potential was stepped to 200 mV, where no Ge should be left on the surface. The surface (image not shown) demonstrated that layer with lines-like features was stripped and the surface was left with additional pits, again suggeting a formation of an alloy.

Figure 3.8a shows the STM image where the potential was held at -600mV. The Au(111) reconstruction was again observed disturbed, however, all reconstructed ridges seem to be observed only in the three main crystallographic directions (120˚ rotations). This surface was already observed modified after the potential of the working electrode was held at -500 mV. As the potential was stepped to -600 mV no visible changes were observed on the imaged spot. The Figure 3.8b demonstrates an image after the potential was stepped to -700 mV. The potential stepping was done while the image was being taken in the “Up” direction, approximately in the middle of the image, as the tip was scanning, and spray-like formations appeared. Figure 3.8c demonstrates the next scan in the “Down” direction. It is observed here that formations are almost gone, but a few small islands. Moreover, the surface looks like it is cut in the direction as the tip was horizontally rastering the imaged area, and the small islands are present on the edges of the cuts. No conditions were changed in between the image b and image c. In Figure 3.8d the scanned area was zoomed out from 170 nm to 300 nm. Piles were observed on both sides where imaging was being performed before, suggesting that the piles were created

as the tip was rastering the surface in the horizontal directions, pushing the deposits on the sides. It is hypothesized that cuts-like features have been caused due to stepping to -700 mV, giving a larger by 100 mV bias, which also could have caused changes in tip conditions as well as due to some salt-like formations could have been caught up on the tip. More negative potential allowed Ge islands to start to form possibly due to Ge presence in alloy surface layer as well as newly reduced Ge atoms. However, these islands seem only weakly bound to the surface and were easily swept from the imaged spot by probably tunneling conditions of the tip. The images were taken apart by 30 s. Interestingly, as the imaged area was zoomed in at a different spot (left top corner of the Figure 3.8d), the surface was found to have herringbone reconstruction, although still to have a lot of rotations in the three main crystallographic directions. And as the potential was still held at -700 mV, appearance of holes was observed (not shown) on the surface similar to Figure 3.6 and what was discussed earlier.

Alternatively, Ge deposits were also observed to grow at around -700 mV, when the potential was not held for too long at the initial potentials (around -400 mV or -500 mV) and the scanned area was large (around 200 nm), which is also assumed to effect Ge deposits formation at the initial deposition stages, probably suggesting that the initial Ge formation is weakly bound to the surface. In these studies the potential was stepped from -400 mV (Figure 3.9a) to -700 mV (Figure 3.9b) stepwise over 7 min. A formation of dips was observed on Au herringbone reconstructed surface (Figure 3.9a), in particular in between the ridges and where the ridges change their direction. Next, formation of islands was observed as the potential was held at -700 mV. The average height was found to be from 0.2 nm to 0.24 nm. It is hypothesized that these are Ge islands, even though it

was observed before that Au islands were formed at -500 mV as the Ge atoms were intercalating into the surface and Au atoms were pushed out and formed islands. But in the present case the potential was stepped to -700 mV relatively fast and Ge might not have intercalated into the surface as fast and homogeneously, as when the potential would be stepped negatively more slowly. Instead, Ge atoms might have entered the Au surface in the appeared dips and as more Ge^{+4} species was reduced, Ge islands started to form on the surface. It also should be noted that the edges of the terrace have wavy shape suggesting that Ge has also entered the surface at the edges. It is very probable that Ge atoms find their way to intercalate into the Au surface faster at the Au terraces edges since they have a higher surface charge. Moreover, as the potential was stepped more negatively, the observed islands continued to grow, eventually completing a layer.

Another set of experiments demonstrates the effect of Ge presence in the Au surface before moving to more negative potentials. In this experiment, first, the potential of the electrode has been stepped from -300 mV up to -700 mV (by about 2 min in between steps of -100 mV). After about 1 min at -700 mV, the potential was stepped positive to 600 mV to oxidize some Ge. Then the potential was again decreased stepwise. At -300 mV the scanned spot still demonstrated herringbone Au reconstructed surface (Figure 3.10a), although due to a low resolution of a tip it is hard to tell if the reconstructed surface is modified. However, as soon as the potential was stepped to -400 mV, islands started to form rapidly. It is hypothesized, that the fast islands formation most probably associated with already present Ge from the previous negative stepping of the potential. Additionally, the rapid Ge deposition might also be associated with created imperfections in the Au surface after pulse stripping at 600 mV. As the potential was held

at -400 mV, the islands were covering homogeneously the scanned area. The continuous growth of the islands was observed as the potential was decreased stepwise again. When the potential reached -800 mV, the first layer of Ge almost completely covered the scanned area, and moreover the second layer started to form. The potential was then stepped to -850 mV and then after about 4 min to -700 mV. A spray-like formation (not shown) was observed again, similar to Figure 3.8b. It should be noted that the bias has been changed due to stepping from 700 mV to 550 mV, meaning the tip was set a little closer to the surface. From described data above it can be concluded that initial Ge deposition is somewhat unstable since slight modifications in tip conditions causing modification of the Ge deposit.

A formation of more than a monolayer was also studied with EC-STM. In Figure 3.11, amount deposited onto the Au substrate corresponds to 2.4 ML (for 4 e^- process). The deposition was performed by scanning the potential to -1.4 V, and without holding the potential it was scanned back to -900 mV, in order to avoid disruption of the Ge deposit by hydrogen evolution. At -900 mV no oxidation or reduction should happen (Figure 3.11). The observed STM image showed the large area covered with Ge deposit. The observed images also demonstrated formation of hexagonal-like surface, however, rather disordered. Figure 3.12a shows the formed Ge on Ge layer. The height of the layer corresponds to 0.35 nm, which is close to low bucked germanene height on germanene layer. The expected atomic distances for buckled germanene, assuming only every other atoms would be imaged as in case of HOPG, should correspond to 0.4 nm. From the observed image (Figure 3.12b) the average atomic distances were about 0.44 ± 0.02 nm. Again, the surface looks rather distorted. Figure 3.12c demonstrates a honeycomb-like

structure of the electrodeposited germanium layer. Figure 3.12d shows the Fast Fourier Transformed (FFT) Figure 3.12c to demonstrate the honeycomb-like structure better. The distance between the holes in the image, which should correspond to the distance between the atoms on the same level in buckled structure, was found to be around 0.46 nm. However, again, it is observed in the structure that domains are rather incoherent and vary throughout the layer. It might be that as germanene patches were growing from different spots, as Ge deposition continues, and if orientations of structures did not match from the different patches, domain boundaries might have been formed as they met. Moreover, it is obvious from the Figure 3.12d that some rings in the honeycomb structure have more than or less than 6 atoms in them. It is possible that the observed defects might be associated with hydrogen evolution, which might have caused reorganization of the germanene domains, or might have introduced defects into its structure. As was shown in studies on defects in graphene that were obtained under electron irradiation, hitting out an atom will lead to a recombination of the rest of the atoms in rings around it, causing a formation of rings with other than 6 atoms in it. [61] There are a few reports on of the defects in the honeycomb structure of graphene. [62-63] The most common ones are cluster defect 5-7-7-5 and 5-8-5 rings, however, the average number of atoms still will be 6. [64] Indeed, after careful inspection of the structures on Figure 3.12d, it could be found that some rings do have those kinds of the cluster defects.

Even though the direct electrodeposition of Ge is self-limited, electrochemical atomic layer deposition (E-ALD) has been utilized by Stickney's group to grow germanium thicker films in an automated flow cell that has been published elsewhere. [50-52] The deposition has been studied on Au and Cu substrates. It has been concluded that

Cu substrates are more suitable for this purpose because it has higher hydrogen overpotential, which turned out to be of significant importance in the beginning of the deposition. The deposits that have been grown on Au substrates were patchy and not as thick as on Cu. The usual deposition of the Ge film utilizing E-ALD would be started by deposition a self-limited Ge layer at -1.4 V first. It should be noted the Ge solution pH in these studies was 9.2. Next, Te layer is deposited at -700 mV, and after exchange of the solution from Te to a blank one, the potential is stepped to -900 mV, where Te is reductively stripped, leaving behind only atomic layer of Te. It should be noted, that the solutions are exchanged in the cycle without losing the potential control. Then, Ge precursor solution is introduced and the potential stepped to -1.4 V to deposit Ge on the Te atomic layer. Then solution is exchanged to a blank one, and the potential is stepped to -1.6 V. At this step the Te layer should reductively be stripped, leaving behind newly deposited Ge layer. The cycle can be repeated as many times as needed to grow Ge films with various thicknesses. At the time of the studies, [52] after performing Raman spectroscopy, it was concluded that the Ge films were amorphous in nature. After examining those deposits recently using micro-Raman it still was found that most of them still showed amorphous signal. However, in one of the samples there were a couple of spots where shift around 290 cm^{-1} was present. Figure 3.13 demonstrates a Raman spectra where a 290 cm^{-1}, shift for germanene, and a 300 cm^{-1}, a shift for Ge wafer, are plotted together. According to the theoretical reports, that shift corresponds to a “G-like” shift in germanene layer. [21-22] Moreover, Carim et al. have studied Ge electrodeposition onto surface-enhanced Raman spectroscopy (SERS)-active Au substrate, where no more than self-limited amount has been deposited. [65] Even though, they were not studying the

germanene formation they also have observed a 290 cm^{-1} shift after -1.2 V in pH 9.2 Ge solution.

Conclusion

The present paper has discussed electrochemical deposition of Ge onto Au and demonstrated the plausibility of germanene formation structure by electrochemical deposition in aqueous media. During initial Ge deposition 0.1 nm layer with “lines-like” features observed to be formed on Au surface. However, if the potential is not held for long time at the around -400 mV and moved to around -600 mV or -700 mV, visible modifications of the Au (111) herringbone reconstruction are found. It is hypothesized that observed changes on the Au surface are associated with either presence of Ge in the Au surface, or it is a result of some Ge species, as was observed in case of adsorption of some organic molecules. First visible Ge islands are observed to appear at around -700 mV. However, studies are showing that if Ge atoms are already present in the surface, Ge islands can be already observed as early as -400 mV. It also can be concluded that initial Ge deposition is somewhat unstable (around -700 or -800 mV), as “salt-like” formation were observed throughout the studies after the potential was stepped to these value. However, studies of more than a monolayer have showed that Ge deposit is more stable under the studied conditions. Moreover, a honeycomb-like structure was found to be formed. According to atomic resolution images, the atomic distances were found to be 0.44 ± 0.02 nm. However, as can be seen from the images, Ge domains look rather incoherent. Moreover, some rings have obviously more or less than 6 atoms. Micro-Raman of one of Ge deposits made with cycle “Bait and Switch”, utilizing Te layer

deposition to help Ge to be deposited and sequential Te stripping, have showed Raman peak around 290 cm^{-1} that corresponds to theoretically predicted one.

The future directions of the current research will be associated with further investigations of mechanisms of germanium electrodeposition by means of EC-STM and micro–Raman flow cell. It is fundamental to understand the nature of the transition between less than a monolayer and more than a monolayer structures as this will help in formation of more coherent domains of germanene structure. It would be also interesting to know what role alloy between Ge and Au atoms plays. It is hypothesized, that formation of the Ge islands has been initiated on the surface where Ge is already present, thus providing a better crystal lattice matches. Furthermore, Ge thick film growth will be studied further, by varying the parameters of the cycle, such as potentials, time hold, and others. Micro-Raman will be used to investigate the structure of the Ge thick film to look for the 290 cm^{-1} shift. Furthermore, it is also interesting to know how Raman spectrum will change for germanene with variation of the thickness, as observed in graphene. [66]

Acknowledgements

Support from the National Science Foundation, DMR #1410109, is gratefully acknowledged.

References

1. Dimoulas, A., Silicene and germanene: Silicon and germanium in the "flatland". *Microelectron Eng* **2015,** *131*, 68-78.

2. Balendhran, S.; Walia, S.; Nili, H.; Sriram, S.; Bhaskaran, M., Elemental Analogues of Graphene: Silicene, Germanene, Stanene, and Phosphorene. *Small* **2015,** *11* (6), 640-652.

3. Kaneko, S.; Tsuchiya, H.; Kamakura, Y.; Mori, N.; Ogawa, M., Theoretical performance estimation of silicene, germanene, and graphene nanoribbon field-effect transistors under ballistic transport. *Appl. Phys. Express* **2014,** *7* (3), 035102/1-035102/4, 4 pp.

4. Zhu, Y.; Murali, S.; Cai, W.; Li, X.; Suk, J. W.; Potts, J. R.; Ruoff, R. S., Graphene and Graphene Oxide: synthesis, Properties, and Applications. *Adv. Mater. (Weinheim, Ger.)* **2010,** *22* (35), 3906-3924.

5. Novoselov, K. S.; Geim, A. K.; Morozov, S. V.; Jiang, D.; Zhang, Y.; Dubonos, S. V.; Grigorieva, I. V.; Firsov, A. A., Electric Field Effect in Atomically Thin Carbon Films. *Science (Washington, DC, U. S.)* **2004,** *306* (5696), 666-669.

6. Li, X.; Zhu, Y.; Cai, W.; Borysiak, M.; Han, B.; Chen, D.; Piner, R. D.; Colombo, L.; Ruoff, R. S., Transfer of Large-Area Graphene Films for High-Performance Transparent Conductive Electrodes. *Nano Lett.* **2009,** *9* (12), 4359-4363.

7. Li, D.; Mueller, M. B.; Gilje, S.; Kaner, R. B.; Wallace, G. G., Processable aqueous dispersions of graphene nanosheets. *Nat. Nanotechnol.* **2008,** *3* (2), 101-105.

8. Hu, S.; Wang, X., Ultrathin nanostructures: smaller size with new phenomena. *Chem. Soc. Rev.* **2013,** *42* (12), 5577-5594.

9. Aufray, B.; Kara, A.; Vizzini, S.; Oughaddou, H.; Leandri, C.; Ealet, B.; Le Lay, G., Graphene-like silicon nanoribbons on Ag(110): A possible formation of silicene. *Applied Physics Letters* **2010,** *96* (18).

10. Kara, A.; Enriquez, H.; Seitsonen, A. P.; Voon, L. C. L. Y.; Vizzini, S.; Aufray, B.; Oughaddou, H., A review on silicene - New candidate for electronics. *Surface Science Reports* **2012,** *67* (1), 1-18.

11. O'Hare, A.; Kusmartsev, F. V.; Kugel, K. I., A Stable "Flat" Form of Two-Dimensional Crystals: Could Graphene, Silicene, Germanene Be Minigap Semiconductors? *Nano Letters* **2012,** *12* (2), 1045-1052.

12. Cahangirov, S.; Topsakal, M.; Akturk, E.; Sahin, H.; Ciraci, S., Two- and One-Dimensional Honeycomb Structures of Silicon and Germanium. *Phys. Rev. Lett.* **2009,** *102* (23), 236804/1-236804/4.

13. Bechstedt, F.; Matthes, L.; Gori, P.; Pulci, O., Infrared absorbance of silicene and germanene. *Applied Physics Letters* **2012,** *100* (26).

14. Derivaz, M.; Dentel, D.; Stephan, R.; Hanf, M.-C.; Mehdaoui, A.; Sonnet, P.; Pirri, C., Continuous germanene layer on Al(111). *Nano Lett.* **2015,** *15* (4), 2510-2516.

15. Li, L.; Zhao, M., First-principles identifications of superstructures of germanene on Ag(111) surface and h-BN substrate. *Physical Chemistry Chemical Physics* **2013,** *15* (39), 16853-16863.

16. Kaloni, T. P.; Schwingenschlogl, U., Stability of germanene under tensile strain. *arXiv.org, e-Print Arch., Condens. Matter* **2013**, 1-11, arXiv:1311.2807v1 [cond-mat.mtrl-sci].

17. Ye, M.; Quhe, R.; Zheng, J.; Ni, Z.; Wang, Y.; Yuan, Y.; Tse, G.; Shi, J.; Gao, Z.; Lu, J., Tunable band gap in germanene by surface adsorption. *Phys. E (Amsterdam, Neth.)* **2014,** *59*, 60-65.

18. Pang, Q.; Zhang, C. L.; Li, L.; Fu, Z. Q.; Wei, X. M.; Song, Y. L., Adsorption of alkali metal atoms on germanene: A first-principles study. *Appl Surf Sci* **2014,** *314*, 15-20.

19. Wang, Y.; Ni, Z.; Liu, Q.; Quhe, R.; Zheng, J.; Ye, M.; Yu, D.; Shi, J.; Yang, J.; Li, J.; Lu, J., All-Metallic Vertical Transistors Based on Stacked Dirac Materials. *Adv. Funct. Mater.* **2015,** *25* (1), 68-77.

20. Houssa, M.; Pourtois, G.; Afanas'ev, V. V.; Stesmans, A., Electronic properties of two-dimensional hexagonal germanium. *Applied Physics Letters* **2010,** *96* (8).

21. Wei, W.; Dai, Y.; Huang, B.; Jacob, T., Many-body effects in silicene, silicane, germanene and germanane. *Physical Chemistry Chemical Physics* **2013,** *15* (22), 8789-8794.

22. Kaltsas, D.; Tsetseris, L., Stability and electronic properties of ultrathin films of silicon and germanium. *Physical Chemistry Chemical Physics* **2013,** *15* (24), 9710-9715.

23. Scalise, E.; Houssa, M.; Pourtois, G.; Broek, B.; Afanas'ev, V.; Stesmans, A., Vibrational properties of silicene and germanene. *Nano Res.* **2013,** *6* (1), 19-28.

24. Matthes, L.; Pulci, O.; Bechstedt, F., Massive Dirac quasiparticles in the optical absorbance of graphene, silicene, germanene, and tinene. *Journal of Physics-Condensed Matter* **2013,** *25* (39).

25. Roome, N. J.; Carey, J. D., Beyond Graphene: Stable Elemental Monolayers of Silicene and Germanene. *ACS Appl. Mater. Interfaces* **2014,** *6* (10), 7743-7750.

26. Tchalala, M. R.; Enriquez, H.; Mayne, A. J.; Kara, A.; Dujardin, G.; Ali, M. A.; Oughaddou, H.; Iop, Atomic structure of silicene nanoribbons on Ag(110). *3rd International Meeting on Silicene (Ims-3)* **2014,** *491*.

27. Li, L.; Lu, S.-z.; Pan, J.; Qin, Z.; Wang, Y.-q.; Wang, Y.; Cao, G.-y.; Du, S.; Gao, H.-J., Buckled Germanene Formation on Pt(111). *Advanced Materials* **2014,** *26* (28), 4820-+.

28. Davila, M. E.; Xian, L.; Cahangirov, S.; Rubio, A.; Le Lay, G., Germanene: a novel two-dimensional germanium allotrope akin to graphene and silicene. *New J. Phys.* **2014,** *16* (Sept.), 095002/1-095002/10, 10 pp.

29. Bampoulis, P.; Zhang, L.; Safaei, A.; van Gastel, R.; Poelsema, B.; Zandvliet, H. J. W., Germanene termination of Ge2Pt crystals on Ge(110). *J. Phys.: Condens. Matter* **2014,** *26* (44), 442001/1-442001/5, 5 pp.

30. Tsai, H.-S.; Chen, Y.-Z.; Medina, H.; Su, T.-Y.; Chou, T.-S.; Chen, Y.-H.; Chueh, Y.-L.; Liang, J.-H., Direct formation of large-scale multi-layered germanene on Si substrate. *Phys. Chem. Chem. Phys.* **2015,** *17* (33), 21389-21393.

31. Bianco, E.; Butler, S.; Jiang, S.; Restrepo, O. D.; Windl, W.; Goldberger, J. E., Stability and Exfoliation of Germanane: A Germanium Graphane Analogue. *Acs Nano* **2013,** *7* (5), 4414-4421.

32. Jayakrishnan, S.; Pushpavanam, M.; Shenoi, B. A., Electrodeposition from organic solutions of metals that are difficult to deposit from aqueous solutions. *Surf. Technol.* **1981,** *13* (3), 225-40.

33. Szekely, G., Electrodeposition of germanium. *J. Electrochem. Soc.* **1951,** *98*, 318-24.

34. Lahiri, A.; Zein El Abedin, S.; Endres, F., UV-Assisted Electrodeposition of Germanium from an Air- and Water-Stable Ionic Liquid. *J. Phys. Chem. C* **2012,** *116* (33), 17739-17745.

35. Wu, M.; Brooks, N. R.; Schaltin, S.; Binnemans, K.; Fransaer, J., Electrodeposition of germanium from the ionic liquid 1-butyl-1-methylpyrrolidinium dicyanamide. *Phys. Chem. Chem. Phys.* **2013,** *15* (14), 4955-4964.

36. Wu, M.; Vanhoutte, G.; Brooks, N. R.; Binnemans, K.; Fransaer, J., Electrodeposition of germanium at elevated temperatures and pressures from ionic liquids. *Phys. Chem. Chem. Phys.* **2015,** *17* (18), 12080-12089.

37. Endres, F.; Schrodt, C., In situ STM studies on germanium tetraiodide electroreduction on Au(111) in the room temperature molten salt 1-butyl-3-methylimidazolium hexafluorophosphate. *Phys. Chem. Chem. Phys.* **2000,** *2* (24), 5517-5520.

38. Endres, F., Electrodeposition of a thin germanium film on gold from a room temperature ionic liquid. *Phys. Chem. Chem. Phys.* **2001,** *3* (15), 3165-3174.

39. Endres, F., Electrodeposition of nanosized germanium from GeBr4 and GeCl4 in an ionic liquid. *Electrochem. Solid-State Lett.* **2002,** *5* (3), C38-C40.

40. Endres, F.; Zein El Abedin, S., Nanoscale electrodeposition of germanium on Au(111) from an ionic liquid: an in situ STM study of phase formation. Part II. Ge from GeCl4. *Phys. Chem. Chem. Phys.* **2002,** *4* (9), 1649-1657.

41. Endres, F.; Zein El Abedin, S., Nanoscale electrodeposition of germanium on Au(111) from an ionic liquid: an in situ STM study of phase formation. Part I. Ge from GeBr4. *Phys. Chem. Chem. Phys.* **2002,** *4* (9), 1640-1648.

42. Mukhopadhyay, I.; Freyland, W., Thickness induced metal-nonmetal transition in ultrathin electrodeposited Ge films. *Chem. Phys. Lett.* **2003,** *377* (1,2), 223-228.

43. Al-Salman, R.; Mallet, J.; Molinari, M.; Fricoteaux, P.; Martineau, F.; Troyon, M.; El Abedin, S. Z.; Endres, F., Template assisted electrodeposition of germanium and silicon nanowires in an ionic liquid. *Phys. Chem. Chem. Phys.* **2008,** *10* (41), 6233-6237.

44. Jawad, M. J.; Hashim, M. R.; Ali, N. K.; Corcoles, E. P.; Sharifabad, M. E., An Alternative Method to Grow Ge Thin Films on Si by Electrochemical Deposition for Photonic Applications. *J. Electrochem. Soc.* **2012,** *159* (2), D124-D128.

45. Ke, J.; Bartlett, P. N.; Cook, D.; Easun, T. L.; George, M. W.; Levason, W.; Reid, G.; Smith, D.; Su, W. T.; Zhang, W. J., Electrodeposition of germanium from supercritical fluids. *Physical Chemistry Chemical Physics* **2012,** *14* (4), 1517-1528.

46. Huang, Q.; Bedell, S. W.; Saenger, K. L.; Copel, M.; Deligianni, H.; Romankiw, L. T., Single-crystalline germanium thin films by electrodeposition and solid-phase epitaxy. *Electrochem Solid St* **2007,** *10* (11), D124-D126.

47. Fahrenkrug, E.; Gu, J.; Jeon, S.; Veneman, P. A.; Goldman, R. S.; Maldonado, S., Room-Temperature Epitaxial Electrodeposition of Single-Crystalline Germanium Nanowires at the Wafer Scale from an Aqueous Solution. *Nano Lett.* **2014,** *14* (2), 847-852.

48. Mahenderkar, N. K.; Liu, Y.-C.; Koza, J. A.; Switzer, J. A., Electrodeposited germanium nanowires. *ACS Nano* **2014,** *8* (9), 9524-9530.

49. Carim, A. I.; Collins, S. M.; Foley, J. M.; Maldonado, S., Benchtop Electrochemical Liquid-Liquid-Solid Growth of Nanostructured Crystalline Germanium. *J. Am. Chem. Soc.* **2011,** *133* (34), 13292-13295.

50. Liang, X.; Jayaraju, N.; Thambidurai, C.; Zhang, Q.; Stickney, J. L., Controlled Electrochemical Formation of GexSbyTez using Atomic Layer Deposition (ALD). *Chem. Mater.* **2011,** *23* (7), 1742-1752.

51. Liang, X.; Kim, Y.-G.; Gebergziabiher, D. K.; Stickney, J. L., Aqueous Electrodeposition of Ge Monolayers. *Langmuir* **2010,** *26* (4), 2877-2884.

52. Liang, X.; Zhang, Q.; Lay, M. D.; Stickney, J. L., Growth of Ge Nanofilms Using Electrochemical Atomic Layer Deposition, with a "Bait and Switch" Surface-Limited Reaction. *J. Am. Chem. Soc.* **2011,** *133* (21), 8199-8204.

53. Clavilier, J.; Faure, R.; Guinet, G.; Durand, R., Preparation of monocrystalline platinum microelectrodes and electrochemical study of the plane surfaces cut in the direction of the {111} and {110} planes. *J. Electroanal. Chem. Interfacial Electrochem.* **1980,** *107* (1), 205-9.

54. Allongue, P.; Cagnon, L.; Gomes, C.; Gundel, A.; Costa, V., Electrodeposition of Co and Ni/Au(111) ultrathin layers. Part I: nucleation and growth mechanisms from in situ STM. *Surface Science* **2004,** *557* (1-3), 41-56.

55. Nahas, Y.; Repain, V.; Chacon, C.; Girard, Y.; Rousset, S., Interplay between ordered growth and intermixing of Pt on patterned Au surfaces. *Surf. Sci.* **2010,** *604* (9-10), 829-833.

56. Campiglio, P.; Repain, V.; Chacon, C.; Fruchart, O.; Lagoute, J.; Girard, Y.; Rousset, S., Quasi unidimensional growth of Co nanostructures on a strained Au(111) surface. *Surf. Sci.* **2011,** *605* (13-14), 1165-1169.

57. Besenbacher, F.; Lauritsen, J. V.; Linderoth, T. R.; Laegsgaard, E.; Vang, R. T.; Wendt, S., Atomic-scale surface science phenomena studied by scanning tunneling icroscopy. *Surface Science* **2009,** *603* (10-12), 1315-1327.

58. Baber, A. E.; Tierney, H. L.; Sykes, E. C. H., Atomic-Scale Geometry and Electronic Structure of Catalytically Important Pd/Au Alloys. *ACS Nano* **2010,** *4* (3), 1637-1645.

59. Sun, J. T.; Gao, L.; He, X. B.; Cheng, Z. H.; Deng, Z. T.; Lin, X.; Hu, H.; Du, S. X.; Liu, F.; Gao, H. J., Surface reconstruction transition of metals induced by molecular adsorption. *Phys. Rev. B: Condens. Matter Mater. Phys.* **2011,** *83* (11), 115419/1-115419/4.

60. Hai, N. T. M.; Van der Auweraer, M.; Mullen, K.; De Feyter, S., Self-Assembly of a Functionalized Alkylated Isophthalic Acid at the Au(111)/Electrolyte Interface: Structure and Dynamics. *J Phys Chem C* **2009,** *113* (27), 11567-11574.

61. Sun, L.; Banhart, F.; Warner, J., Two-dimensional materials under electron irradiation. *MRS Bull.* **2015,** *40* (1), 29-37.

62. Ajayan, P. M.; Yakobson, B. I., Graphene. Pushing the boundaries. *Nat. Mater.* **2011,** *10* (6), 415-417.

63. Huang, P. Y.; Ruiz-Vargas, C. S.; van der Zande, A. M.; Whitney, W. S.; Levendorf, M. P.; Kevek, J. W.; Garg, S.; Alden, J. S.; Hustedt, C. J.; Zhu, Y.; Park, J.; McEuen, P. L.; Muller, D. A., Grains and grain boundaries in single-layer graphene atomic patchwork quilts. *Nature (London, U. K.)* **2011,** *469* (7330), 389-392.

64. Araujo, P. T.; Terrones, M.; Dresselhaus, M. S., Defects and impurities in graphene-like materials. *Mater. Today (Oxford, U. K.)* **2012,** *15* (3), 98-109.

65. Carim, A. I.; Gu, J.; Maldonado, S., Overlayer Surface-Enhanced Raman Spectroscopy for Studying the Electrodeposition and Interfacial Chemistry of Ultrathin Ge on a Nanostructured Support. *ACS Nano* **2011,** *5* (3), 1818-1830.

66. Green, A. A.; Hersam, M. C., Solution Phase Production of Graphene with Controlled Thickness via Density Differentiation. *Nano Lett.* **2009,** *9* (12), 4031-4036.

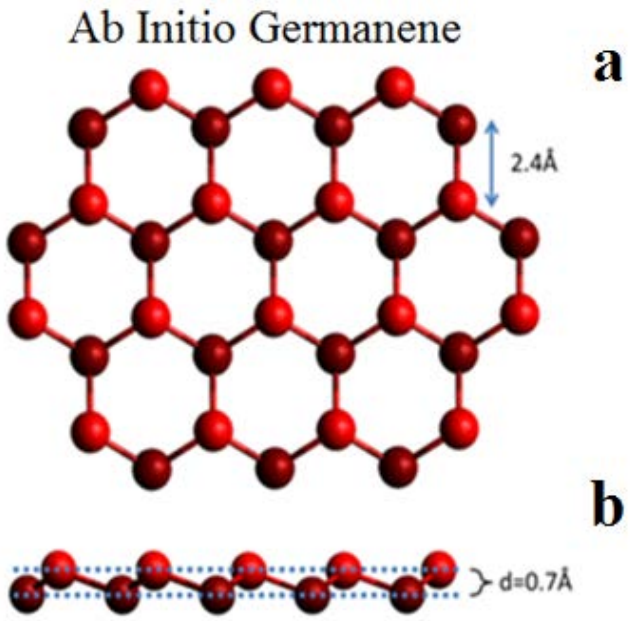

Figure 3.1. Proposed low buckled germanene structure. One half of the Ge atoms are 0.07 nm higher than the other half.

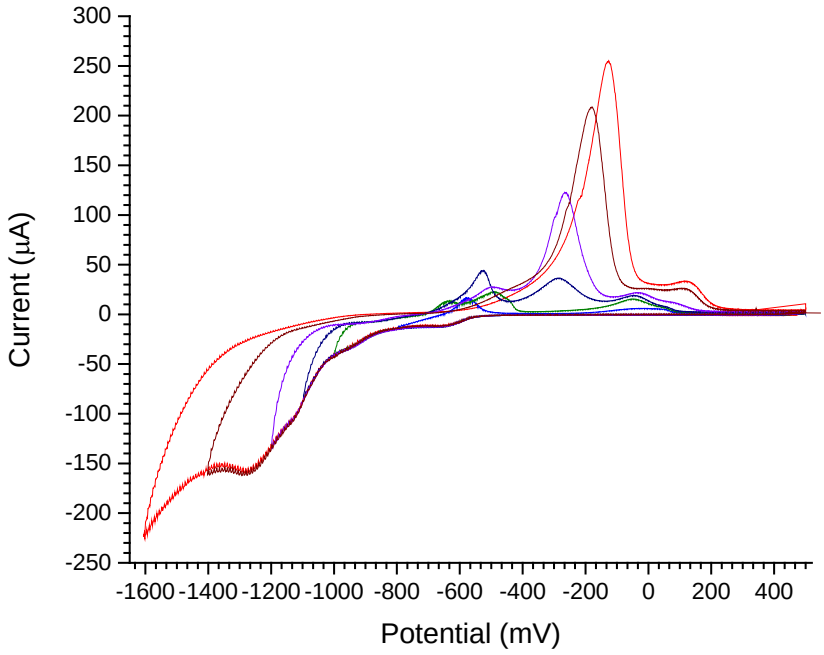

Figure 3.2. Window opening CVs of 0.5 mM GeO_2, 0.1 M $NaClO_4$ (pH 4.5) on a polycrystalline Au substrate from cathodic limits of -400 mV to -1600 mV while the anodic limit was kept to 500 mV for each cycle. The scan rate used was 10 mV/s.

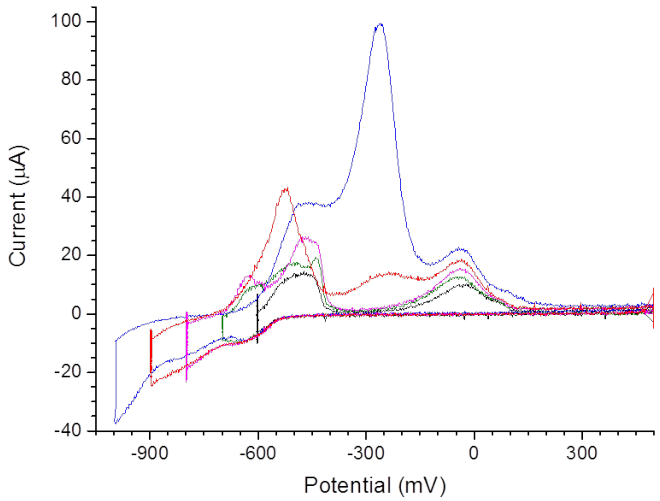

Figure 3.3. Window opening CVs of 0.5 mM GeO_2, 0.1 M $NaClO_4$ (pH 4.5) on a polycrystalline Au substrate from cathodic limits of -400 mV to -1000 mV, holding at these potentials for 700 sec, while the anodic limit was kept to 500 mV for each cycle. The scan rate used was 10 mV/s.

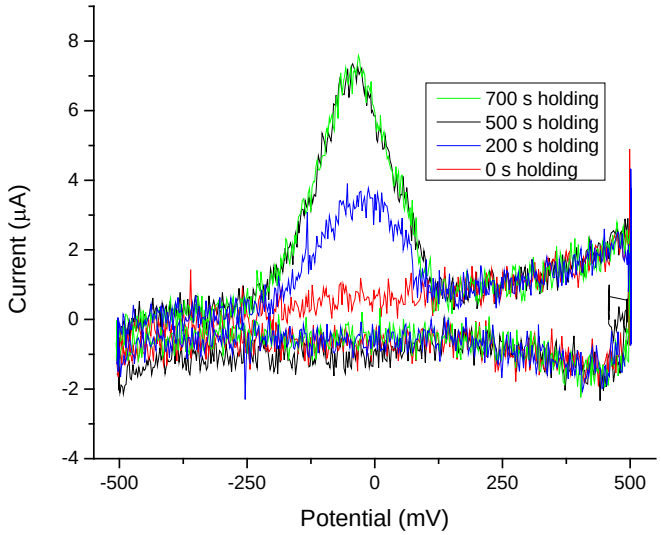

Figure 3.4. Oxidative stripping scans in 0.5 mM GeO_2, 0.1 M $NaClO_4$ (pH 4.7) on a polycrystalline Au substrate, after holding the potential at -500 mV for 0, 200, 500, or 700 s. The stripping scan was performed at 10 mV/s, without solution flowing in the electrochemical flow cell. Assuming a 4 e^- process, the oxidation peak at -50 mV indicated the presences of 0.062 ML of Ge after 700s & 500s, and 0.036 ML of Ge after 200s.

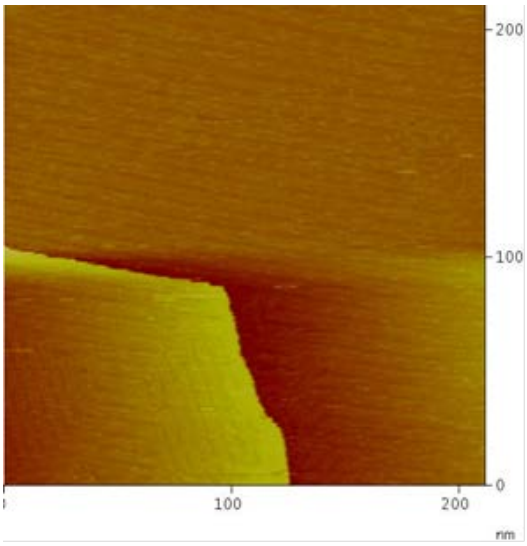

Figure 3.5. STM image of Au(111) herringbone reconstruction in 1 mM GeO_2 and 0.1 M $KClO_4$ (pH 4.2) before Ge deposition, at -300 mV vs Ag/AgCl.

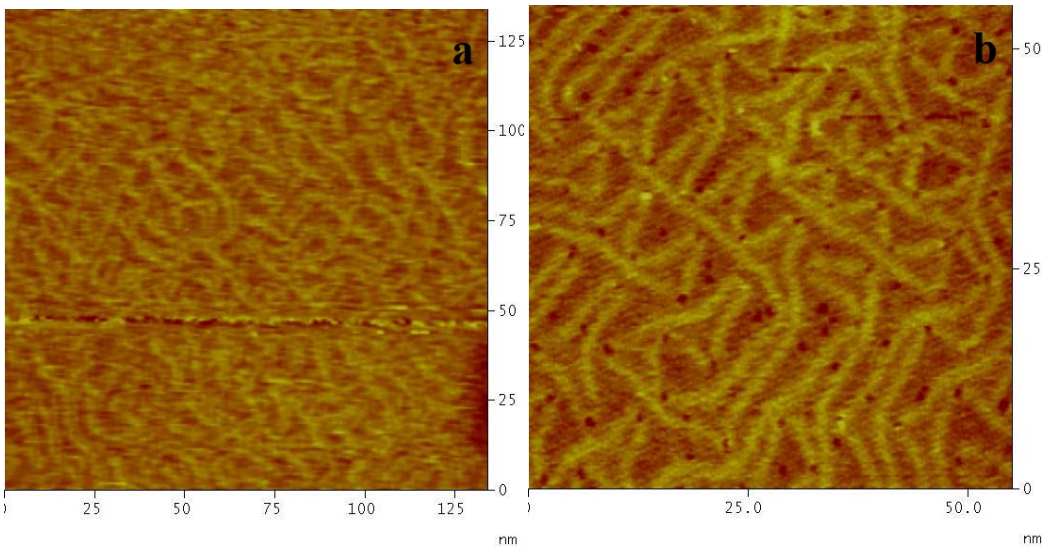

Figure 3.6. STM image of Au(111) in 1 mM GeO_2 and 0.1 M $KClO_4$ (pH 4.2) at -600 mV vs. Ag/AgCl.

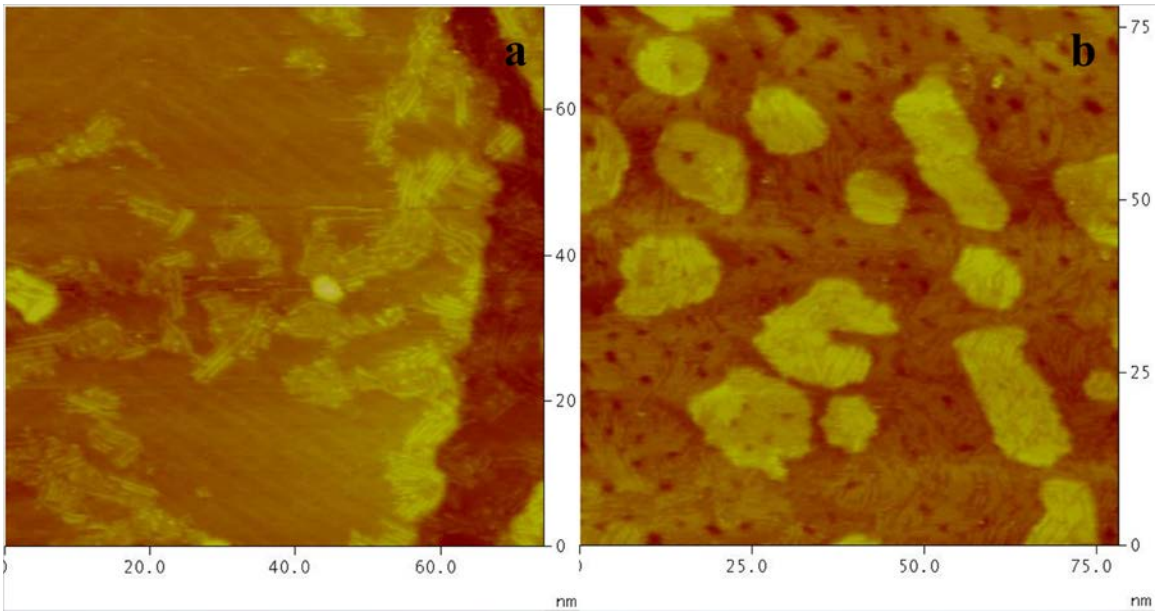

Figure 3.7. STM image of Au(111) in 1 mM GeO_2 and 0.1 M $KClO_4$ (pH 4.2) at – 400 mV vs. Ag/AgCl a) no pretreatment; b) after Ge was deposited and stripped, the potential was stepped to -400 mV vs. Ag/AgCl.

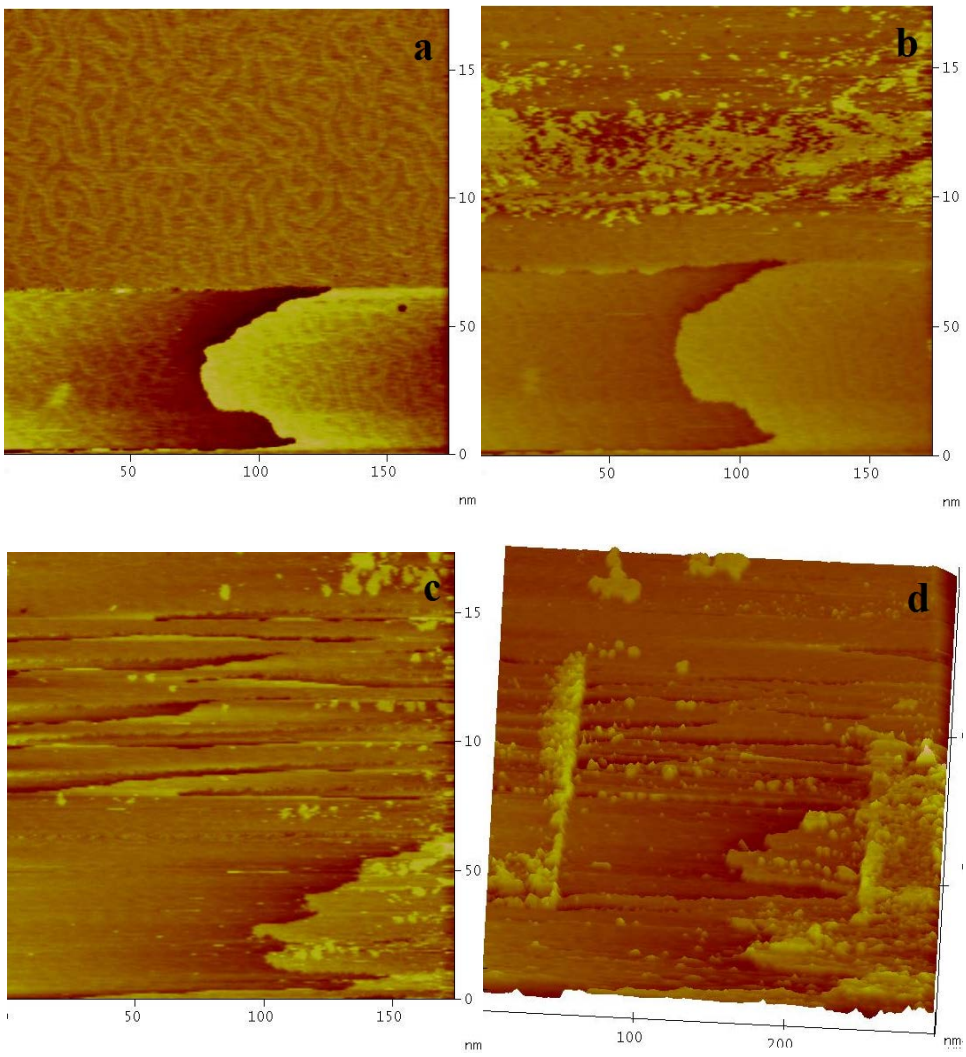

Figure 3.8. STM images of Au(111) in 1 mM GeO_2 and 0.1 M $KClO_4$ (pH 4.2) taken 30 s apart. a) at -600 mV vs. Ag/AgCl; b) after the potential was stepped to -700 mV; c) no change in conditions; d) no conditions were changed, however the scan area was expanded to show the piles of Ge.

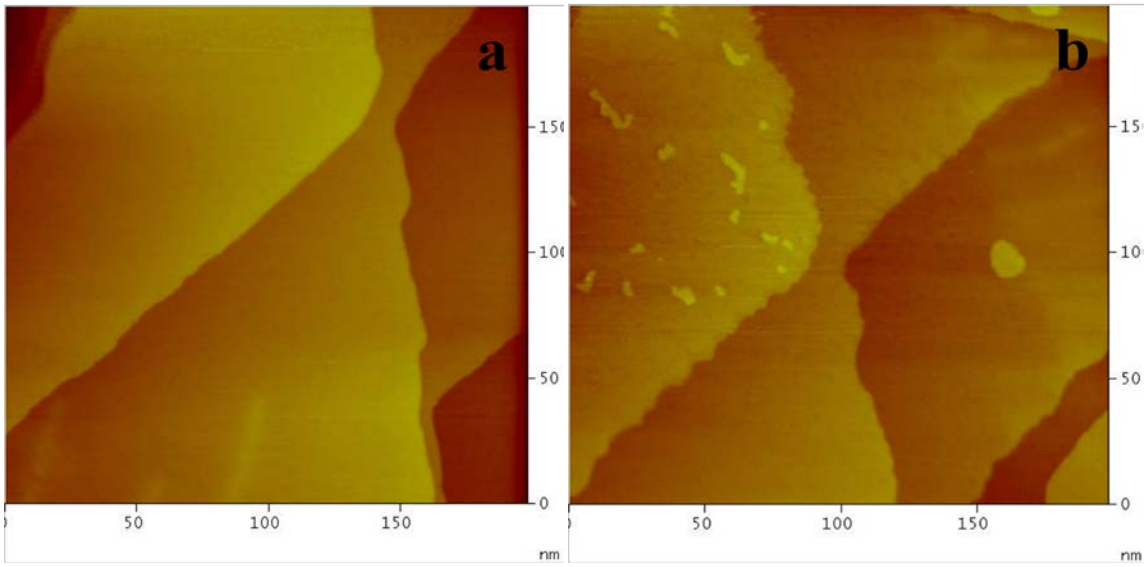

Figure 3.9. STM images of Au(111) in 1 mM GeO_2 and 0.1 M $KClO_4$ (pH 4.2). a) -400 mV; b) at -700 mV.

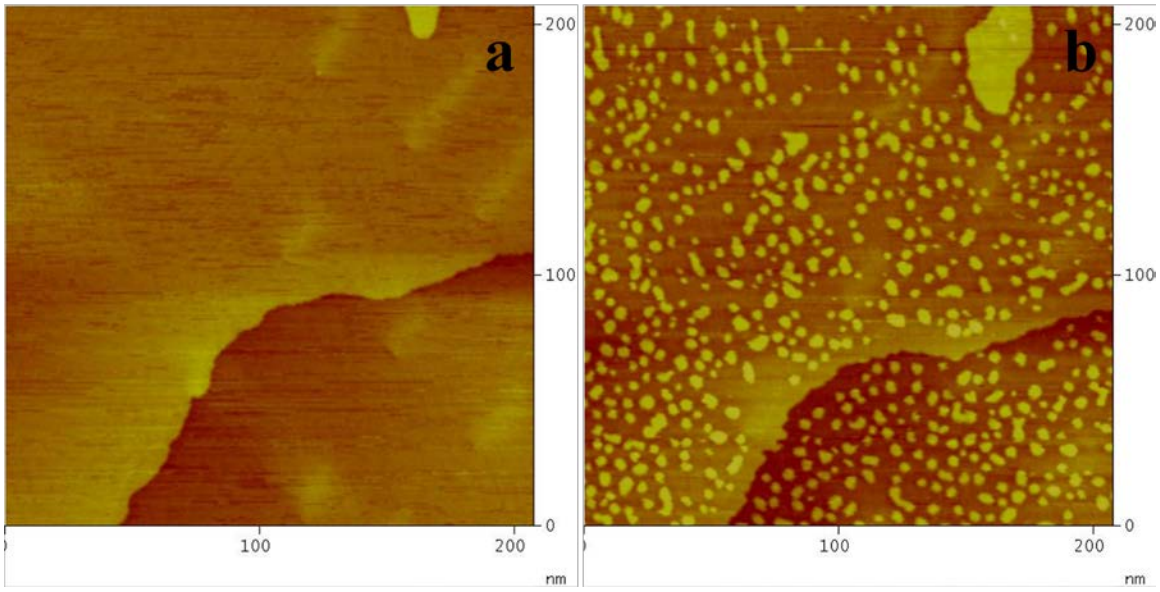

Figure 3.10. STM images of Au(111) in 1 mM GeO_2 and 0.1 M $KClO_4$ (pH 4.2). a) -300 mV; b) after 4 min at -400 mV.

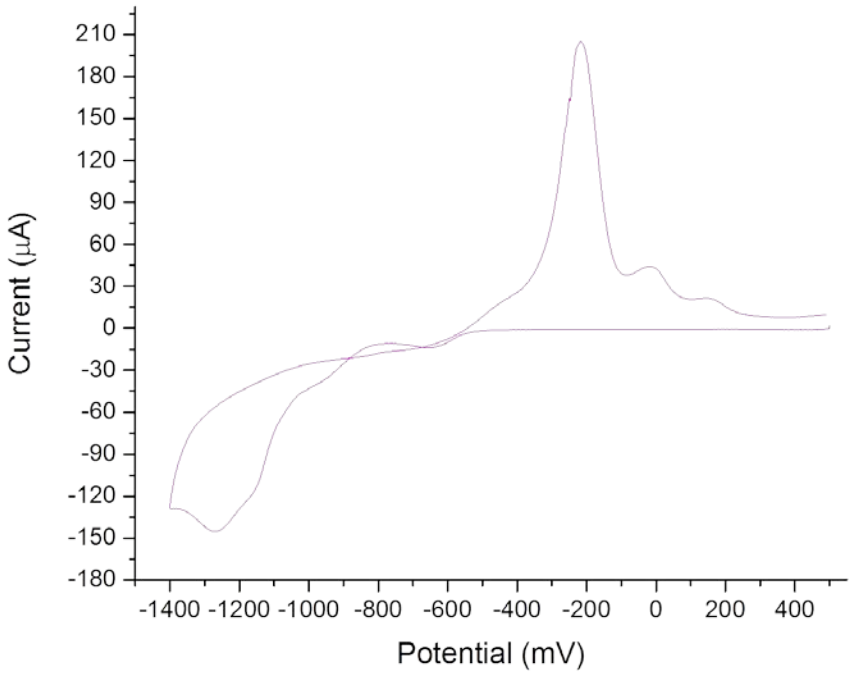

Figure 3.11. CV of Au electrode in 0.5 mM GeO_2, 0.1 M $NaClO_4$ (pH 4.5).

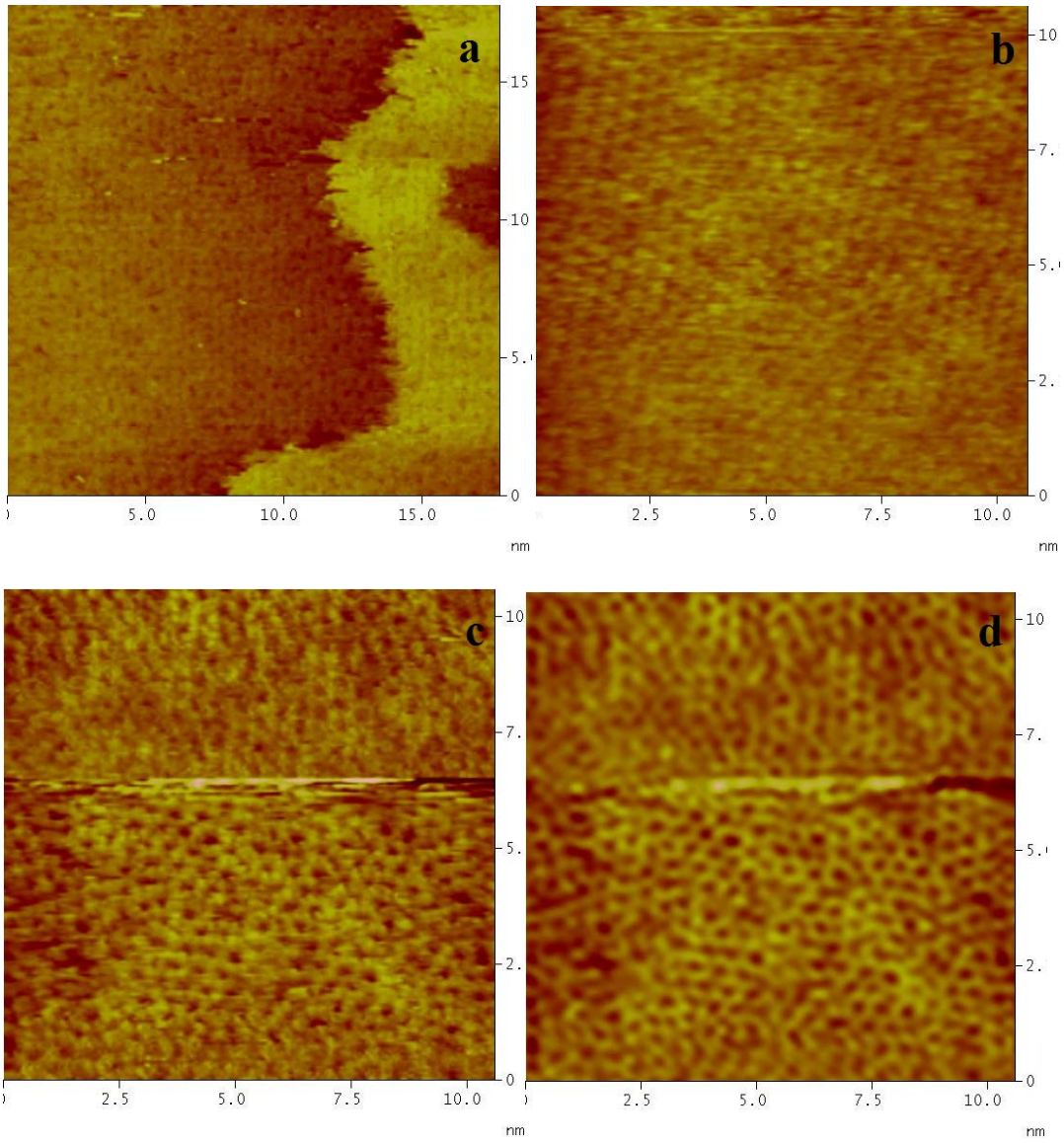

Figure 3.12. a-d are STM images of Au(111) in 1 mM GeO_2 and 0.1 M $KClO_4$ (pH 4.2) after the potential was scanned to -1.4 V and then to -900 mV vs Ag/AgCl. Atomic resolution on image b is 0.44 ± 0.02 nm. Image d is FFT processed image c to show honeycomb structure.

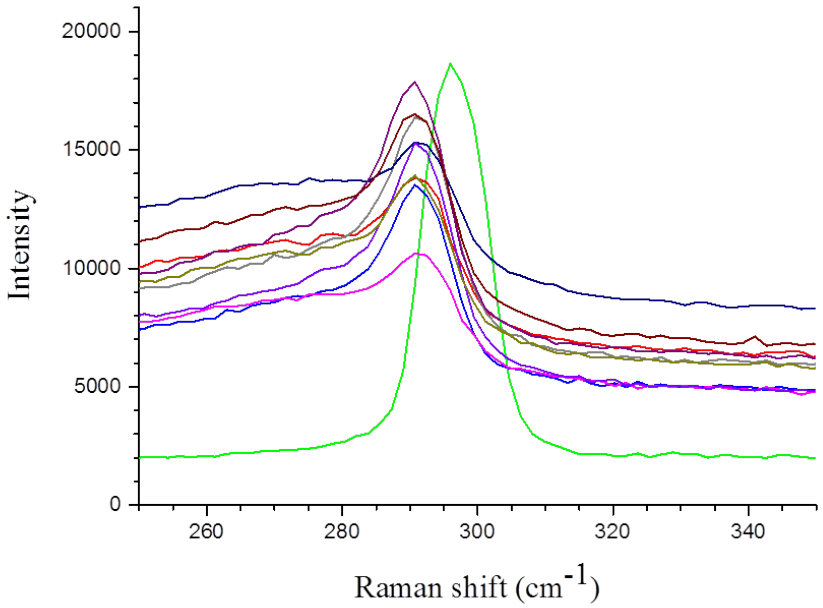

Figure 3.13. Raman spectra of Ge wafer (green line) and appearance of 290 cm^{-1} band for Ge deposit (other colors) corresponding to germanene. The 290 cm^{-1} band has only been observed in a very limited area of one sample.

CHAPTER 4

PRELIMINARY ELECTROCHEMICAL STUDIES OF TELLURIUM DEPOSITION ON GE(100) WAFER[1]

[1] M.A. Ledina and J.L. Stickney, To be submitted to *Journal of the Electrochemical Society*

Abstract

Electrochemical investigations into Te deposition were performed on Ge(100) wafer from solution at pH 9.1. Studies were done by means of cyclic voltammetry and ultrahigh vacuum surface (UHV) analysis techniques such as Low Energy Electron Diffraction (LEED) and Auger Electron Spectroscopy (AES), combined with electrochemical experiments (UHV-EC) without exposure of substrate to the air. A series of potentials was studied to identify where a self-limited Te atomic layer deposition takes place as well as where no Te would be present on the surface. LEED patterns of atomic layer Te terminated Ge surface was observed to show (1 × 1) structure. Te electrodeposition onto Ge wafer at around -0.6 V to about -0.85 V vs. Ag/AgCl resulted in Te bulk amount. At -0.94 V a reduction of Te bulk layer has produced an atomic layer of Te left on Ge surface. Finally, no Te signal according to AES was observed after deposition at -1.6 V and lower.

Introduction

Germanium is one of the important semiconductors and is becoming even more essential nowadays in electronics, for example, due to reaching a critical thickness of SiO_2. [1] However, since germanium does not have an oxide similar to that on Si, studies of Ge passivation have been performed and discussed in the literature. [2-3] A few reports were published about S terminated Ge surface. [4-5] Roche et al. have reported formation of S layer on top of Ge from an electrochemical cell attached to UHV system. [5] It was reported that at 200˚C, S-Ge reacted phase desorbs from surface, leaving behind a clean Ge surface. Another group, Fleischmann et al., have demonstrated studies of S monolayer

adsorption from $(NH_4)_2S$ solution also onto Ge(100) surface. It was identified that S forms bridge bonds to two Ge atoms, rather than to H. [6] Gregory et al. also showed studies for preparation of atomically smooth germanium substrates, where Te deposition from acidic solutions were also used onto Ge(111) surface to passivated it. It was reported that the Te layer was protecting the surface from oxidation which were demonstrated by Auger ratios values and in ex situ Scanning Tunneling Microscopy (STM) images. [7]

Tellurium deposition onto semiconductors is utilized for passivation of surfaces as well as for formation of compounds. [8-11] Tellurium electrodeposition onto Ge substrate can also be used as a sacrificial layer during electrochemical growth of Ge nanofilms from aqueous solution. [12] The electrodeposition of Ge from aqueous solution is known to be ceased due to Ge deposition thermodynamically occurring below hydrogen evolution. [13-15] Only a self-limited Ge layer can be deposited before HER (hydrogen evolution reaction) takes over. However, Liang et al. have developed a cycle where Ge nanofilms can be grown in aqueous media utilizing a Te layer to entice Ge to be deposited by electrochemical atomic layer deposition (E-ALD). [12] E-ALD is a method for nanofilms formation by usage of surface-limited reactions to grow films in a layer by layer manner. [10, 16-21] Surface-limited reactions usually referred to as underpotential deposition (UPD), a phenomenon where an atomic layer of one element is deposited on a second at a potential prior to (under) that needed form a bulk deposit of an element.

In the cycle[12] Te is deposited as a bulk amount first, and then is reductively stripped to obtain only an atomic layer on the surface. Ge is electrodeposited on Te atomic layer, which (Te atomic layer) is then reductively stripped from the surface as Te^{-2}

soluble species, leaving behind newly deposited Ge. The cycle is repeated as many times as needed to grow various thicknesses Ge films. However, some films grown utilizing this cycle have produced patchy deposits, especially on Au substrates. The most probable reason for formation of such films on Au is low hydrogen overpotential, since to reductively and completely strip Te atomic layer from the surface, a very negative potential (-1.6 V vs. Ag/AgCl) is needed to be used. However, Ge deposits grown on Cu substrate were a better quality, since Cu has higher hydrogen overpotential. Moreover, one of Ge nanofilms grown on Cu substrate showed a Raman signal for a germanene structure, which is a 2D honeycomb structure of germanium similar to graphene. [22]

An attempt is made in the present report to better understand the nature of Te electrodeposition onto Ge surface utilizing UHV surface characterization techniques combined with electrochemical experiments. The identification of better conditions for Te atomic layer formation is needed to improve the quality of Ge nanofilms growth.

Experimental

Experiments were performed in ultrahigh vacuum (UHV) system coupled through a 4.5″ gate valve with antechamber. The main chamber (UHV chamber, base pressure was usually about 1×10^{-9} Torr) was equipped with surface analysis instrumentation to conduct Auger Electron Spectroscopy or AES (Perkin-Elmer) and Low Energy Electron Diffraction or LEED (Princeton Research Instruments, Inc.). The electrochemical experiments were performed in antechamber backfilled to an atmospheric pressure with Ultrahigh Purity (UHP) Ar gas. A routine procedure was usually started from immersing a clean substrate (working electrode) into the electrochemical cell with solution of

interest which contained Ag/AgCl (Basi, 3 M NaCl) and gold wire as a reference and an auxiliary electrodes, respectfully. All potentials reported here are vs. Ag/AgCl. After the experiment was finished the electrochemical cell was removed, and antechamber was pumped down to UHV to match the pressure in the UHV chamber. Then the substrate was transferred through the gate valve into the main chamber, thus without exposure to air, where the surface analysis was performed. After the surface characterization was finished the substrate was cleaned with Ar^+ -ion bombardment and annealed to be used in next experiment.

N-type Ge(100) single crystal wafer was used as a substrate for Te deposition studies. The wafer, initially covered with SiO_2, was treated in 10% HF to etch the protective oxide and rinsed with DI water. Then the wafer was ultrasonically cleaned in acetone and in DI water. The Ge substrate top part was wrapped with Au foil (for an ohmic contact) and was put between two molybdenum plates, which were then attached with tungsten wire to a puck. [8] Furthermore, the wafer was UV ozone cleaned in order to oxidize any carbon contaminations left. The oxidized substrate was then transferred into the antechamber backfilled with UHP Ar gas through a transporter. The oxidized surface was electrochemically reduced and, after the antechamber was pumped down, transferred into the main chamber where it was cleaned with Ar^+ -ion bombardment and annealed.

Chemicals used were reagent grade or better. Blank and Te solutions (pH 9.1) contained 30 mM potassium perchlorate (Aldrich) as a supporting electrolyte and 1mM sodium borate as a buffer, as well as 0.1 mM TeO_2 (Aldrich) in Te one. The solutions were made with ultrapure DI water filtered with Milipore-Q System (> 18 MΩ). All solutions were purged for at least 30 min with UHP Ar gas prior the experiment in order

to exclude oxygen content. μAutolab type-III was utilized for all electrochemical experiments.

Results and discussions

Figure 4.1 demonstrates a LEED pattern of clean Ge(100) (2 × 1) wafer, typical reconstructed surface for Ge(100), [23-24] which was routinely obtained after hot IBB, during which the substrate was cleaned by Ar^{+} -ion bombardment and annealed at the same time, before every experiment. Figure 4.2 shows a cyclic voltammogram (CV) of Ge(100) wafer in 0.1 mM Te solution (pH 9.1). Two reductive peaks were identified in CV. The first peak, which centers at about -0.75 V, corresponds to reduction of Te^{+4} (tellurite) species to Te^{0}. The second peak at -0.94 V is assigned to a formation of soluble telluride species, Te^{-2}. The reduction that starts at -0.96 V is due to HER (Hydrogen evolution reaction). The potential on Figure 4.2 was scanned up to -1.6 V and scanned back to -1.1 V (not shown). The substrate then was emersed from Te solution and transferred to the main chamber. At -1.1 V only a Te atomic layer should be present on the surface since the potential was not scanned more positive than -1.1 V. Figure 4.3 demonstrates a LEED pattern after the substrate was taken out at -1.1 V at the same electron energy as the LEED pattern of clean Ge(100) wafer. As can be seen instead of (2 × 1) a (1 × 1) structure is obtained. Similar reconstruction structure has been observed in case of sulfur terminated Ge(100) surface. [5] Figure 4.4 shows an Auger spectrum of Ge(100) wafer covered with Te atomic layer with assigned peaks where each element produced a peak. Spectrum shows presence of oxygen, since not the whole Ge surface was covered with Te, as well as chlorine and potassium, which are due traces of

electrolyte present on the surface (from potassium perchlorate). It should be noted, though, that sensitivities for Cl and K are more twice as higher than for Te signal.

It should be noted that no UPD Te peaks were observed in CV on Ge(100) wafer contrary to the studies on Au surfaces. [18] Peak for Te electrodeposition at -0.75 V discussed earlier corresponds to formation of bulk Te which was confirmed by a series of CVs in Figure 4.5. The last demonstrates window opening CVs in a negative direction, where for all scans positive limit was -0.6 V and negative limit was decreased by -0.1 V for every new scan, starting from -0.7 V and finishing at -1.1 V. As can be seen in black, red and blue scans, reduction currents were decreasing with time for every new scan, however, still observed, which means Te was still being deposited. After the potential was scanned to -1 V, a large reductive peak was observed. However, in the next scan, after the potential was scanned to -1.1 V, the peak at -0.94 V was more than 4 times smaller. As the potential was scanned several times through -0.75 V before going more negative than -0.85 V, Te^0 was continuing to form on the surface, an when the potential was finally scanned through -0.94 V, bulk Te was reduced to telluride, soluble species, leaving behind an atomic layer. Thus it is no surprise that during the next scan to -1.1 V, since less Te was deposited onto the surface during green scan, the reductive peak shows up smaller.

To understand the dependence of Te amount deposition versus applied potential in Te solution pH 9.1, a series of experiments was performed. First, Ge wafer was cleaned according to the procedure described before, after which same as LEED pattern shown in Figure 4.1 and same as Auger spectrum in Figure 4.6a were obtained. Then the substrate was immersed into Te solution and potential was stepped to a certain chosen

value for 3 min. After holding a potential was finished the substrate was rinsed twice with DI water to wash off traces of electrolyte and transported into the main chamber to obtain LEED pattern and Auger spectrum. The studied potentials were in the range from -0.5 V and till -1.8 V. At potentials higher than -0.5 V oxidative currents were observed due to Ge oxidation. Figure 4.6 shows Auger spectra b-e after holding the potentials at -0.5 V, -0.7 V, -0.95 V and -1.6 V, respectfully. In the spectra the increase of Te signal at 483 eV until -0.7 V can be clearly seen and then sequential decrease at lower potentials. Figure 4.7 shows Auger ratios for Te/Ge and O/Ge vs. different potentials applied, where ratios were calculated from Auger spectra some of which were shown in Figure 4.6. Figure 4.7 shows volcano-like shape of Te/Ge graph which peaks at a ratio of about 1.2 at -0.7 V. The ratios at -0.5 V and -0.9 V and -0.95 V were found to be very close. However, it is known that kinetics for Te deposition is slow and longer times can be applied to deposit more at initial potentials. The ratios at -0.9 V and -0.95 V, on the other hand, are self-limited. Moreover, the Te/Ge ratios were decreasing as more negative potentials were used. Partially it might be associated with hydrogen evolution process faster kinetics, and hence being the preferred reaction. Furthermore, no Te signal was observed after -1.6 V. The ratios for O/Ge were around 0.1-0.2 and no particular dependence was observed. It should be noted, though, that no thick GeO layer should be formed because GeO is soluble in water. [3] Thus

Conclusion

The present paper reports the results for studies of Te electrodeposition onto Ge(100) wafer from pH 9.1 solution at various potentials. The particular results are of

interest for its use in Ge nanofilm growth cycle where Te is deposited as a sacrificial layer and after a new layer of Ge is deposited onto it, stripped, leaving behind newly deposited Ge. Thus, by repeating the cycle a Ge nanofilm can be grown in aqueous media. Thus it is necessary to identify the potentials where a self-limited amount of Te will be formed and where no Te will be left on the Ge surface. Electrochemical deposition of Te was studied without exposure to air by ultrahigh vacuum characterization techniques as LEED and AES. LEED pattern of Te atomic layer on Ge(100) wafer demonstrated (1 × 1) reconstruction. It was identified that bulk amount of Te is deposited before -0.85 V, whereas a self-limited amount of Te can be obtained at about -0.94 V. No Te was observed according to Auger spectra after -1.6 V.

Acknowledgements

Support from the National Science Foundation, DMR #1410109, is gratefully acknowledged.

References

1. Kamata, Y., High-k/Ge MOSFETs for future nanoelectronics. *Mater. Today (Oxford, U. K.)* **2008,** *11* (1-2), 29-38.

2. Fleischmann, C.; Schouteden, K.; Merckling, C.; Sioncke, S.; Meuris, M.; Van Haesendonck, C.; Temst, K.; Vantomme, A., Adsorption of O2 on Ge(100): Atomic Geometry and Site-Specific Electronic Structure. *J. Phys. Chem. C* **2012,** *116* (18), 9925-9929.

3. Okumura, H.; Akane, T.; Matsumoto, S., Carbon contamination free Ge(100) surface cleaning for MBE. *Appl. Surf. Sci.* **1998,** *125* (1), 125-128.

4. Rohlfing, M.; Krueger, P.; Pollmann, J., Quasiparticle band structures of clean, hydrogen-, and sulfur-terminated Ge(001) surfaces. *Phys. Rev. B: Condens. Matter* **1996,** *54* (19), 13759-13766.

5. Roche, J.; Ryan, P.; Hughes, G. J., Core level photoemission studies of the sulphur terminated Ge(100) surface. *Appl. Surf. Sci.* **2001,** *174* (3-4), 271-274.

6. Fleischmann, C.; Houssa, M.; Muller, M.; Beckhoff, B.; Boyen, H.-G.; Meuris, M.; Temst, K.; Vantomme, A., Liquid-Phase Adsorption of Sulfur on Germanium: Reaction Mechanism and Atomic Geometry. *J. Phys. Chem. C* **2013,** *117* (15), 7451-7458.

7. Gregory, B. W.; Thomas, S.; Stephens, S. M.; Dluhy, R. A.; Bottomley, L. A., Preparation of Atomically Smooth Germanium Substrates for Infrared Spectroscopic and Scanning Probe Microscopic Characterization of Organic Monolayers. *Langmuir* **1997,** *13* (23), 6146-6150.

8. Kim, J. Y.; Stickney, J. L., Ultrahigh Vacuum Surface Studies of the Electrochemical Atomic Layer Deposition of Indium Telluride on n-Type GaAs(100). *J. Phys. Chem. C* **2008,** *112* (15), 5966-5971.

9. Gebregziabiher, D. K.; Ledina, M. A.; Preisser, R.; Stickney, J. L., Cu(111) surface passivation with atomic layers of Te, Se or I, studied using auger spectroscopy. *J. Electrochem. Soc.* **2012,** *159* (8), H675-H679.

10. Varazo, K.; Lay, M. D.; Sorenson, T. A.; Stickney, J. L., Formation of the first monolayers of CdTe on Au(111) by electrochemical atomic layer epitaxy (EC-ALE):

studied by LEED, Auger, XPS, and in-situ STM. *J. Electroanal. Chem.* **2002,** *522* (1), 104-114.

11. Vaidyanathan, R.; Cox, S. M.; Happek, U.; Banga, D.; Mathe, M. K.; Stickney, J. L., Preliminary Studies in the Electrodeposition of PbSe/PbTe Superlattice Thin Films via Electrochemical Atomic Layer Deposition (ALD). *Langmuir* **2006,** *22* (25), 10590-10595.

12. Liang, X.; Zhang, Q.; Lay, M. D.; Stickney, J. L., Growth of Ge Nanofilms Using Electrochemical Atomic Layer Deposition, with a "Bait and Switch" Surface-Limited Reaction. *J. Am. Chem. Soc.* **2011,** *133* (21), 8199-8204.

13. Pourbaix, M., *Atlas of Electrochemical Equilibria in Aqueous Solutions*. Pergamon Press: 1966.

14. Liang, X.; Kim, Y.-G.; Gebergziabiher, D. K.; Stickney, J. L., Aqueous electrodeposition of Ge monolayers. *Langmuir* **2010,** *26* (4), 2877-84.

15. Carim, A. I.; Gu, J.; Maldonado, S., Overlayer Surface-Enhanced Raman Spectroscopy for Studying the Electrodeposition and Interfacial Chemistry of Ultrathin Ge on a Nanostructured Support. *ACS Nano* **2011,** *5* (3), 1818-1830.

16. Lister, T. E.; Colletti, L. P.; Stickney, J. L., Electrochemical formation of CdSe monolayers on the low index planes of Au. *Isr. J. Chem.* **1997,** *37* (2-3), 287-295.

17. Sorenson, T. A.; Varazo, K.; Suggs, D. W.; Stickney, J. L., Formation of and phase transitions in electrodeposited tellurium atomic layers on Au(111). *Surf. Sci.* **2001,** *470* (3), 197-214.

18. Lay, M. D.; Stickney, J. L., EC-STM Studies of Te and CdTe Atomic Layer Formation from a Basic Te Solution. *J. Electrochem. Soc.* **2004,** *151* (6), C431-C435.

19. Kim, Y.-G.; Kim, J. Y.; Vairavapandian, D.; Stickney, J. L., Platinum Nanofilm Formation by EC-ALE via Redox Replacement of UPD Copper: Studies Using in-Situ Scanning Tunneling Microscopy. *J. Phys. Chem. B* **2006,** *110* (36), 17998-18006.

20. Thambidurai, C.; Kim, Y.-G.; Stickney, J. L., Electrodeposition of Ru by atomic layer deposition (ALD). *Electrochim. Acta* **2008,** *53* (21), 6157-6164.

21. Sheridan, L. B.; Kim, Y.-G.; Perdue, B. R.; Jagannathan, K.; Stickney, J. L.; Robinson, D. B., Hydrogen Adsorption, Absorption, and Desorption at Palladium Nanofilms formed on Au(111) by Electrochemical Atomic Layer Deposition (E-ALD): Studies using Voltammetry and In Situ Scanning Tunneling Microscopy. *J. Phys. Chem. C* **2013,** *117* (30), 15728-15740.

22. Ledina, M.; Liang, X.; Kim, Y.-G.; Jung, J.; Perdue, B.; Tsang, C.; Soriaga, M. P.; Stickney, J. L., (Invited) Investigations into the Formation of Germanene Using Electrochemical Atomic Layer Deposition (E-ALD). *Ecs Transactions* **2015,** *66* (6), 129-140.

23. Cvetko, D.; Floreano, L.; Crottini, A.; Morgante, A.; Tommasini, F., Disordering of the Ge(001) surface studied by He atom scattering. *Surf. Sci.* **2000,** *447* (1-3), L147-L151.

24. Bock, W.; Gnaser, H.; Oechsner, H., Modification of crystalline semiconductor surfaces by low-energy argon(1+) bombardment: silicon(111) and germanium(100). *Surf. Sci.* **1993,** *282* (3), 333-41.

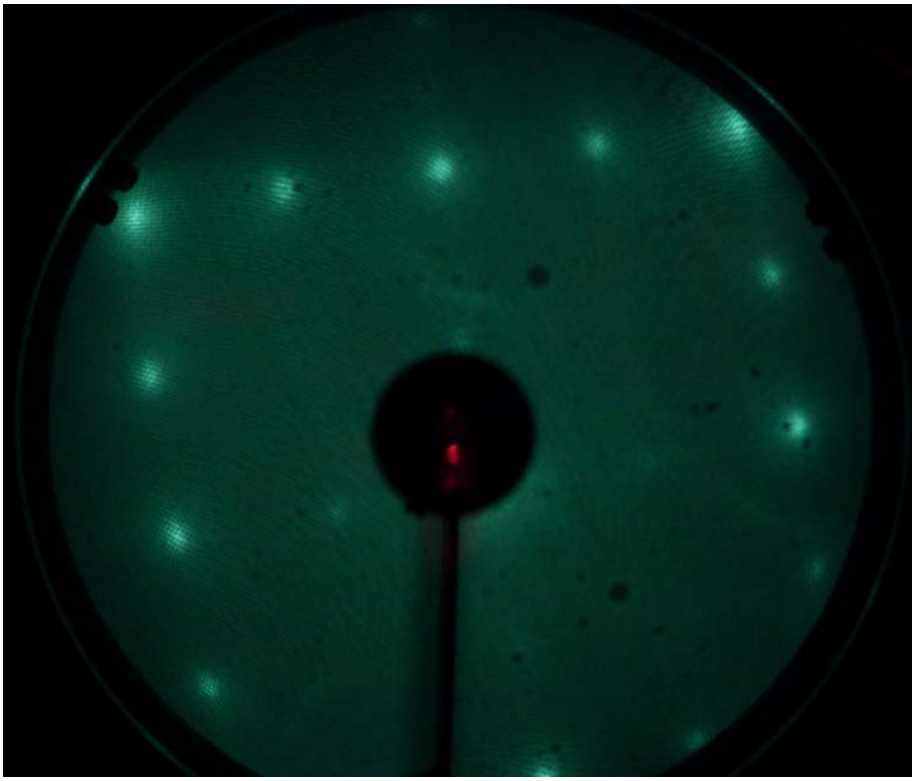

Figure 4.1. LEED pattern of clean Ge(100) (2 × 1) wafer. Electron energy for LEED was 39 eV.

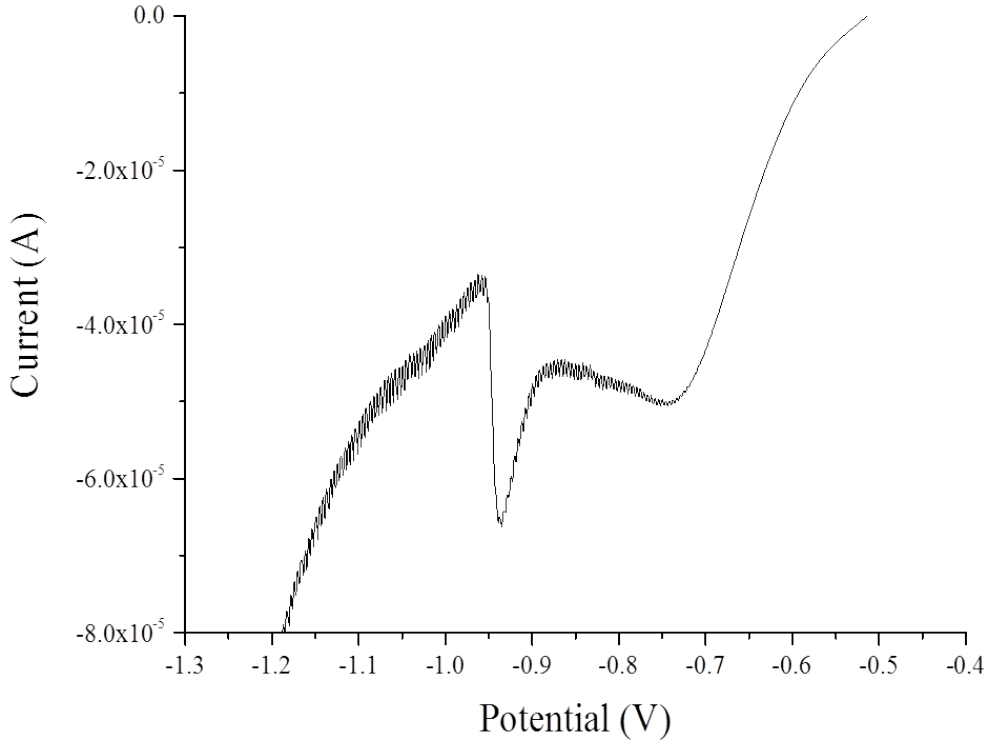

Figure 4.2. CV of Ge(100) wafer in 0.1 mM Te solution (pH 9.1).

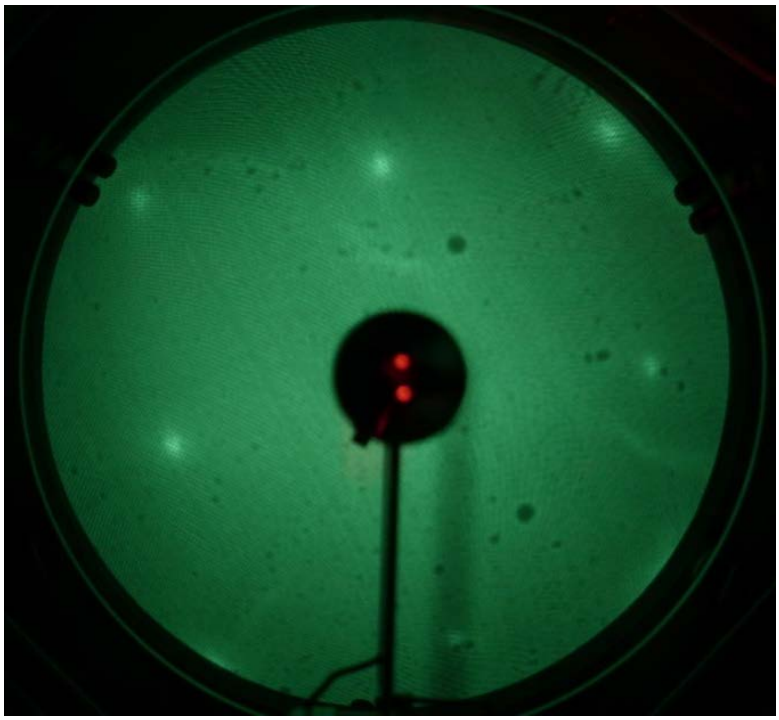

Figure 4.3. LEED pattern of Ge(100) wafer after CV in Te solution (pH 9.1). Electron energy for LEED was 41 eV.

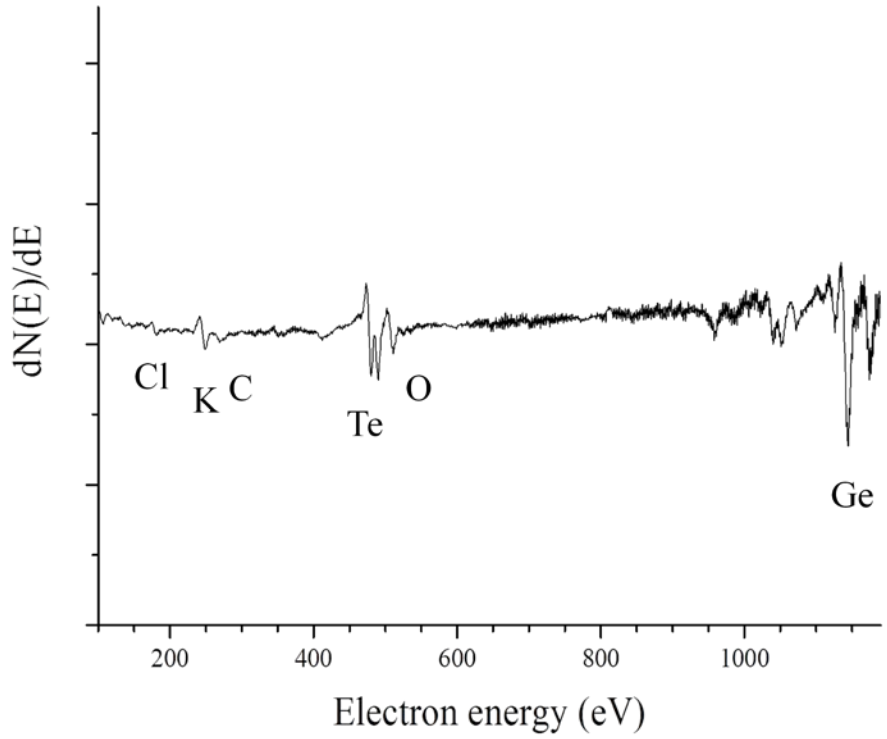

Figure 4.4. Auger spectrum of Ge(100) wafer after CV in Te solution (pH 9.1).

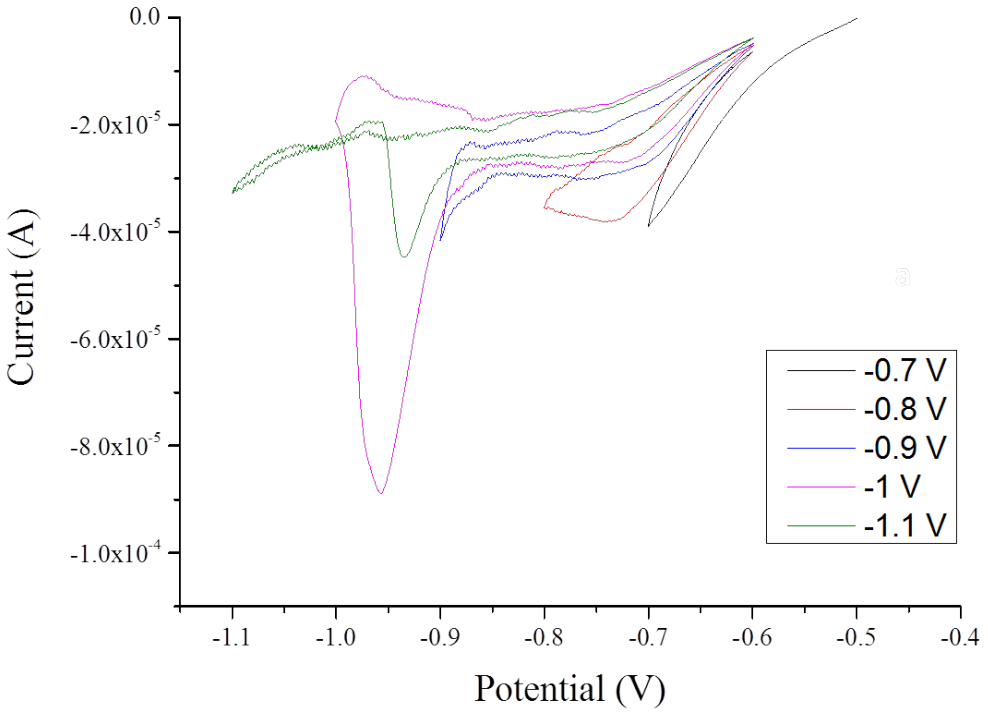

Figure 4.5. CVs of Ge(100) wafer in 0.1 mM Te solution (pH 9.1).

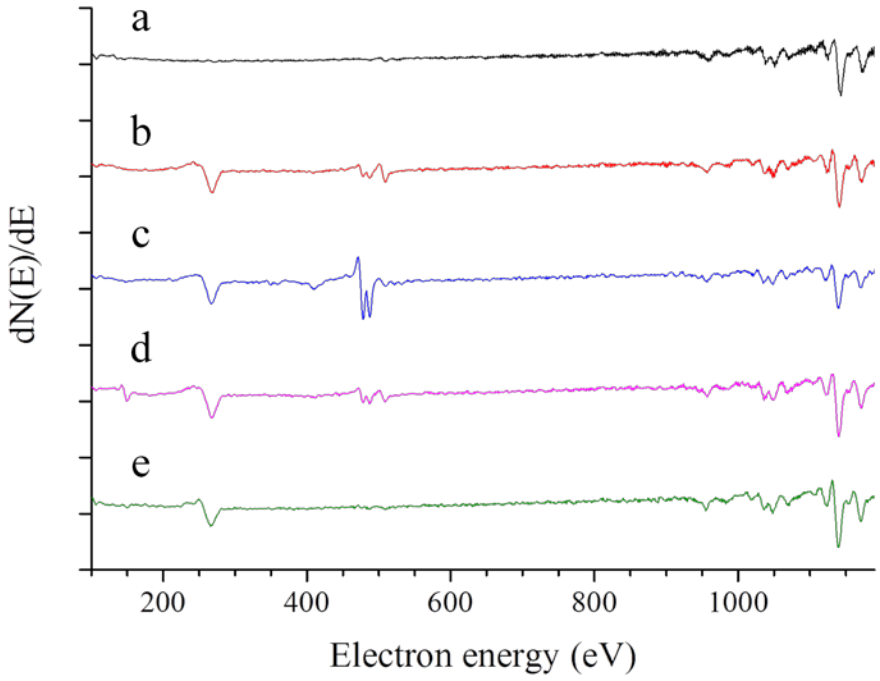

Figure 4.6. Auger spectra of Ge wafer. a). Clean surface; after 3 min in Te solution at b). -0.5 V, c). -0.7 V, d). -0.95 V, e). -1.6 V.

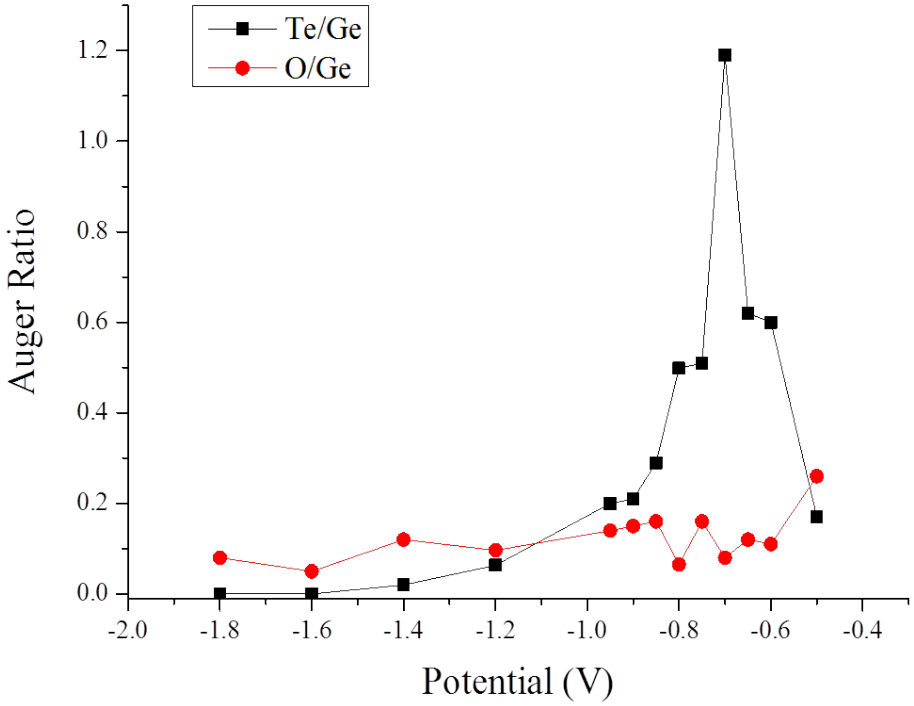

Figure 4.7. Auger ratios for Te/Ge and O/Ge after 3 min of Te deposition onto Ge(100) wafer at various potentials.

CHAPTER 5

CONCLUSION AND FUTURE STUDIES

The electrochemical studies of initial deposition of germanium as well as investigation into the formation of germanene performed by means of cyclic voltammetry, coulometry, electrochemical Scanning Tunneling Microscopy (EC-STM) and Raman Spectroscopy were discussed in this dissertation. The electrochemical nature of germanium is self-limited to only a couple of monolayers in aqueous solutions due to high overpotential of germanium deposition and low hydrogen overpotential. The self-limited coverage of germanium will depend on value of potential applied and the maximum coverage will be reached only when the potential is held at a particular value. Moreover, the total maximum coverage will also depend on the pH of the aqueous solution used, thus the maximum Ge deposition can be reached in pH 9.2 which will correspond to about 4 ML. Furthermore, electrochemical Te deposition onto Ge(100) wafer has been studied in aqueous solutions. The investigations were conducted in order to identify the potentials for a Te atomic layer formation on Ge surface as well as the potential where no Te is present on the surface.

Second chapter demonstrates results for the coverages less than a monolayer. It was found that alloy between Ge atoms and Au surface started to be formed as early as -300 mV vs. Ag/AgCl in pH 4.5 germanium solution. The alloy was identified as “lines”-like features formed in on the Au(111) herringbone surface, however, only if the potential was held long enough. The observed “lines” structures were tend to form in parallel

manner to each other rows the length of which was found to less than 10 nm. According to EC-STM images, the distances in between “lines” were measured to correspond to around 0.9 nm and the distances in between atoms were identified as 0.5 nm, or $\sqrt{3}$ relative to the Au(111) surface. The “lines” were observed to be forming up to -600 mV, after that the layer formed would look rough and none of the “lines” could have been differentiated. The height of that layer was measured to be about 0.1 nm. Moreover, if the potential would not be held at such initial for Ge deposition potentials the “lines” would not be observed. At -700 mV, where the coverage would correspond to a third of a monolayer relative to a Au(111) surface, the formation of holes would be observed, due to place exchange, which be increasing in size with time if the potential would be hold. These holes are where Ge atoms are intercalating into the Au surface. A modified Au(111) herringbone reconstructed surface has been observed in EC-STM images. Broken-like double ridges were identified on the images instead of normally looking double soliton walls of herringbone reconstruction which would only change its direction by 120˚. Even a more dramatically changed Au(111) reconstructed surface has been demonstrated. The double ridges were separated and the single soliton were forming triangles, the sides of which were in $[1\bar{1}0]$ direction instead of usual $[11\bar{2}]$ direction. This behavior implies that due to Ge species presence in the surface or Ge species adsorbed onto the Au have caused a relaxation of the Au herringbone reconstruction. Additionally, at the same potential, -700 mV, ribbons-like features were observed to be formed. However, interestingly, it was evident that no uplifting of the herringbone reconstruction has happened. Instead the ribbons were very mobile and were appearing and disappearing as the imaging process was taking place. It was also observed that the

ribbons were growing in string of what looked like molecules. The distance between the molecules in the ribbon was measure to be about 1 nm and the distance between the ribbons was identified around 1.1 nm. The alloy formed at -800 mV, the height of which was about 0.1 nm, was growing in a ”flower”-like manner, with pits-like features in the structure. The atomic distances in that alloy structure was found to be around 0.5 nm, and was close to correspond to $\sqrt{3} \times \sqrt{3}$ structure relative to the Au(111).

The third chapter demonstrates a continuation of electrochemical results with different coverages of Ge on Au(111) electrode. It was found that at -700 mV the Ge deposit formed, which is assigned to be alloy between Ge atoms and Au surface, seemed to be not stable and was easily swiped away from the imaged window. Such behavior was not once observed around -700 mV and -800 mV. It might be that the tunneling conditions of the tip might be causing the disruption of the grown Ge-Au alloy. Coverages of more than a monolayer were also studied in this chapter. In order to deposit a higher coverage the potential of the Au (working electrode) was scanned to -1.4 V and then scanned back to -0.9 V to avoid any other reactions happening on the substrate, such as reduction or oxidation processes. The observed EC-STM images demonstrated the height between two Ge layers was measured to be around 0.35 nm, which would be consistent with the buckled structure of germanene. Moreover, a honeycomb-like structure was obtained, where the distance between the holes corresponded to 0.44 ± 0.02 nm, which is very close to the values expected for germanene structure. However, it was also obvious from the EC-STM images the structure had multiple small domains, which means presence of a lot of domain boundaries in the deposit. Additionally, micro-Raman spectroscopy performed on one of the Ge nanofilms grown on copper substrate, showed a

shift that corresponded to the theoretically predicted one for germanene structure. Taking into account the EC-STM and Raman data, it is obvious that the quality of the deposits have to be improved in order to more consistently produce Raman signal.

The forth chapter discusses the electrochemical deposition of Te on Ge(100) wafer from pH 9.1 solution. The investigations were performed utilizing UHV characterization techniques such as AES and LEED after electrochemical experiment without exposure of the substrate to the air. LEED pattern of a Te atomic layer on Ge(100) (2 × 1) surface have demonstrated a (1 × 1) structure. The Auger ratios of Te/Ge after electrochemical experiment at a range of potentials have shown that Te bulk was formed between -0.6 V to -0.85 V, whereas the an atomic layer of Te has been formed at about -0.94 V. No Te signal was observed after Te deposition at -1.6 V and lower.

Future studies of the germanene formation will include EC-STM investigation of the structures that are formed in between -800 mV and -1.4 V in pH 4.7 germanium solution. Currently, it is not clear what is the transition between the observed structures. Moreover, studies are needed to be done in other pH value of aqueous solution, to understand how pH affects Ge electrodeposition and whether germanene structure can be formed. Furthermore, the continuation of electrochemical formation of Ge nanofilms studies are needed to find conditions to grow a better quality Ge deposits and to identify which conditions are producing Raman signal for germanene structure. For that purpose in situ Raman will be utilized and Surface Enhanced Raman spectroscopy (SERS) which uses modified substrates to increase the Raman signal of the deposit. A reason for utilization of in situ Raman spectroscopy is that Raman signal might not be reproducible because the germanene deposit is oxidized since it has to be carried through air before it

can be measured in the Raman instrument. Additionally, if the oxidation of the germanene structure is the case, means for its protection has to be identified. Moreover, a continuation of Te deposition studies onto Ge wafer needs to be performed, such as variation of time deposition and different pH of Te solution, to understand the nature of Te layer formation in detail, in order to utilize it in Ge growth cycle.